Ground states of spin-$\frac{1}{2}$ triangular antiferromagnets in a magnetic field

Ru Chen,[1] Hyejin Ju,[1] Hong-Chen Jiang,[2] Oleg A. Starykh,[3] and Leon Balents[2]
[1]*Department of Physics, University of California, Santa Barbara, Santa Barbara, California, 93106, USA*
[2]*Kavli Institute of Theoretical Physics, University of California, Santa Barbara, Santa Barbara, California, 93106, USA*
[3]*Department of Physics and Astronomy, University of Utah, Salt Lake City, Utah 84112, USA*
(Received 9 November 2012; revised manuscript received 11 March 2013; published 17 April 2013)

We use a combination of numerical density matrix renormalization group calculations and several analytical approaches to comprehensively study a simplified model for a spatially anisotropic spin-$\frac{1}{2}$ triangular lattice Heisenberg antiferromagnet: the three-leg triangular spin tube (TST). The model is described by three Heisenberg chains, with exchange constant J, coupled antiferromagnetically with exchange constant J' along the diagonals of the ladder system, with periodic boundary conditions in the shorter direction. Here, we determine the full phase diagram of this model as a function of both spatial anisotropy (between the isotropic and decoupled chain limits) and magnetic field. We find a rich phase diagram, which is remarkably dominated by quantum states: the phase corresponding to the classical ground state appears only in an exceedingly small region. Among the dominant phases generated by quantum effects are commensurate and incommensurate coplanar quasiordered states, which appear in the vicinity of the isotropic region for most fields, and in the high-field region for most anisotropies. The coplanar states, while not classical ground states, can at least be understood semiclassically. Even more strikingly, the largest region of phase space is occupied by a spin density wave phase, which has incommensurate collinear correlations along the field. This phase has no semiclassical analog, and may be ascribed to enhanced one-dimensional fluctuations due to frustration. Cutting across the phase diagram is a magnetization plateau, with a gap to all excitations and "up-up-down" spin order, with a quantized magnetization equal to $\frac{1}{3}$ of the saturation value. In the TST, this plateau extends almost but not quite to the decoupled chains limit. Most of the above features are expected to carry over to the two-dimensional system, which we also discuss. At low field, a dimerized phase appears, which is particular to the one-dimensional nature of the TST, and which can be understood from quantum Berry phase arguments.

DOI: 10.1103/PhysRevB.87.165123 PACS number(s): 75.10.Jm, 75.40.Cx, 75.50.Ee

I. INTRODUCTION

The nearest-neighbor spin-$\frac{1}{2}$ Heisenberg antiferromagnet on the triangular lattice is an archetypal model of frustrated quantum magnetism. While the isotropic model in zero field is rather well understood and is known to order into a coplanar "120°" state,[1] away from this limit the situation is less clear. Two deformations of the Hamiltonian are of particular physical and experimental importance: the application of an external magnetic field and the introduction of spatial anisotropy into the exchange interactions.

The spatial anisotropy is introduced by decomposing the lattice into chains with bonds of strength J, arranged into a parallel array, with interchain interactions of strength J' (see Fig. 1). Here, we define $R \equiv 1 - J'/J$ as the degree of anisotropy, and h measures the applied magnetic field. There have been many extensive studies that consider these effects separately. However, a two-dimensional (2D) phase diagram, taking both effects together, remains to be understood. This problem is of considerable experimental interest. The application of a magnetic field is one of the few general means to tune quantum magnets *in situ*, and provides very important information on the quantum dynamics, as well as clues to the underlying spin Hamiltonian, which is often not well known. Two materials whose behavior in magnetic fields has been extensively studied are Cs_2CuCl_4 and Cs_2CuBr_4, which are known to be approximately described by the spatially anisotropic version of the model, with larger anisotropy in the chloride ($R \approx 0.7$) than the bromide ($R \approx 0.3$–0.5). Both materials exhibit a rich structure of multiple phases in applied magnetic fields, for which a theoretical view of the phase diagram would be quite helpful.

The solution of the ground state of a fully two-dimensional frustrated quantum spin model in a two-parameter phase space is quite ambitious. Here, we consider a somewhat simpler task by concentrating on the problem defined by the model confined to a cylinder with a circumference of three lattice spacings (i.e., making y periodic with period 3), which we refer to as a *triangular spin tube*, or TST (see Fig. 2). By a combination of analytical approaches and extensive numerical simulations using the density matrix renormalization group[2] (DMRG), we reveal a rich and complex phase diagram for the TST, shown in Fig. 3. We argue in the Discussion (Sec. VIII) that much of this diagram translates to the fully 2D model. Whenever possible, we use a nomenclature for the ground-state phases which translates directly to two dimensions, although there are, of course, differences due to the absence of spontaneously broken continuous symmetry in one dimension.

Different parts of this phase diagram will be discussed in detail in the bulk of the paper, but we will highlight a few aspects here, where strong quantum features occur. First, the isotropic line $R = 0$ as a function of magnetic field has been considered many times in the two-dimensional limit. There, semiclassical methods[3,4] predict the stabilization of both coplanar spin configurations by quantum fluctuations, and, most interestingly, a magnetization plateau, at which the magnetization of the system is fixed (at $T = 0$) at $\frac{1}{3}$ of the saturation magnetization over a range of magnetic fields. We will refer to this state as the "$\frac{1}{3}$ plateau" throughout this text.

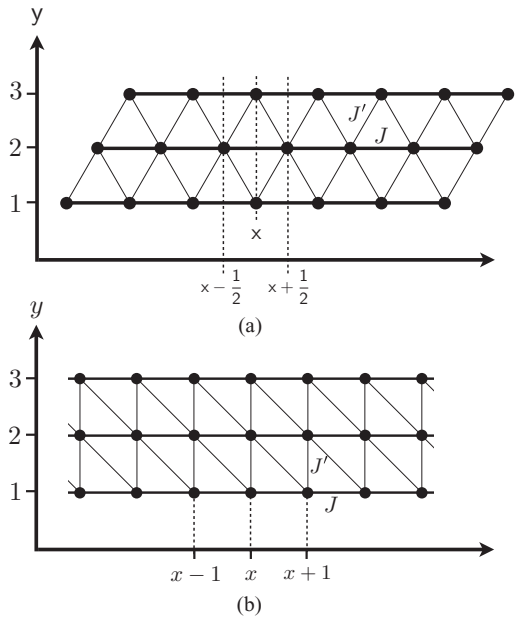

FIG. 1. TST in (a) Cartesian and (b) sheared coordinates with intrachain interactions J and interchain interactions J'.

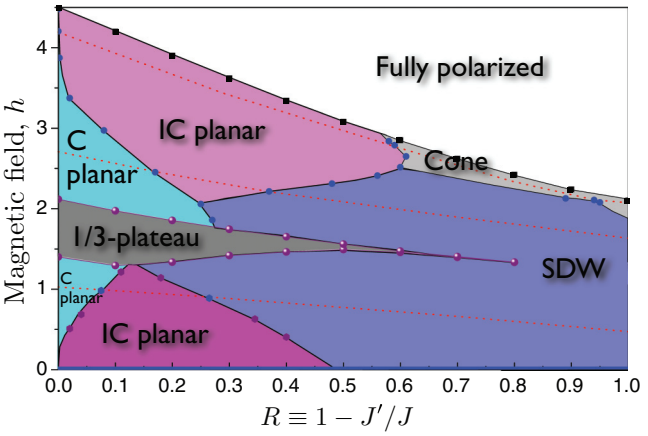

FIG. 3. (Color online) Phase diagram for the spatially anisotropic spin-$\frac{1}{2}$ TST in a magnetic field. Here, we use the following abbreviations to label the various phases of the diagram: C = commensurate; IC = incommensurate; SDW = spin density wave. $R \equiv 1 - J'/J$ is the degree of anisotropy. The dashed lines indicate constant magnetization lines, where the upper, middle, and lower ones are at $M/M_s = \frac{5}{6}$, $\frac{1}{2}$, and $\frac{1}{6}$, respectively.

On the plateau, the spins order into a collinear configuration. Stabilization of such a plateau is very much a quantum effect and is one of the more striking quantum features of the TST. The presence of the plateau has been confirmed for both the one-dimensional[5–7] and the two-dimensional spin-$\frac{1}{2}$ Heisenberg models by exact diagonalization,[8] coupled-cluster,[9] and variational[10] methods. Our DMRG study of the TST is also consistent with the semiclassical picture along the $R = 0$ line. We directly confirm the two "coplanar" phases, and accurately locate the boundaries of the $\frac{1}{3}$ plateau.

Another regime of strong quantum fluctuations occurs when R is close to 1, where the system is composed of weakly coupled (strictly) one-dimensional (1D) chains. There, an approach based on scaling and bosonization methods is possible, following Refs. 11 and 12. Those techniques (explained in this context in Sec. V) predict a *spin density wave* (SDW) state over a wide range of applied fields. In this SDW state, the dominant spin correlations are those of the Ising component parallel to the field, in sharp contrast to the classical behavior. Our DMRG simulations show that the SDW state dominates a remarkably broad region of the phase diagram, extending far beyond the decoupled line $R = 1$.

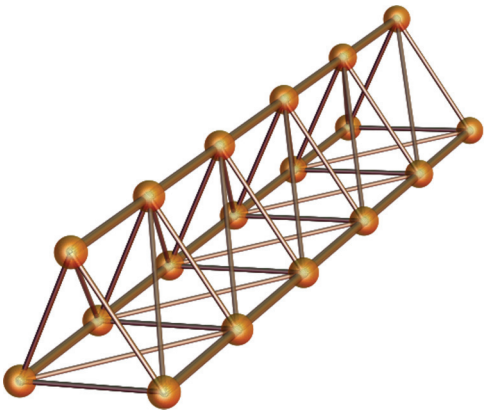

FIG. 2. (Color online) TST in sheared coordinates with period of three lattice spacings in the y direction. It is *crucial* to note that this geometry allows one to write $\sum_{y=1}^{3}\sum_x \mathcal{O}_y\mathcal{O}_{y+1} = \sum_{y=1}^{3}\sum_x \mathcal{O}_y\mathcal{O}_{y+2}$ for an operator $\mathcal{O}$.

In two dimensions, the quasi-1D approach of Refs. 11 and 12 shows the existence of a (very narrow) $\frac{1}{3}$ plateau arising out of the SDW phase, leading to the speculation that the plateau persists for all R in two dimensions. In the TST, we find that the plateau is also very robust, and persists almost, but not quite, to the 1D limit. The suppression relative to two dimensions can be understood as a result of enhanced fluctuations due to the one dimensionality of the TST. To check this, we have also carried out some DMRG studies of wider cylinders consisting of six and nine sites in the periodic direction. Our results appear consistent with the existence of a plateau for all R in two dimensions.

The last quantum regime we discuss here is clearly specific to the periodic boundary conditions imposed around the TST. This occurs at zero field, where for all values of R, we observe a spontaneously dimerized ground state. The dimerization is most clearly observed in the entanglement entropy, which shows a pronounced oscillatory behavior along the chain. We argue that this can be understood as an effect of one-dimensional quantum fluctuations upon an underlying short-range spiral magnetically ordered state, somewhat similar to the formation of a Haldane gap in integer spin chains with collinear classical states. The elementary excitations of the dimerized state are solitons, and we show how the behavior at small magnetization can be understood in terms of a dilute system of such solitons.

The remainder of the paper is organized as follows. In Sec. II, we introduce the model and then describe key technical aspects of our DMRG simulations, including the procedure to determine the phase boundaries using the second derivative

of the ground-state energy and entanglement entropy, and careful finite-size scaling. In Sec. III, we review and compare the semiclassical predictions to the DMRG results in the isotropic limit. Next, we discuss the high-field region in Sec. IV. In the vicinity of the saturation field, the problem can be modeled as a dilute system of spin-flip bosons. We compare an analysis of this limit, built upon an analytic solution of the Bethe-Salpeter equation, to the DMRG, and find a transition between coplanar and cone phases, and a commensurate-incommensurate transition. In Sec. V, we study the regime of weakly coupled chains, and in particular discuss the spin density wave (SDW) state and show that the $\frac{1}{3}$ plateau terminates in a Kosterlitz-Thouless transition around $R \sim 0.7 \pm 0.1$ for the TST. We consider the low-field region in Sec. VII, showing the persistent dimerization, the evidence for solitons at small magnetization, and the commensurate to incommensurate transition near $R = 0$. DMRG numerical results will be presented throughout these sections, presenting the important features used to identify each phase. Physical quantities, such as entanglement entropy, vector chirality, and the spin density profile will be shown for some representative large system size. Finally, we conclude in Sec. VIII with a summary and discuss some generalizations of our results to larger spin and two-dimensional systems.

II. MODEL AND DMRG METHOD

A. Hamiltonian and notation

The explicit Hamiltonian studied in this paper is written as

$$H = \sum_{x,y} [J\, \mathbf{S}_{x,y} \cdot \mathbf{S}_{x+1,y} + J'\, \mathbf{S}_{x,y} \cdot (\mathbf{S}_{x,y+1} + \mathbf{S}_{x-1,y+1})] - h \sum_{x,y} \mathbf{S}^z_{x,y}, \quad (1)$$

where x is the direction along the chains, and y is perpendicular to it, and h is the magnetic field. Importantly, we choose coordinates, as shown in Fig. 1(b), where the triangular lattice is "sheared" to embed it in a square one. This is convenient for the application of periodic boundary conditions in the TST.

Many previous works on the anisotropic triangular lattice in two dimensions, including those by some of the authors,[11,13] use instead "Cartesian" coordinates, as shown in Fig. 1(a). Both for convenience in certain calculations (especially in the quasi-one-dimensional limit), and to clarify the connection to this prior work, we give the relation between the sheared and Cartesian coordinates here. In Cartesian coordinates, we take the distance between sites along the chains and the (normal) distance between chains to unity. Defining the Cartesian coordinates as x,y, and $\mathsf{r} = (\mathsf{x},\mathsf{y})$, then

$$\mathsf{x} = x + y/2, \quad \mathsf{y} = y. \quad (2)$$

From this, we may also obtain the relationship between wave vectors in the two coordinate frames. We require $\mathbf{q} \cdot \mathbf{r} = \mathsf{q} \cdot \mathsf{r}$, which implies

$$q_x = \mathsf{q}_x, \quad q_y = \tfrac{1}{2}\mathsf{q}_x + \mathsf{q}_y. \quad (3)$$

B. DMRG

Throughout this paper, we rely extensively on DMRG simulations. For this study, we kept up to $m = 3072$ states in the DMRG block, performing more than 24 sweeps to obtain fully converged results. In doing so, we find that our truncation error is of the order 10^{-7}. We also take advantage of the cylindrical boundary condition to study large systems and to reduce finite-size effects for a more reliable extrapolation to the thermodynamic limit. In particular, in the regions above the $\frac{1}{3}$ plateau, we find that observables have much better convergence, with a truncation error of the order 10^{-9}. Even in the regions below the $\frac{1}{3}$ plateau not close to the dimerized phase, we find reasonable convergence, with a slightly larger truncation error on the order of 10^{-7}. However, when we approach the dimerized phase near zero magnetization, finite-size effects dominate: system sizes up to $N = 180 \times 3$ do not provide a reliable extrapolation to the thermodynamic limit.

The phase boundaries in Fig. 3 were determined from the simulations. We describe the methodology for doing so here, leaving the characterization of the phases which occur for subsequent sections. For the case of continuous transitions, it is common to calculate the second derivative of the ground-state energy $\frac{\partial^2 E_0}{\partial R^2}$. The calculation follows standard procedure of using three data points at $R + dR$, R, and $R - dR$, according to the formula $\partial^2 E_0/\partial R^2 = [E_0(R + dR) + E_0(R - dR) - 2E_0(R)]/dR^2$. The derivative diverges when the infinite-size system undergoes a transition. For finite systems, however, one will observe a finite peak that increases with system size. We then determine the phase boundaries numerically by looking at the peak position as a function of tuning parameter R. For example, as shown in Fig. 4(a), sharp peaks are located at $R = 0.6$. We observe that the peak value increases significantly with sample size, for all system sizes studied. We have not attempted to carry out detailed finite-size scaling analyses of the peaks, as our focus here is on the phases, not the critical behavior at the transitions between them. This transition corresponds to the upper dashed line in Fig. 3, where there is a transition between an incommensurate planar and a cone phase. We use similar procedures to determine phase boundaries at other magnetizations, e.g., $M/M_s = \frac{1}{2}, \frac{1}{6}$ in Figs. 4(b) and 4(c) correspond to the middle and lower dashed lines in Fig. 3, respectively.

In addition to these divergent peaks, there are some other features (which are *not* phase transitions) due to finite-size effects. For example, in Fig. 4(a) for $M/M_s = \frac{5}{6}$, a broad peak near $R = 0.8$ actually decreases (and eventually goes to zero) in the thermodynamic limit. Therefore, we can confidently say that the cone phase dominates in the region $R > 0.6$, and that there is no transition at $R = 0.8$. Similarly, for Figs. 4(b) and 4(c), the fluctuations in the plots near $R \approx 0.7, 0.45$, respectively, are finite-size effects and vanish in the thermodynamic limit.

Finally, we use the structure factor

$$S^{\mu\mu}(q) = \frac{1}{N} \sum_{\mathbf{r},\mathbf{r}'} e^{-i\mathbf{q}\cdot(\mathbf{r}-\mathbf{r}')} \langle S^\mu_{\mathbf{r}} S^\mu_{\mathbf{r}'} \rangle \quad (4)$$

to determine the boundaries between the commensurate and incommensurate phases. For example, for small R, the transverse and longitudinal components of the structure factor peak at

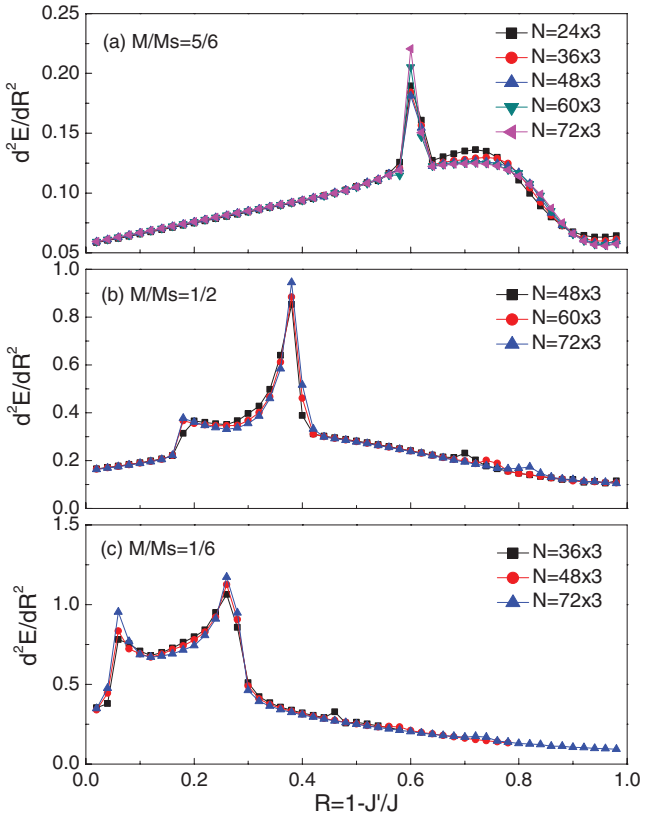

FIG. 4. (Color online) Second derivative of the ground-state energy with respect to R, for different values of magnetization. These plots are used to locate the phase boundaries in Fig. 3.

commensurate momenta $\mathbf{Q} = (4\pi/3, 2\pi/3)$ and $(2\pi/3, 4\pi/3)$, respectively. This defines the "C planar" regions in Fig. 3.

III. SEMICLASSICAL BEHAVIOR IN THE ISOTROPIC CASE

A. Two-dimensional model

The isotropic model $J' = J$ has been extensively studied in two dimensions, and it is believed that a semiclassical description, with weak quantum fluctuations included via spin wave theory, is qualitatively correct in this case.[3] We find that the semiclassical analysis largely carries over to the TST, with small modifications to allow for one-dimensional fluctuations. Therefore, we review the established semiclassical results first.

In the classical limit, where spins are described as O(3) vectors, the isotropic problem is known to display an "accidental" degeneracy in a nonzero applied magnetic field.[14] This can be seen from the fact that this model can be rewritten as

$$H = \frac{J}{2} \sum_{\triangle} \left(\mathbf{S}_{\triangle} - \frac{h}{3J} \hat{\mathbf{z}} \right)^2, \tag{5}$$

where $\mathbf{S}_{\triangle} = \mathbf{S}_1 + \mathbf{S}_2 + \mathbf{S}_3$ is the sum of the spins on a triangle, and the sum is over all triangles on the lattice. The ground-state configuration is given by the constraint

$$\mathbf{S}_{\triangle} - \frac{h}{3J} \hat{\mathbf{z}} = 0. \tag{6}$$

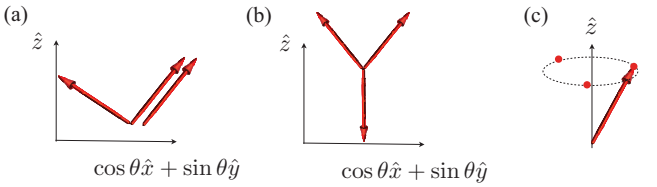

FIG. 5. (Color online) Degenerate classical spin configurations in the isotropic limit. With the magnetic field taken in the z direction, (a) shows the "V" configuration above the $\frac{1}{3}$ plateau, (b) depicts the "Y" phase below the $\frac{1}{3}$ plateau, while (c) shows the cone (or umbrella) state.

At zero magnetization, this constraint is solved by placing all spins in a plane, with the three spins in each triangle at 120° angles to one another in a three-sublattice structure. A specific ground state is specified by three angles, e.g., two determining the plane of the spins and one determining the angle within the plane. All such states are related by O(3) spin symmetry; so, this is a symmetry-demanded degeneracy. A previous DMRG study[15] on the 2D model also confirms the three-sublattice structure.

In a nonzero field, the ground states retain a three-sublattice structure, with three arbitrary angles remaining to determine the specific ground state. However, the presence of the field reduces the O(3) symmetry to O(2) [or U(1)], and only one of these angular degrees of freedom is symmetry demanded. The remaining two angular degrees of freedom constitute an *accidental* degeneracy. Two simple states within the degenerate manifold are the coplanar and umbrella ones, shown in Fig. 5.

As first shown by Chubukov and Golosov,[3] this accidental degeneracy is lifted by quantum fluctuations. They showed by a $1/S$ spin wave expansion that the degeneracy is lifted in favor of the coplanar states. Additionally, they demonstrated the existence of the $\frac{1}{3}$ plateau, in which the spins adopt a three-sublattice "up-up-down" structure. Away from the plateau, the coplanar state retains a three-sublattice structure with ordering wave vector $\mathbf{Q} = (4\pi/3, 0)$, or $\mathbf{Q} = (4\pi/3, 2\pi/3)$.[3,4,16] Below the plateau, the three spins form a "Y" with one spin antiparallel to the field and two spins with equal positive projection to the field but at opposite angles from each other. This can be viewed as a deformation of the 120° state with spins in a plane containing the magnetic field. Here, the spin configurations can be parametrized by

$$\begin{aligned} \langle S^+_{\mathbf{r}} \rangle &= a e^{i\theta} \sin(\mathbf{Q} \cdot \mathbf{r}), \\ \langle S^z_{\mathbf{r}} \rangle &= b - c \cos^2(\mathbf{Q} \cdot \mathbf{r}), \end{aligned} \tag{7}$$

where θ is an arbitrary angle specifying the plane of the spins, while a, b, c are constants dependent upon the field magnitude. Since $\mathbf{Q} \cdot \mathbf{r} = 2\pi(2x + y)/3$, we see from Eq. (7) that when $2x + y$ is a multiple of 3, one of the spin is aligned with the magnetic field. Above the plateau, one finds instead a "V" configuration, with two spins identical and the third chosen to give zero moment normal to z. In this case, we have

$$\begin{aligned} \langle S^+_{\mathbf{r}} \rangle &= a e^{i\theta} \cos(\mathbf{Q} \cdot \mathbf{r}) \\ \langle S^z_{\mathbf{r}} \rangle &= b - c \cos^2(\mathbf{Q} \cdot \mathbf{r}). \end{aligned} \tag{8}$$

Note that the cosine in the first line of Eq. (8) never vanishes on lattice sites, so that spins are never parallel to the field in the V state.

B. One dimension

We will see that the semiclassical results summarized in the previous section for the two-dimensional case remain qualitatively correct, at least at short distances, in the TST. However, we must still account for the effects of quantum fluctuations on long length scales since the one-dimensional system *can not* break the U(1) spin-rotational symmetry about the field axis. Since the U(1) symmetry is unbroken in the plateau state, there are no essential effects of one-dimensional fluctuations there. However, they have qualitative effects in the Y and V phases since $\langle S_r^+ \rangle = 0$ there, in contrast to Eqs. (7) and (8). Note that the modulation of $\langle S_r^z \rangle$ is perfectly consistent with one dimensionality, and is expected to persist directly without qualitative modifications.

To incorporate one-dimensional fluctuations, we regard the semiclassical results in Eqs. (7) and (8) as defining the local spin ordering, with a *fluctuating* quantum phase $\theta(x,\tau)$ (τ is imaginary time), that is, we make the replacement

$$S_r^+(\tau) \to a e^{i\theta(x,\tau)} \sin(\mathbf{Q}\cdot\mathbf{r}) \tag{9}$$

in the Y phase, and

$$S_r^+(\tau) \to a e^{i\theta(x,\tau)} \cos(\mathbf{Q}\cdot\mathbf{r}) \tag{10}$$

in the V phase. Note that these formulas are *not* invariant under translations, reflecting the three-sublattice structure of the coplanar phases. This can also be seen from the oscillations in the $\langle S_r^z \rangle$ expectation values. Even when one-dimensional fluctuations are taken into account, translational symmetry is broken. This is still consistent with the Mermin-Wagner theorem since the broken translational symmetry is discrete. Translating by one or two lattice spacings, one obtains two other symmetry-related but distinct ground states.

In both the Y and V phases, the field $\theta(x,\tau)$, representing the "would-be" Goldstone mode of the spontaneously broken U(1) symmetry, is governed by the usual massless free relativistic boson action

$$S_\theta = \int dx d\tau \left\{ \frac{vK}{2}(\partial_x\theta)^2 + \frac{K}{2v}(\partial_\tau\theta)^2 \right\}. \tag{11}$$

C. Comparison to DMRG

We now turn to a comparison of the semiclassical predictions, corrected as in the previous section for one-dimensional fluctuations, to the DMRG.

1. Entanglement entropy

The simplest comparison arises immediately from Eq. (11): the low-energy physics is that of a single massless scalar field, which is a conformal field theory with central charge $c = 1$. This central charge can be directly measured using the entanglement entropy.

According to conformal field theory,[17] in a one-dimensional critical system with open boundary conditions and total length L, the von Neumann entanglement entropy associated to a region with length x and its complement of length $L - x$ is given by

$$S(x,L) = \frac{c}{6} \ln\left[\frac{L}{\pi} \sin\left(\frac{\pi x}{L} \right) \right]. \tag{12}$$

By plotting the entropy $S(x,L)$ versus the reduced coordinate $x' = \ln[\frac{L}{\pi}\sin(\frac{\pi x}{L})]$, we can directly extract c from the numerics. As shown in Fig. 6, we can indeed obtain $c = 1$ with high accuracy for both Y and V phases. For example, the obtained central charge $c = 0.98$ at $M/M_s = \frac{1}{6}$ in the Y phase below the plateau, and $c = 0.97$ at $M/M_s = \frac{1}{2}$ in the V phase above the plateau. Both are consistent with the theoretical prediction.

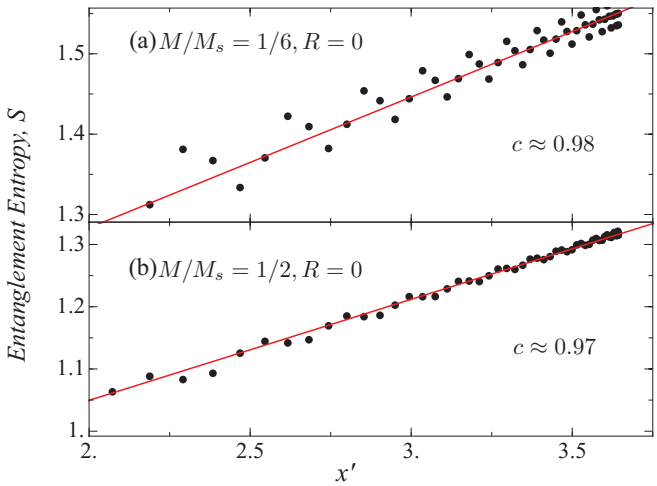

FIG. 6. (Color online) Entanglement entropy in the isotropic limit $R = 0$ for system size $N_x = 120$. Note that the reduced coordinate $x' \equiv \ln[\frac{L}{\pi}\sin(\frac{\pi x}{L})]$ is plotted on the x axis. We show the von Neumann entanglement entropy for (a) $M/M_s = \frac{1}{6}$, the commensurate Y phase and (b) $M/M_s = \frac{1}{2}$, the commensurate V state. The solid line is a linear fit, where by Eq. (12), we can extract the central charge c.

2. S^z profile

The modulation of $\langle S_{\mathbf{r}}^z \rangle$ predicted by the semiclassical theory in Eqs. (7) and (8) can be directly compared to the DMRG results. This is shown in Figs. 7 and 8. Note that a particular symmetry-broken state is chosen in the simulations, presumably due to pinning by the boundaries, which explicitly break translational symmetry. The origin of the coordinate $\mathbf{r}$ in Eqs. (7) and (8) must be appropriately chosen to match the chosen ground state.

3. $S^\pm$ correlations

Due to quantum fluctuations of the phase θ, the single-spin expectation value $\langle S_r^+ \rangle = 0$. Therefore, we must instead turn to correlation functions to detect the Y and V structures of the local ordering. Using Eq. (9), we obtain

$$\langle S_{\mathbf{r}}^+ S_{\mathbf{r}'}^- \rangle \sim a^2 \sin(\mathbf{Q}\cdot\mathbf{r}) \sin(\mathbf{Q}\cdot\mathbf{r}') \langle e^{i[\theta(x)-\theta(x')]} \rangle, \tag{13}$$

in the Y phase below the $\frac{1}{3}$ plateau. A similar formula, with the sines replaced by cosines, describes the correlation function of the V phase above the plateau. The correlation function is evaluated with respect to Eq. (11), where a finite-size form,

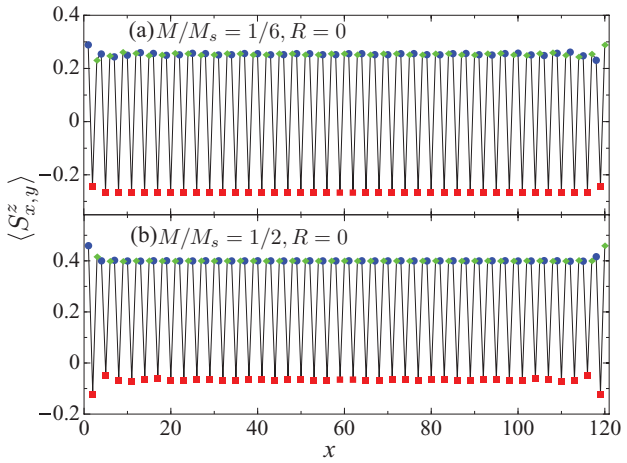

FIG. 7. (Color online) S^z profile in the isotropic limit $R = 0$ at (a) $M/M_s = \frac{1}{6}$, the commensurate Y phase, and (b) $M/M_s = \frac{1}{2}$, the commensurate V state. The square (red), diamond (green), and circle (blue) data points show the three-sublattice structure of the isotropic case. The magnitude of S^z does not decay because the discrete translational symmetry is spontaneously broken in these states.

first derived in Ref. 18, is as follows:

$$\langle e^{i[\theta(x)-\theta(x')]} \rangle = C_\eta(x,x'), \tag{14}$$

where

$$C_\eta(x,x') = a_0^\eta \frac{[f(2x)f(2x')]^{\eta/2}}{[f(x-x')f(x+x')]^\eta},$$
$$f(x) = \left[\frac{2(L+1)}{\pi} \sin\left(\frac{\pi|x|}{2(L+1)}\right)\right]. \tag{15}$$

Here, a_0 is a cutoff-dependent factor, which we can take to unity, absorbing the dependence in a in Eq. (13). The function $f(x)$ originates from a quantum average over the normal modes of the bosonic field θ. One is now able to fit the DMRG measurement of the transverse spin-spin correlation function to Eqs. (13) and (14) to obtain the ordering wave vector and the additional fit parameter η. A comparison is plotted in Fig. 9, where we show the correlation function along each chain (i.e., $y = 1,2,3$) for $R = 0$ and $M/M_s = \frac{1}{6}, \frac{1}{2}$. The fitting in Fig. 9(a) yields a commensurate wave vector $\mathbf{Q} = (4\pi/3, 2\pi/3)$ and $\eta = 0.65$ for $M/M_s = \frac{1}{6}$, which corresponds to the Y phase below the plateau. Above the plateau, in the V phase shown in Fig. 9(b), the ordering wave vector still shows commensurability $\mathbf{Q} = (4\pi/3, 2\pi/3)$ with $\eta = 0.43$. One can show that in the thermodynamic limit, the correlation function in Eq. (14) reduces to a simple power-law relation $\propto |x - x'|^{-\eta}$, which is reflected by our data for distances $|x - x'| \ll L/2$.

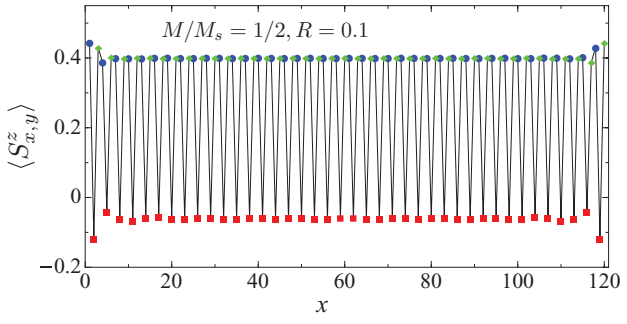

FIG. 8. (Color online) S^z profile for the commensurate V phase at $M/M_s = \frac{1}{2}$ and $R = 0.1$. We find that the wave vector remains commensurate, even for a nonzero, but small, R.

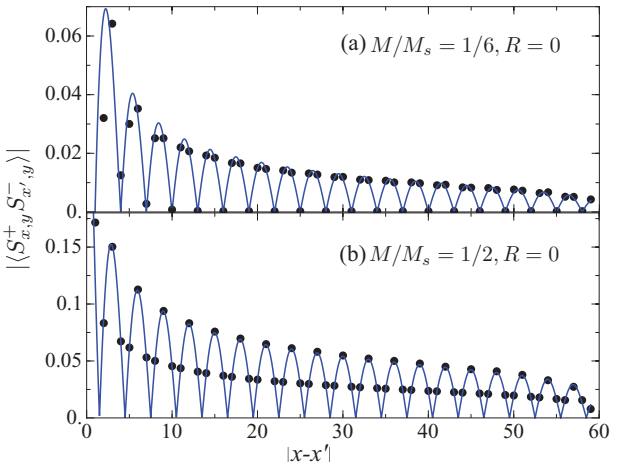

FIG. 9. (Color online) Transverse spin-spin correlations in the isotropic limit $R = 0$ in the (a) commensurate Y phase and (b) V phase for $N_x = 120$ and $x' = N_x/2$. Data points are shown as (black) circles, while the theoretical fit from Eq. (14) is shown as the (blue) line.

D. Behavior for small nonzero R

If we perturb slightly away from the isotropic limit, i.e., $0 < R \ll 1$, we expect the semiclassical picture to still hold. This has been analyzed in Refs. 4 and 16. Classically, the minimum energy spin configuration changes immediately when $R > 0$ from a commensurate state to an incommensurate one, with an ordering wave vector $\mathbf{Q} \neq (4\pi/3, 0)$ or $\mathbf{Q} \neq (4\pi/3, 2\pi/3)$. However, we expect that quantum fluctuations will stabilize the commensurate state for a range of anisotropies for a generic value of the magnetic field. The reason is that coplanar phases break discrete translational symmetries of the lattice. Since there are three equivalent ground states connected by translations, the symmetry breaking can be described by a $\mathbb{Z}_3$ order parameter. Specifically, the combination

$$\zeta_r = S^z_r e^{2\pi i(x+2y)/3} \tag{16}$$

defines a $\mathbb{Z}_3$ order parameter with $\langle \zeta_r \rangle = |\zeta| e^{i\vartheta}$ and $\vartheta = 0, 2\pi/3, 4\pi/3$ in the three distinct $\mathbb{Z}_3$ domains. To restore this discrete symmetry, a phase transition is required. More specifically, there are topological excitations of the coplanar state which are domain walls, also called solitons, connecting different symmetry-broken states. There is a nonzero energy gap to create a domain wall in any phase with long-range $\mathbb{Z}_3$ order. For the $\mathbb{Z}_3$ order to be destroyed, solitons must proliferate in the ground state. Small changes of parameters, such as R, can not instantly lower the gap for the domain walls to zero, which implies stability of the phase for a range of R values. This is correct, at least, away from the exceptional points where $h = 0$ (where the symmetry breaking becomes continuous) and $h = h_{\text{sat}}$ (where the symmetry breaking

vanishes). We will discuss the vicinity of these exceptional points in subsequent sections.

In general, with increasing anisotropy R, we will encounter a phase transition to an incommensurate phase, which corresponds to the proliferation of solitons and a vanishing of their gap. Beyond that point, $\langle \zeta_r \rangle$ becomes zero, and S^z correlations peak at a wave vector other than $\mathbf{Q} = (4\pi/3, 2\pi/3)$. This transition is discussed in Sec. IV E.

A useful test for this phase is the measurement of the central charge via entanglement entropy. In the commensurate regions, even for $R > 0$, we expect $c = 1$, while incommensurate phases may have $c > 1$. We observe this effect in Fig. 6, which shows $c = 1$ in the commensurate state, whereas Fig. 11 shows $c = 2$ in the incommensurate state. In addition, we can check for commensurability using structure factor measurements, as discussed in Sec. II B.

E. Phenomenological analysis at low field

We now address the region slightly away from $R = 0$ and at low applied magnetic field. We begin the discussion from a 2D point of view, although it largely applies to the TST as well. Commensurate coplanar spin order is described by the order parameter $\mathbf{d} = \mathbf{n}_1 - i\mathbf{n}_2$, where $\mathbf{n}_1$, $\mathbf{n}_2$ are mutually orthogonal vectors with identical norm spanning the plane of the spin order. Then, a spin at coordinate $\mathbf{r}$ can be written as

$$\mathbf{S}_\mathbf{r} = M + \mathrm{Re}(\mathbf{d}e^{i\mathbf{Q}\cdot\mathbf{r}}) = M + \mathbf{n}_1 \cos[\mathbf{Q}\cdot\mathbf{r}] + \mathbf{n}_2 \sin[\mathbf{Q}\cdot\mathbf{r}]. \tag{17}$$

Lattice translations transform $\mathbf{d} \to \mathbf{d}e^{-i2\pi/3}$, while lattice inversion $\mathbf{r} \to -\mathbf{r}$ results in complex conjugation $\mathbf{d} \to \mathbf{d}^*$. The effective Ginzburg-Landau Hamiltonian describing the coplanar state should remain invariant under these operations (see Ref. 19 for a closely related discussion). Then,

$$\begin{aligned} H_{\mathrm{comm}} = {} & -r\mathbf{d}^*\cdot\mathbf{d} + a_0|\partial_x\mathbf{d}|^2 + a_1(\mathbf{d}^*\cdot\mathbf{d})^2 + a_2|\mathbf{d}\cdot\mathbf{d}|^2 \\ & + \chi_1 h^2 \mathbf{d}^*\cdot\mathbf{d} + \chi_2|\mathbf{h}\cdot\mathbf{d}|^2 \\ & + \tfrac{1}{2}\chi_3[(\mathbf{h}\cdot\mathbf{d})^3 + (\mathbf{h}\cdot\mathbf{d}^*)^3]. \end{aligned} \tag{18}$$

Here, at mean-field level, $r > 0$ is required to obtain nonzero $\mathbf{n}_{1,2}$, and $a_{0,1} > 0$, for stability in the ordered phase. Furthermore, $a_2 > 0$ energetically imposes the orthogonality condition $\mathbf{n}_1 \cdot \mathbf{n}_2 = 0$ in zero field. To favor coplanar (rather than umbrella) spin structures in a finite magnetic field requires $\chi_2 < 0$. We may expect that χ_2 is a function of the anisotropy, being negative for the isotropic limit $R = 0$ and changing sign to positive values for sufficiently large R, where the order-by-disorder physics favoring coplanar states gives way to the classical energetic preference for umbrella states. Here, we restrict ourselves to the small anisotropy regime, for which we expect χ_2 to remain negative. With the preference for coplanar states set by $\chi_2 < 0$, for field oriented along $\hat{z}$, the preferred configurations of $\mathbf{d}$ may be parametrized as

$$\mathbf{d} = |d|e^{i\tilde{\theta}}[\hat{\mathbf{z}} + i(\cos\theta\hat{\mathbf{x}} + \sin\theta\hat{\mathbf{y}})], \tag{19}$$

where θ describes the orientation of the plane of the spins, and $\tilde{\theta}$ the angle of the spins within that plane. With this form for $\mathbf{d}$, we obtain the spin operators as

$$\begin{aligned} S^z_{x,y} &\sim M + |d|\cos(\mathbf{Q}\cdot\mathbf{r} + \tilde{\theta}), \\ S^+_{x,y} &\sim -|d|e^{-i\theta}\sin(\mathbf{Q}\cdot\mathbf{r} + \tilde{\theta}). \end{aligned} \tag{20}$$

The last term in Eq. (18) describes the commensurate locking of the spin to the lattice by the finite magnetic field. Using Eq. (19), it may be rewritten as a sine-Gordon term

$$H_{sg} = \chi_3|d|^3h^3\cos[3\tilde{\theta}]. \tag{21}$$

The sign $\chi_3 > 0$ is fixed by the condition that one of the three spins in a sublattice must be oriented opposite to the external field in the commensurate state. Thus, in the commensurate state, $\tilde{\theta} = \pi$ in Eq. (19).

Now, we move away from the isotropic line to $R > 0$. Here, threefold rotational symmetry is broken, which allows the introduction of an additional term, linear in derivatives, into the effective Hamiltonian:

$$H_{\mathrm{incomm}} = \frac{i}{2}b_1(\mathbf{d}^*\cdot\partial_x\mathbf{d} - \mathbf{d}\cdot\partial_x\mathbf{d}^*) = -b_1|d|^2\partial_x\tilde{\theta}. \tag{22}$$

Since this term must vanish at $R = 0$ and be analytic, $b_1 \sim R$. This term competes with the sine-Gordon term in Eq. (21), with the commensurate state with constant $\tilde{\theta}$ favored at small R and destabilized at larger R. Thus, the commensurate-incommensurate transition in two dimensions can be described by a Hamiltonian of the phase

$$H_{\text{C-IC}} = \int d^2\mathbf{r}\{\tilde{a}_0(\partial_x\tilde{\theta})^2 - \tilde{b}_1\partial_x\tilde{\theta} + \tilde{\chi}_3h^3\cos[3\tilde{\theta}]\}. \tag{23}$$

Here, the coefficients with tildes, $\tilde{a}_0, \tilde{b}_1, \tilde{\chi}_3$, are rescaled by unimportant factors, such as the amplitude $|d|$.

The sine-Gordon model of the form in Eq. (23) appears in several guises in this paper, and is analyzed in Appendix A. It encodes a commensurate-incommensurate transition (CIT) with increasing $\tilde{b}_1$. This transition is mean-field like for $d = 2$, and we may apply the results of Appendix A 1. This gives a critical value for the CIT of $\tilde{b}_{1,\mathrm{cr}} \sim \sqrt{\tilde{a}_0\tilde{\chi}_3h^3}$ for the incommensurate state, which translates to

$$h_{\text{C-IC}} \sim R^{2/3} \tag{24}$$

since $\tilde{b}_1 \sim R$. This is roughly consistent with shape of the boundary in the lower left corner of Fig. 3.

For the TST, the situation is complicated by one-dimensional fluctuations. At zero field $h = 0$, we know that, in fact, the ground state is *not* a spiral but rather a dimerized phase. Hence, we can not directly apply the above analysis at the lowest fields. The dimerized phase is broken fairly rapidly by the field, and so, above some small critical field, we may expect to be able to use results of this type. Even so, we should really use results for the $d = 1$ case, where a non-mean-field analysis applies, as described in Appendix A 2. Using Eq. (A16), the critical value $\tilde{b}_{1,\mathrm{cr}}$ is suppressed by a factor of $(\tilde{\chi}_3h^3/\tilde{a}_0)^{\Delta_3/(4-2\Delta_3)}$, so that the net result is $\tilde{b}_{1,\mathrm{cr}} \sim h^{\frac{3-\Delta_3}{2-\Delta_3}}$, and hence

$$h_{\text{C-IC}} \sim R^{\frac{2-\Delta_3}{3-\Delta_3}}. \tag{25}$$

Here, Δ_3 is the scaling dimension of the $\cos 3\tilde{\theta}$ term. Assuming the commensurate phase is at all stable for small R implies $\Delta_3 < 2$, so that the cosine term is relevant in the isotropic case

$R = 0$. It is also bounded below by zero, so that the exponent in Eq. (25) varies between 0 and $\frac{2}{3}$. Once again, we caution that the expression must be taken with care since it does not in fact apply at the lowest fields.

IV. HIGH-FIELD REGION

A. Spin-flip bosons

In this section, we study the phase diagram near saturation, i.e., for applied fields sufficiently large that the magnetization is close to its maximum of $\frac{1}{2}$ per site. *At* saturation, the ground state of the model is the trivial product state with all spins aligned in the direction selected by the field. For fields above the saturation field, this is the exact ground state, and the lowest excited states consist of single magnons, in which just one spin has been flipped relative to the saturated state. These magnons are bosons with $S^z = 1$, and upon reducing the field to the saturation value, the minimum energy required to create a magnon vanishes. Below the saturation field, therefore, we can expect Bose-Einstein condensation (BEC) of these magnons. In the one-dimensional TST, strict BEC is not possible due to phase fluctuations, but these fluctuations are readily taken into account and a quasicondensate description remains appropriate.

To formalize the magnon BEC picture, one may transform the spin model to a bosonic one,[20–25] using the equivalence of the spin $s = \frac{1}{2}$ Hilbert space to that of hard-core bosons:

$$S^+_{\mathbf{r}} = \mathcal{P}_{\mathbf{r}}\, b_{\mathbf{r}}\, \mathcal{P}_{\mathbf{r}}, \tag{26}$$

$$S^z_{\mathbf{r}} = \tfrac{1}{2} - n_{\mathbf{r}}, \tag{27}$$

where $n_{\mathbf{r}} = b^\dagger_{\mathbf{r}} b_{\mathbf{r}}$ is the boson occupation number, and one must project onto the space of no-double-boson occupancy $\mathcal{P}_{\mathbf{r}} = |n_{\mathbf{r}} = 0\rangle\langle n_{\mathbf{r}} = 0| + |n_{\mathbf{r}} = 1\rangle\langle n_{\mathbf{r}} = 1|$. Equation (26) is equivalent to the Holstein-Primakoff bosonization formula, truncated to quadratic order in boson operators and taking $s = \frac{1}{2}$, provided the no-double-occupancy constraint is imposed. The generalization to $s > \frac{1}{2}$ will be briefly discussed later in Sec. VIII B 1.

It is convenient to implement the no-double-occupancy constraint by first relaxing the constraint, adding an onsite interaction U to the Hamiltonian, and then realizing the projection by taking the $U \to \infty$ limit. In this way, we can proceed simply by rewriting the Heisenberg model using Eq. (26), forgetting the projection operators, i.e., taking $\mathcal{P}_{\mathbf{r}} \to 1$. We thereby obtain a boson Hamiltonian with hopping terms (J), onsite energies (J,h), an onsite (U), and nearest-neighbor (J,J') interactions. Fourier transforming to diagonalize the quadratic terms, we find

$$H = \sum_{\mathbf{k}} [\epsilon(\mathbf{k}) - \mu]\, b^\dagger_{\mathbf{k}} b_{\mathbf{k}} + \frac{1}{2N} \sum_{\mathbf{k},\mathbf{k}',\mathbf{q}} V(\mathbf{q}) b^\dagger_{\mathbf{k}+\mathbf{q}} b^\dagger_{\mathbf{k}'-\mathbf{q}} b_{\mathbf{k}'} b_{\mathbf{k}}, \tag{28}$$

where

$$\epsilon(\mathbf{k}) = J(\mathbf{k}) - J_{\min}, \tag{29}$$

$$\mu = h_{\rm sat} - h, \quad \text{where} \quad h_{\rm sat} = J(0) - J_{\min}, \tag{30}$$

$$V(\mathbf{k}) = 2\,[\epsilon(\mathbf{k}) + U]\,. \tag{31}$$

Here, $J(\mathbf{k})$ is the Fourier transform of the exchange interaction, μ is the bosonic chemical potential, and $h_{\rm sat}$ is the saturation field. We will use this formalism to derive an effective action for the dilute bosons, and also to locate (if any) a transition between the planar and cone phases near saturation.

B. Effective field theory for dilute bosons

For $h > h_{\rm sat}$, the vacuum is an exact ground state of this Hamiltonian, i.e., $b_{\mathbf{k}}|0\rangle = 0$. Below the saturation field, a finite density of magnons is introduced into the system, and a BEC or quasi-BEC is expected. The phase of the system, and correspondingly the magnetic order (correlations), is determined by the structure of this condensate (or quasicondensate). To determine this structure, we construct an effective model. The lowest-energy magnon excitations in the triangular lattice occur at nonzero momenta $\pm\mathbf{Q}$, which minimize the dispersion.[23,24] In our (sheared) coordinates, the dispersion relation is

$$J_{\rm TST}(\mathbf{k}) = J\cos k_x + J'[\cos k_y + \cos(k_y - k_x)]. \tag{32}$$

In two dimensions, we can choose arbitrary k_x and k_y, and the minima occur at $\mathbf{k} = \pm\mathbf{Q}_{\rm 2D}$, with $\mathbf{Q}_{\rm 2D} = (Q_{\rm 2D}, Q_{\rm 2D}/2)$, and

$$Q_{\rm 2D} = 2\arccos\left[-\frac{J'}{2J}\right]. \tag{33}$$

Note that in the conventional Cartesian coordinates, this wave vector is $\mathbf{Q} = (Q_{\rm 2D},0)$. For the TST, we must quantize $k_y = 0, 2\pi/3, 4\pi/3$. With this restricted choice of k_y, the 2D wave vector $\mathbf{Q}_{\rm 2D}$ can not generally be achieved. Instead, we find that the minimum energy wave vector is $\mathbf{k}_{\rm TST} = \pm\mathbf{Q}_{\rm TST} = \pm(Q_{\rm 1D}, 2\pi/3)$, with

$$Q_{\rm 1D} = \pi + \arctan\left(\frac{\sqrt{3}J'}{2J - J'}\right). \tag{34}$$

The two wave vectors coincide when $J = J'$.

In a low-energy description, the modes away from these two minima may be integrated out, leaving an effective theory in terms of two "flavors" of bosons ψ_1 and ψ_2 defined via

$$b_{\mathbf{k}} = \psi_{1,\mathbf{Q}+\mathbf{k}} + \psi_{2,-\mathbf{Q}+\mathbf{k}} + \bar{b}_{\mathbf{k}}. \tag{35}$$

Here, $\psi_{1,\mathbf{q}}$ ($\psi_{2,\mathbf{q}}$) is defined as a boson "centered" on the minimum energy momentum $\mathbf{Q}$ ($-\mathbf{Q}$), with weight only for small $|q| < \Lambda$, where $\Lambda \ll 2\pi$ is a cutoff introduced by integrating out the modes away from the minima. The third operator $\bar{b}_{\mathbf{k}}$ represents the high-energy modes which remain uncondensed, and are integrated out. In two dimensions, Fourier transforming in q_x, q_y back to real space leads to slowly varying continuum fields $\psi_a(\mathbf{r})$, where $\mathbf{r}$ is a two-dimensional spatial coordinate. For the TST, we need to keep only the mode with minimum energy q_y, and so, we Fourier transform only in q_x, which leads to a continuum field dependent only on the position along the chain x.

In this continuum limit, the boson fields are governed by an effective action of the form

$$\mathcal{S}=\int d^d\mathbf{r}\,d\tau\,\left\{\psi_1^\dagger\left(\partial_\tau-\frac{1}{2m}\nabla^2\right)\psi_1+\psi_2^\dagger\left(\partial_\tau-\frac{1}{2m}\nabla^2\right)\psi_2 -\mu(\rho_1+\rho_2)+\frac{1}{2}\Gamma_1\left(\rho_1^2+\rho_2^2\right)+\Gamma_2\rho_1\rho_2\right\}, \tag{36}$$

where $\rho_\alpha=|\psi_\alpha|^2$. We have written the action (36) in a form which includes both the TST ($d=1$) and two-dimensional ($d=2$) cases. We expand to fourth order in $|\psi_a|$ and to lowest order in derivatives, which is justified near saturation due to the diluteness of the magnons. The quadratic terms in Eq. (36) can be readily extracted from the exact single-magnon dispersion, which is given in Eq. (29) [in general in two dimensions the quadratic term may have an anisotropic effective mass tensor,[24] which is not explicitly shown in Eq. (36)]. The quartic interaction terms are more subtle because although the magnons may be assumed dilute, the lattice-scale interactions in Eq. (28) are not weak. Therefore, the parameters Γ_1,Γ_2 must be obtained from a more careful analysis, which we return to below.

C. Order-parameter structure

Taking for the moment the Γ_a as phenomenological parameters, we discuss the structure of the condensed or quasicondensed phase. If $\mu<0$, there are no bosons in the system, and the vacuum is the ground state. When $\mu>0$, a finite density of bosons is present. Depending upon their interactions, different phases may result.[23] To discuss the nature of these phases, a mean-field analysis of Eq. (36) is sufficient. We comment on the modifications to the mean-field results at the end of this section.

In mean-field theory, we simply minimize $\mathcal{S}$ in Eq. (36) for constant values of ψ_α. When $\mu>0$ and $\Gamma_1<\Gamma_2$, then $\rho_1\neq 0,\rho_2=0$ or vice versa, which means that the magnons condense at one of the two minima: a single-Q condensate. Here, in minimizing the energy, one finds that $\rho_1=\langle\rho_1\rangle=\mu/\Gamma_1$ and $E/N=-\mu^2/(2\Gamma_1)$. By taking $\psi_{1,2}=\sqrt{\rho_{1,2}}e^{i\theta_{1,2}}$, one can write the spin operator as follows:

$$S^+_{\mathbf{r}}=\overline{\psi}\,e^{i(\mathbf{Q}\cdot\mathbf{r}+\theta_1)}, \tag{37}$$

$$S^z_{\mathbf{r}}=\tfrac{1}{2}-\langle\rho_1\rangle, \tag{38}$$

where $\overline{\psi}=\sqrt{\langle\rho_1\rangle}$ in mean-field theory. We see that the z component of the spins is nonzero but constant in space, while the xy components rotate as one moves in space. Such a configuration is called a cone or umbrella phase because the spins trace out a cone as one proceeds through the lattice [see Fig. 5(c)].

When $\Gamma_2<\Gamma_1$, then $\rho_1=\rho_2$, which means that the bosons condense at both $+\mathbf{Q}$ and $-\mathbf{Q}$. This is a double-Q condensate with density $\langle\rho\rangle=\langle\rho_1\rangle+\langle\rho_2\rangle=\mu/(\Gamma_1+\Gamma_2)$ in mean-field theory. Here, the energy $E/N=\mu^2/(\Gamma_1+\Gamma_2)$. Again, by letting $\psi_{1,2}=\sqrt{\rho_{1,2}}e^{i\theta_{1,2}}$ and $\theta_{1,2}=\theta\pm\tilde{\theta}$,

$$S^+_{\mathbf{r}}=2\overline{\psi}\,e^{i\theta}\cos(\mathbf{Q}\cdot\mathbf{r}+\tilde{\theta}), \tag{39}$$

$$S^z_{\mathbf{r}}=\tfrac{1}{2}-4\langle\rho\rangle\cos^2(\mathbf{Q}\cdot\mathbf{r}+\tilde{\theta}), \tag{40}$$

where $\overline{\psi}=\sqrt{\langle\rho\rangle}$ in mean-field theory. In this phase, the z component of the spins is not constant, but the phase of S_r^+ is constant. This implies that the spins remain in a plane, i.e., this is a coplanar phase. Instead of a cone, the spins in this phase sweep out a "fan," so this is sometimes called a fan state.

How much of this survives beyond mean-field theory? In general, the dependence of the density on chemical potential is affected by fluctuations. Note that in the original spin problem, this dependence gives the behavior of the magnetization versus field in the vicinity of saturation, as is seen from Eq. (26). As is well known,[26] the BEC transition at $\mu=0$ is a very simple example of a quantum critical point, whose upper critical dimension is $d=2$. Thus, in two dimensions, the deviations from mean-field theory are minimal and consist just of logarithmic corrections. However, in $d=1$ the corrections are much more significant, and the dependence of the density on chemical potential is quite different.

In mean-field theory, we see that there is a first-order transition between the cone and fan states upon varying $\Gamma_1-\Gamma_2$ through zero. In fact, the location of this transition at $\Gamma_1=\Gamma_2$ is correct and, moreover, exact, beyond mean-field theory. To see this, note that when $\Gamma_1=\Gamma_2=\Gamma$, the interaction terms may be rewritten as $\frac{\Gamma}{2}(\rho_1+\rho_2)^2$, which implies that the action has an enlarged SU(2) symmetry under rotations $\psi_\alpha\to\sum_\beta U_{\alpha\beta}\psi_\beta$, where U is an arbitrary SU(2) matrix. This guarantees the degeneracy of the cone and fan states at this point since one can be rotated into the other by such an SU(2) rotation, and therefore, fixes the location of the cone to coplanar transition.

When $\Gamma_1\neq\Gamma_2$, the SU(2) symmetry of Eq. (36) is reduced to U(1) × U(1), corresponding to independent phase rotations of ψ_1 and ψ_2. As a consequence, there will be one gapless mode in the theory described by Eq. (36) for each Bose field with nonzero amplitude, i.e., one in the cone state and two in the fan. The fluctuations of these gapless modes lead, in the one-dimensional TST, to power-law correlations of the spin components transverse to the magnetic field, rather than the long-range order (broken-symmetry states) obtained in mean field.

Physically, the overall U(1) symmetry under simultaneous and equal rotations of both fields reflects conservation of S^z and is microscopically mandated by the Heisenberg model. The "orthogonal" symmetry under the rotation of the two boson fields by opposite phases is *emergent*, however. It is a consequence of the *discrete* translational symmetry of the lattice and the (generically) incommensurate nature of the wave vector Q. In general, this symmetry is broken by terms [which should be added to $\mathcal{S}$ in Eq. (36)] of the form

$$\mathcal{S}'=-\sum_n w_n\int d^d\mathbf{x}\,d\tau\,(\psi_1^\dagger\psi_2)^n\,e^{-in\mathbf{q}_n\cdot\mathbf{r}}+\text{H.c.}, \tag{41}$$

where naïvely $\mathbf{q}_n=2\mathbf{Q}$, but in fact we can take $\mathbf{q}_n=2\mathbf{Q}-\mathbf{K}/n$, where $\mathbf{K}$ is any reciprocal lattice (RL) vector, since $\mathbf{r}$ is a lattice coordinate. So, henceforth we work with

$$\mathbf{q}_n=\min_{\mathbf{K}\in\text{RL}}[2\mathbf{Q}-\mathbf{K}/n], \tag{42}$$

i.e., we choose $\mathbf{K}$ to minimize the magnitude of $\mathbf{q}_n$. When the wave vector $\mathbf{Q}$ is incommensurate and the magnitude of these terms is small, their oscillations average to zero

over short distances, and they can thereby be neglected. However, if $2n\mathbf{Q}$ is close to a reciprocal lattice vector, then $\mathbf{q}_n$ is small and the corresponding w_n term becomes slowly varying, and it can have effects that persist into the continuum theory. This occurs only if $2n\mathbf{Q}$ is close to a reciprocal lattice vector *and* the amplitude of both ψ_1 and ψ_2 is nonzero, i.e., within the coplanar or fan state. This leads to commensurate-incommensurate transitions, discussed in Sec. IV E.

In the cone state, such effects are not important. In this case, we expect one gapless "Goldstone" mode (θ_1) and power-law transverse spin correlations. But, actually there is some hidden long-range order. Note that in Eq. (37) we have (arbitrarily) chosen the minimum with $\rho_1 \neq 0$ and $\rho_2 = 0$ instead of the one with $\rho_1 = 0$, $\rho_2 \neq 0$. In doing so, the system spontaneously breaks discrete symmetries. In particular, for the TST, this choice breaks both inversion symmetry and a "charge-conjugation" symmetry, the latter being the antiunitary symmetry of the Scrödinger equation under complex conjugation of the wave function. Although the fluctuations of the phase θ_1 above will reduce the mean-field magnetic order to quasi-long-range order in the TST, the discrete symmetry breaking is robust to one-dimensional fluctuations. This symmetry breaking can be most directly sensed by the vector chirality[7,27]

$$V_{x,y} = \hat{z} \cdot \langle \mathbf{S}_{x,y} \times \mathbf{S}_{x+1,y} \rangle. \tag{43}$$

Replacing S_r^+ in Eq. (43) by the ansatz in Eq. (37), we find $V = \overline{\psi}^2 \sin Q$, i.e., a nonzero and constant value in the cone state. The opposite sign would be obtained for the solution with $\rho_1 = 0, \rho_2 \neq 0$, so this serves as an Ising-type order parameter for the cone state.

D. Incommensurate planar-to-cone-state transition at the saturation

1. Bethe-Salpeter equation

Now that we have described the phases of Eq. (36), we will briefly outline the methods to compute Γ_1, Γ_2. When the external field is sufficiently close to the saturation field, then the density of magnons, or spin flips, is dilute. In this case, we can safely use the ladder approximation[28–30] to renormalize the interaction vertex in a controlled manner. In fact, we (strictly speaking) analyze the interactions for fields *above* the saturation field, where there are no bosons present in the ground state, and we consider just two bosons interacting pairwise above the vacuum. We require the behavior in the limit in which the saturation field is approached, i.e., in which the energy of the two interacting bosons approaches zero. This limit should be familiar from ultracold atomic systems, in which the complicated interactions between atoms can be replaced by one or a few scattering lengths, which represent the effective interactions in the dilute limit. Here, we obtain the effective interactions from the Bethe-Salpeter (BS) equation, which reads as

$$\Gamma(k,k';q) = V(q) - \int_p \frac{V(q-p)\Gamma(k,k';p)}{\epsilon(k+p)+\epsilon(k'-p)+\Omega}. \tag{44}$$

Here, $\Gamma(k,k';q)$ is the irreducible four-point interaction vertex taken with all external frequencies equal to zero, and $\Omega = 2(h - h_{\rm sat}) = -2\mu$. The k,k' are the incoming momenta and $k+q, k'-q$ are the outgoing momenta, as shown in Fig. 10. From this, one obtains that $\Gamma_1 = \Gamma(Q,Q,0)$ and $\Gamma_2 = \Gamma(Q,-Q,0) + \Gamma(Q,-Q,-2Q)$. In Eq. (29), we introduced a factor of U into the definition of $V(q)$ to enforce the spin-$\frac{1}{2}$ constraint, which is equivalent to taking the limit $U \to \infty$. This limit in the BS language, Eq. (44), provides us with an additional constraint which reads as[21,23]

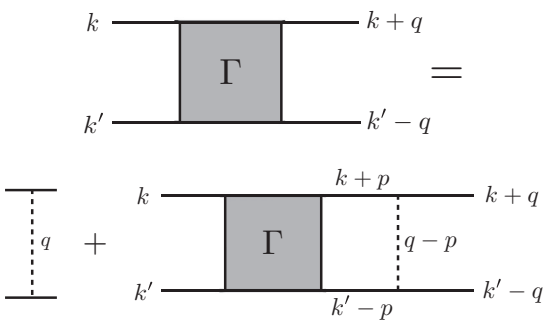

FIG. 10. Ladder approximation of Eq. (44). Here, k,k' are incoming momenta while $k+q, k'-q$ are outgoing momenta.

$$\int_p \frac{\Gamma(k,k';p)}{\epsilon(k+p)+\epsilon(k'-p)+\Omega} = 1. \tag{45}$$

Both Eqs. (44) and (45) can be applied either in two or three dimensions, or for the one-dimensional TST; in the latter case, the integral over p should be regarded as an integral over p_x and a *sum* over the discrete $p_y = 0, 2\pi/3, 4\pi/3$. Notice that in two or fewer dimensions, since $\epsilon(k) \sim k^2, V(k) \sim 1$ near $k = 0$, the integral is at least logarithmically divergent when Ω approaches zero. This reflects the fact that weak interactions are marginally relevant at the zero-density fixed point in $d = 2$, and relevant for $d < 2$. We use this to our advantage since we are interested precisely in this limit: the singular parts dominate the vertex function as $\Omega \to 0^+$, and we extract these dominant singular terms analytically to obtain the asymptotic behavior. For $d > 2$, the integrals become nonsingular, and one can directly take the $\Omega = 0$ limit.

2. Calculation of Γ_1 and Γ_2 in 2D

We first give a brief summary of our calculations for the 2D case. The dispersion minima occur at $\mathbf{k},\mathbf{k}' = \pm\mathbf{Q}_{\rm 2D} = \pm(Q_{\rm 2D}, Q_{\rm 2D}/2)$, where $Q_{\rm 2D}$ is given in Eq. (33). To solve the BS equation, we use the following ansatz:

$$\begin{aligned}\Gamma(k,k';q;\Omega) = {} & A_0 + A_1 \cos q_x + A_2 \sin q_x \\ & + A_3 \cos q_y + A_4 \sin q_y + A_5 \cos(q_y - q_x) \\ & + A_6 \sin(q_y - q_x),\end{aligned} \tag{46}$$

where A_i are coefficients dependent on k, k', J, J', and Ω. With Eqs. (44)–(46), one can solve a set of linear equations for the coefficients A_i, which give an explicit form of $\Gamma(q)$ for a given set of k, k', J, J', and Ω. Details of the 2D case are given in Appendix B 1. From the solution, we simply obtain

$$\Gamma_1 > \Gamma_2 \quad \text{for} \quad 0 < R < 1, \tag{47}$$

which implies that *for all range of anisotropies* $0 \leqslant R \leqslant 1$, *the ground state near saturation field is always an incommensurate planar (or fan) state*.

To see how the incommensurate planar state dominates over the cone state in the weakly coupled chains region, we expand the expression of Γ's in the leading order of both $1/\ln\Omega$ and $j \equiv J'/J$:

$$\begin{aligned}\Gamma_1/J &= \left[-4\pi j + \frac{\pi}{2}j^3 + O(j^5)\right]\frac{1}{\ln\Omega} \\ &\quad + [-8j\pi\ln(4j) + \alpha + O(j^3)]\frac{1}{(\ln\Omega)^2} + \cdots, \\ \Gamma_2/J &= \left[-4\pi j + \frac{\pi}{2}j^3 + O(j^5)\right]\frac{1}{\ln\Omega} \\ &\quad + [-8j\pi\ln(4j) + O(j^3)]\frac{1}{(\ln\Omega)^2} + \cdots, \\ \alpha &= \frac{8j\pi(24 - 16\ln 2 - 3\pi\ln 2)}{16 + 3\pi} > 0.\end{aligned} \tag{48}$$

Since the extra factor α is always larger than zero, the ground state always prefers the fan state in the limit of decoupled chains.

One can analytically check this result in the same limit $J' \ll J$. We discuss this extension in Appendix B 3.

3. *Calculation of* Γ_1 *and* Γ_2 *in the TST*

We now present a brief overview of our calculations on the TST. We consider an infinitely long system, where q_x is continuous and $q_y = 0, 2\pi/3, 4\pi/3$ is discretized by periodic boundary conditions. The dispersion minima occur at $\mathbf{k}, \mathbf{k}' = \pm\mathbf{Q}_{1D} = \pm(Q_{1D}, 2\pi/3)$, given in Eq. (34). We are now in a position to solve the BS equation, where we follow similar procedures as the two-dimensional case. We use the same ansatz (46) to solve for the coefficients A_i. From these coefficients, we can obtain the explicit forms of $\Gamma(q)$, for which we provide details in Appendix B 2. Our results are as follows:

$$\begin{aligned}&\Gamma_1 > \Gamma_2 \quad \text{for} \quad 0 < R < 0.48, \\ &\Gamma_1 < \Gamma_2 \quad \text{for} \quad 0.48 < R < 1.\end{aligned} \tag{49}$$

This tells us that for $R < R_c = 0.48$, the incommensurate (fan) state is favored, while for $R > R_c$, the cone (umbrella) state is favored. This result is in agreement with the analytical result, in Appendix B 3, where it was shown that spins order into a cone state in the decoupled chains limit.

E. Commensurate-incommensurate transitions (CIT)

In the previous section, we found that near saturation, the ground state of the two-dimensional model for all R and of the TST for $R > 0.48$ is coplanar, with modulation of the z component of the spin at wave vector $2Q$. As mentioned in Sec. IV C, this implies spontaneous breaking of the discrete translational symmetry, which is sensitive to commensurability effects via the terms in Eq. (41). In particular, we expect that the wave vector Q will *lock* to commensurate values, where $2Qn$ is a reciprocal lattice vector, over a finite range of field and anisotropy R. We now turn to a description of these commensurate-incommensurate transitions (CITs), both in the 2D case and for the TST.

To study the CITs, we must now consider the full action [Eqs. (36) and (41)] for $h < h_{sat}$, i.e., for $\mu > 0$, where the bosons are at nonzero density. In two dimensions, we can regard them as condensed, while in the TST, true condensation is impossible but the system can be viewed as a quasicondensate or a Luttinger liquid. In either case, amplitude fluctuations of the ψ_α fields are small, and we can write the effective action in terms of the phases θ_α, where $\psi_\alpha \sim \psi_0 e^{-i\theta_\alpha}$ in the coplanar/fan region.

Conceptually, the effective action for the phase fields is obtained by first following the renormalization of the system away from the zero-density fixed point $\mu = 0$, where amplitude fluctuations are still important. Once the energy scale set by μ is reached, these fluctuations are quenched, and it is sufficient to consider only small fluctuations in the amplitudes. To achieve this, we simply make the assumption of small amplitude fluctuations in Eqs. (36) and (41), but with the bare couplings replaced by *fully renormalized ones, at the scale* μ. We believe this procedure properly captures the scaling for small μ, although it is not quantitatively reliable.

Because the low-energy dispersion of the single-magnon states is exactly known and described by the quadratic terms in Eq. (36), the corresponding couplings are unrenormalized. The interactions Γ_1 and Γ_2, however, are renormalized by multiple scatterings, which is exactly what is captured by the BS equation discussed in Sec. IV D. From this analysis, we simply take as our renormalized couplings $\Gamma_\alpha(\Omega = 2\mu)$. Note that this would be exactly correct if we replaced μ by $|\mu|$ for the case $\mu < 0$, but on scaling grounds it should give the correct dependence even for $\mu > 0$.

The renormalized interactions can be approximately represented for small μ as

$$\Gamma_\alpha(\mu) \sim \frac{u_\alpha}{1 + m u_\alpha/\zeta(m\mu)}, \tag{50}$$

where

$$\zeta(m\mu) = \begin{cases}(m\mu)^{1/2}, & d = 1 \\ 1/|\ln(m\mu)|, & d = 2\end{cases} \tag{51}$$

and u_α are constants related to the "bare" values of Γ_α. We can in principle use the renormalized $\Gamma_\alpha(\mu)$ for the original lattice spin model, which have the same leading and first subleading terms for small μ (up to second order in $\zeta \ll 1$) as in Eq. (50), but with considerably more complicated coefficients. Beyond second order in ζ, the lattice Γ_α differs somewhat, and the expression is unwieldy. The above form is sufficient for our purposes, and is exact for a continuum model.

Once the $\Gamma_\alpha(\mu)$ are known, the analysis is straightforward.[24] We write $\psi_\alpha = [\overline{\rho} + \sigma_\alpha]^{1/2} e^{-i\theta_\alpha}$, and assume small fluctuations in σ_α around the saddle-point value for

$$\overline{\rho} = \frac{\mu}{[\Gamma_1(\mu) + \Gamma_2(\mu)]}. \tag{52}$$

[Here, we assume $\Gamma_1(\mu) > \Gamma_2(\mu)$.] Equation (52) properly captures, through the dependence of Γ_α on μ, the non-mean-field dependence of the boson density on chemical potential. In particular, it yields $\overline{\rho} \sim \mu^{1/2}$ in $1+1$ dimensions, consistent with the fact that repulsively interacting bosons behave with an effective hard core at low density, and consequently have an equation of state similar to free fermions.

Expanding the action to quadratic order in σ_α and neglecting irrelevant terms involving derivatives of σ_α and their couplings to higher derivatives of θ_α, we obtain (neglecting constant

terms)

$$\mathcal{S} = \int d^d\mathbf{r}d\tau \Big\{ i(\sigma_1\partial_\tau\theta_1 + \sigma_2\partial_\tau\theta_2) + \frac{\overline{\rho}}{2m}(|\nabla\theta_1|^2 + |\nabla\theta_2|^2) + \frac{\Gamma_1}{2}\left(\sigma_1^2+\sigma_2^2\right) + \Gamma_2\sigma_1\sigma_2 \Big\}. \tag{53}$$

Next, we integrate out the σ_α fields, and express the resulting action in terms of new linear combinations

$$\theta = \theta_1 + \theta_2, \quad \tilde{\theta} = \theta_1 - \theta_2. \tag{54}$$

The result is

$$\mathcal{S} = \mathcal{S}_\theta + \mathcal{S}_{\tilde{\theta}}, \tag{55}$$

where

$$\mathcal{S}_\theta = \int d^d\mathbf{r}d\tau \left\{ \frac{\kappa_c}{2}(\partial_\tau\theta)^2 + \frac{\rho_c}{2}(\nabla\theta)^2 \right\}, \tag{56}$$

with

$$\kappa_c = \frac{1}{2[\Gamma_1(\mu)+\Gamma_2(\mu)]}, \quad \rho_c = \frac{\overline{\rho}}{2m}, \tag{57}$$

and

$$\mathcal{S}_{\tilde{\theta}} = \int d^d\mathbf{r}d\tau \left\{ \frac{\kappa}{2}(\partial_\tau\tilde{\theta})^2 + \frac{\rho}{2}(\nabla\tilde{\theta})^2 - \sum_n \lambda_n \cos[n(\tilde{\theta} - \mathbf{q}_n\cdot\mathbf{r})] \right\}, \tag{58}$$

with

$$\kappa = \frac{1}{2[\Gamma_1(\mu)-\Gamma_2(\mu)]}, \quad \rho = \frac{\overline{\rho}}{2m}, \quad \lambda_n = 2w_n\overline{\rho}^n. \tag{59}$$

Here, we have restored the term resulting from $\mathcal{S}'$ in Eq. (41). Note that the "charge" field θ describes the Goldstone mode of the broken (or quasibroken in 1D) U(1) symmetry, and thus remains exactly massless. It completely decouples from the $\tilde{\theta}$ field, and can be neglected in the analysis of the CIT.

We are now in a position to analyze the CIT using Eqs. (58) and (59) and the results of Appendix A. This is strongly dimension dependent, so we treat the cases of two dimensions and one dimension separately.

1. Two dimensions

In two dimensions, we begin by presuming that *one* of the cosines in Eq. (58) is almost nonoscillating, i.e., when one of the q_n is close to zero. Generically, this will happen for one specific minimal n, when

$$Q_{2D} = \frac{\pi m}{n} + \delta Q \tag{60}$$

for some specific m,n, with $|\delta Q| \ll 1$. The other rapidly oscillating cosines can be neglected, and we retain only the weakly oscillatory one. Then, in the x,y coordinates, the action takes the form given in Eq. (A1), with $\lambda_n = \lambda$ and $q = q_n = 2\delta Q$.

We can now directly apply the results of Appendix A 1. Using $\delta = \rho q = 2\rho\delta Q$, and Eq. (A6), we obtain that the commensurate state is stable for $|\delta Q| < \delta Q_c$, which defines the location δQ_c of the CIT as

$$\delta Q_c \sim \sqrt{\lambda_n/\rho} \sim \sqrt{m w_n}\,\overline{\rho}^{(n-1)/2} \sim \sqrt{m w_n}[\Upsilon(\mu)\mu]^{(n-1)/2}, \tag{61}$$

where we used Eq. (59) for $d = 2$, and, of course, we assume $\mu > 0$. Here,

$$\Upsilon(\mu) = \frac{1}{\Gamma_1(\mu)+\Gamma_2(\mu)} \sim \frac{2|\ln(m\mu)|}{m} \quad \text{for} \quad \mu \ll 1 \tag{62}$$

is a weak logarithmic function of μ.

For the commensurate state centered around $R = 0$ ($J' = J$), we have $n = 3$, and the phase boundary for the C-IC transition is linear in μ, up to logarithmic corrections. However, as n increases, the widths of the commensurate phases decrease.

2. One dimension

In the TST, to derive the 1D theory we must sum over discrete y. This restricts the λ_n terms in Eq. (58) to n which are multiples of 3, so that the y component of $\mathbf{q}_n$ ($=2nQ_y$) is a multiple of 2π.

Following the discussion for two dimensions, we again consider wave vectors

$$Q_{1D} = \frac{\pi m}{n} + \delta Q, \tag{63}$$

with appropriate m,n such that $|\delta Q| \ll 1$, and keep only the dominant cosine term of order n, which then matches the sine-Gordon form in Eq. (A1) with $q = 2\delta Q$. Then, we take over results from Appendix A 2.

According to that discussion, a commensurate phase is stabilized whenever the scaling dimension of the cosine term Δ_n is less than two. Using the result in Eq. (A12) and also Eq. (59), we obtain

$$\Delta_n = \frac{n^2}{\sqrt{2}\pi}\left(\frac{\mu}{m}\right)^{1/4}\sqrt{\frac{u_1-u_2}{u_1u_2}}, \tag{64}$$

so that $\Delta_n \ll 1$ for $\mu \ll 1$. This shows that $\Delta_n < 2$, and the commensurate phase is indeed realized. Note that if we approximate $\Delta_n = 0$, then this becomes the same classical estimate as in the previous section, except that $\Gamma_a(\mu)$ has a different dependence in one dimension. While this is in principle appropriate for very small μ, the $\frac{1}{4}$ exponent in Eq. (64) indicates that Δ_n can be substantial nonetheless, so we will proceed with the estimate taking $\Delta_n \neq 0$.

Using $\delta = 2\rho\delta Q$ and the estimate for the critical δ_c in Eq. (A16), and applying Eqs. (52) and (59), we find the location of the 1D CIT as

$$\delta Q_c \sim \left(w_n m^{\frac{n+1}{2}} n^{\Delta_n}\mu^{\frac{n-1}{2}}\right)^{\frac{1}{2-\Delta_n}}. \tag{65}$$

For $n = 3$ and assuming $\Delta_n \to 0$, this predicts $\delta Q_c \sim \mu^{1/2}$, which does not agree with $\mu \sim R$ scaling of the C-IC boundary in the upper left corner of the phase diagram in Fig. 3. However, the range of μ there is not particularly small, h changes from 4.5 to approximately 3 as R changes from 0 to 0.1. This observation calls for a more careful analysis of behavior predicted by Eqs. (64) and (65) for $\mu \sim O(1)$. We find that numerical coefficients in (64) make $\Delta_{n=3}$ to vary in the interval 0.5–1 for μ relevant to the C-IC boundary in Fig. 3, resulting in an almost linear dependence $\delta Q_c \sim \mu$ away from the strict

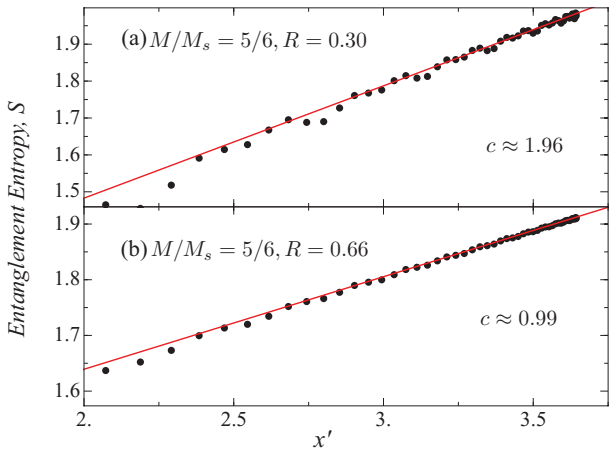

FIG. 11. (Color online) Entanglement entropy at (a) $M/M_s = \frac{5}{6}$, $R = 0.3$, the incommensurate coplanar phase, and (b) $M/M_s = \frac{5}{6}$, $R = 0.66$, the cone (or umbrella) phase. We take a system size of $N_x = 120$.

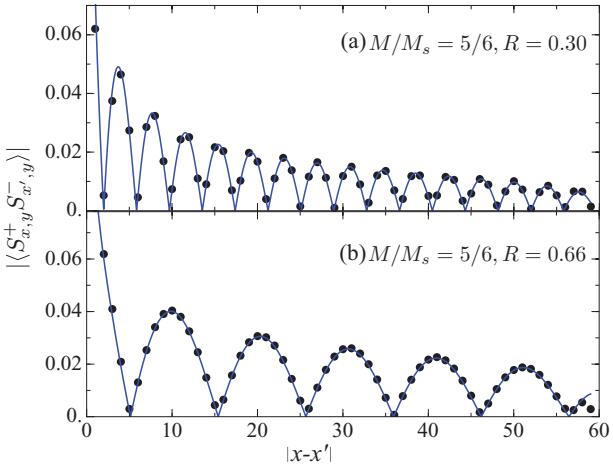

FIG. 12. (Color online) Transverse spin-spin correlation function for $M/M_s = \frac{5}{6}$, $N_x = 120$, and $x' = N_x/2$ at (a) $R = 0.30$ in the incommensurate coplanar state and (b) $R = 0.66$ in the cone state. Our DMRG data points are plotted in (black) circles, while the theoretical fit [Eq. (66)] is shown as a solid (blue) line.

$\mu \to 0$ limit and in qualitative agreement between our analysis here and the numerical data in Fig. 3.

F. DMRG results

In Sec. IV C, we show that the cone state corresponds to a single-Q condensate bosonic field, while the incommensurate planar state corresponds to double-Q condensate. This is verified by the central charge measurement, where we find $c = 2$ to describe the coplanar phase as shown in Fig. 11(a), as opposed to $c = 1$ for the cone in Fig. 11(b).

The transverse spin-spin correlation function for the cone state can be written as

$$\begin{aligned}\langle S^+_{\mathbf{r}} S^-_{\mathbf{r}'}\rangle &\sim \overline{\psi}^2 \cos[\mathbf{Q}\cdot(\mathbf{r}-\mathbf{r}')]\langle e^{i[\theta(\mathbf{r})-\theta(\mathbf{r}')]}\rangle \\ &\sim \overline{\psi}^2 \cos[\mathbf{Q}\cdot(\mathbf{r}-\mathbf{r}')]C_\eta(x,x') \qquad (66)\end{aligned}$$

with $C_\eta(x,x')$ given in Eq. (15). We fit the DMRG results to this formula in Fig. 12(b). The transverse correlation shows a clear sinusoidal pattern with incommensurate wave vector $\mathbf{Q} = (1.10\pi, 2\pi/3)$ and $\eta = 0.37$ at $M/M_s = \frac{5}{6}$, $R = 0.66$. Figure 12(b) shows an excellent fit which yields the exponent $\eta = 0.37$.

The whole procedure is repeated for the incommensurate planar state

$$\begin{aligned}\langle S^+_{\mathbf{r}} S^-_{\mathbf{r}'}\rangle &\sim 4\overline{\psi}^2 \langle \cos(\mathbf{Q}\cdot\mathbf{r} + \tilde{\theta}(x)) \cos(\mathbf{Q}\cdot\mathbf{r}' + \tilde{\theta}(x'))\rangle \\ &\quad \times \langle e^{i(\theta(x)-\theta(x'))}\rangle \\ &= \frac{\overline{\psi}^2}{2} \cos[\mathbf{Q}\cdot(\mathbf{r}-\mathbf{r}')]C_{\eta+\tilde{\eta}}(x,x'). \qquad (67)\end{aligned}$$

The exponent η and $\tilde{\eta}$ come from averaging the θ and $\tilde{\theta}$ fields, respectively. The fitting estimates $\mathbf{Q} = (1.26\pi, 2\pi/3)$ and $\eta + \tilde{\eta} = 0.54$ at $M/M_s = \frac{5}{6}$, $R = 0.3$, shown in Fig. 12(a).

Next, we consider the vector chirality (VC), which is defined as $V_{x,y} = \hat{z}\cdot\langle S_{x,y} \times S_{x+1,y}\rangle$ in Eq. (43). As discussed in Sec. IV C, since the cone state favors XY order, the VC should be a nonzero and constant value. Indeed, as shown in Fig. 13, the VC correlation function does not decay with distance in the cone state, i.e., $R = 0.66$ and 0.80, and the finite-size scaling [Fig. 13(b)] shows that the corresponding VC order parameter remains finite in the thermodynamic limit. Instead, for planar states, the spins are confined to one plane, so the VC correlation decays exponentially (see $R = 0.4$ data in Fig. 13).

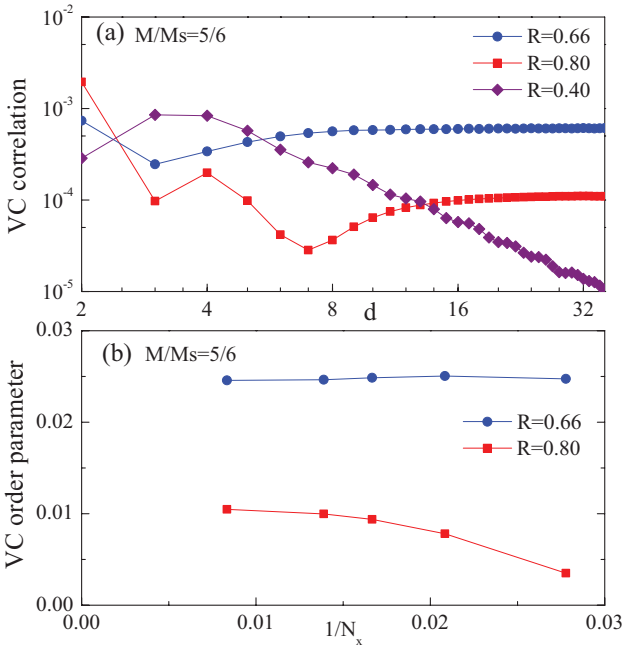

FIG. 13. (Color online) Spin vector chirality (VC) correlation function, as defined in Eq. (43), at $M/M_s = \frac{5}{6}$ with system size $N_x = 120$ and $x' = N_x/2$. In (a), we show $R = 0.4$ (purple diamond) where the system orders into an incommensurate coplanar phase. Furthermore, $R = 0.66, 0.80$, where the system is in the cone phase, is shown on the same plot. We can see that the VC approaches a constant in the cone phase while decaying in the coplanar phase. In (b), we show the finite-size scaling of the VC order parameter in the cone phase.

V. WEAKLY COUPLED CHAINS

A. Bosonization of a Heisenberg chain

In this section, we give a brief overview of applying Abelian bosonization to a single spin-$\frac{1}{2}$ Heisenberg chain in a magnetic field. The Hamiltonian of interest is as follows:

$$H_{ch} = J\sum_{x=1}^{L}\mathbf{S}(x)\cdot\mathbf{S}(x+1) - h\sum_{x=1}^{L}S^z(x), \tag{68}$$

where the magnetic field is chosen along the z direction, and the lattice spacing has been set to 1. Here, the magnetization $M \equiv \sum_x \frac{1}{L}S^z(x)$ is conserved and hence, the magnetic field h can be treated as a chemical potential to relate the properties at $h \neq 0$ to those at $h = 0$. For any magnetizations less than saturation, i.e., $M < M_{\rm sat} = \frac{1}{2}$, the low-energy theory can be described by a canonical set of a massless scalar field θ and its dual field ϕ:

$$H_0 = \int dx \frac{v}{2}[(\partial_x\phi)^2 + (\partial_x\theta)^2]. \tag{69}$$

These two fields satisfy the familiar commutation relations

$$[\theta(x),\phi(x')] = -i\Theta(x-x'), \tag{70}$$

where Θ is the Heaviside step function. The spin velocity v in Eq. (69) is a function of the magnetization M. When $M = 0$, $v/J = \pi/2$, and the SU(2) symmetry is restored. For the case when $M > 0$, v decreases continuously and is numerically determined by the Bethe-ansatz integral equations (see Fig. 9 of Ref. 31).

At a fixed magnetization, both the longitudinal (along the field direction) and transverse (perpendicular to the field axis) spin fluctuations have gapless excitations. The longitudinal modes occur at commensurate wave vector $k_x = 0$ and incommensurate ones $k_x = \pi \pm 2\delta$, where $\delta = \pi M$, while the transverse modes are at commensurate wave vector $k_x = \pi$ and incommensurate vectors $k_x = \pm 2\delta$. Then, one can expand the spin operator around these low-energy gapless modes, i.e.,

$$\begin{aligned} S^z(x) &= M + \mathcal{S}^z_0(x) + e^{i(\pi-2\delta)x}\mathcal{S}^z_{\pi-2\delta}(x) \\ &\quad + e^{-i(\pi-2\delta)x}\mathcal{S}^z_{\pi+2\delta}(x), \\ S^+(x) &= e^{-i2\delta x}\mathcal{S}^+_{-2\delta}(x) + e^{i2\delta x}\mathcal{S}^+_{2\delta}(x) + (-1)^x\mathcal{S}^+_{\pi}(x), \end{aligned} \tag{71}$$

where S^z_0, $\mathcal{S}^z_{\pi\pm2\delta}(x)$, $\mathcal{S}^+_{\pm2\delta}(x)$, and $\mathcal{S}_\pi$ are operators whose scaling dimensions depend on M. One can rewrite these operators in terms of the bosonic fields ϕ and θ:

$$\begin{aligned} &\mathcal{S}^z_0(x) = \beta^{-1}\partial_x\phi, \quad \mathcal{S}^z_{\pi-2\delta}(x) = -\frac{i}{2}A_1 e^{-2\pi i\phi/\beta}, \\ &\mathcal{S}^+_{\pm2\delta}(x) = \pm\frac{i}{2}A_2 e^{i\beta\theta}e^{\pm i2\pi\phi/\beta}, \quad \mathcal{S}^+_{\pi}(x) = A_3 e^{i\beta\theta}. \end{aligned} \tag{72}$$

Here, the parameter $\beta \equiv 2\pi\mathcal{R}$ is related to the compactification radius $\mathcal{R}$ and can be calculated by solving the integral equations, which can be found in Refs. 32–34. The compactification radius takes on a simple form $2\pi\mathcal{R}^2 = 1$ at zero magnetization, and approaches $2\pi\mathcal{R}^2 = 1/2$ as $M \to M_{\rm sat} = 1/2$. The constants A_1, A_2, and A_3 are determined numerically.[18] Furthermore, at $M = 0$, the scaling dimension of S^z_0 and $\mathcal{S}^+_{\pm2\delta}(x)$ is 1, and these operators can be written in its SU(2)-symmetric form $\mathbf{M} = \mathbf{J}_R + \mathbf{J}_L$. The scaling dimension of $\mathcal{S}^z_{\pi\pm2\delta}(x)$ and $\mathcal{S}_\pi$, however, is $\frac{1}{2}$ at zero magnetization and is related to the staggered Néel order $\mathbf{N}$ and dimerization ϵ. Further details for the $M = 0$ case are provided in Appendix C 1.

Now, in order to compare our DMRG results to this analysis, we must enforce open boundary conditions (BC) along the chain direction to mimic DMRG's BC. This can be achieved by introducing two additional "phantom sites" at $x = 0$ and $x = L+1$.[35] At these positions, we enforce boundary conditions on the bosonic field ϕ, where $\phi(x=0) = 0$ and $\phi(x = L+1) = 0$. The sum in Eq. (68) now runs from site index 0 to L, and we effectively obtain a periodicity of $L+1$ using these phantom sites. We can now substitute Eq. (72) into Eq. (71), and enforce the open boundary conditions. The spin operators can now be written as (for brevity, we suppress chain index y)

$$\begin{aligned} S^z(x) &= \tilde{M} + \frac{1}{\beta}\frac{d\phi}{dx} - A_1\sin\left(\frac{2\pi}{\beta}\phi(x) - (\pi - 2\tilde{\delta})x\right), \\ S^+(x) &= e^{i\beta\theta(x)}\left[A_3(-1)^x + A_2\sin\left(\frac{2\pi}{\beta}\phi(x) + 2\tilde{\delta}x\right)\right], \end{aligned} \tag{73}$$

where $\tilde{M} = ML/(L+1)$ and $\tilde{\delta} = \pi\tilde{M}$. The bosonic field ϕ can also be expanded in terms of its lattice modes as

$$\phi(x) = \sum_{n=1}^{\infty}\frac{\sin(q_n x)}{\sqrt{\pi n}}(a_n + a_n^+), \tag{74}$$

where $q_n = \pi n/(L+1)$. Here, a_n and a_n^+ are the annihilation and creation operators and satisfy the commutation relation $[a_n, a_{n'}^+] = \delta_{n,n'}$.

B. Triangular spin tube

We now extend our previous discussion to study the behavior of the TST, described by Eq. (1), in the limit of weak coupling $J' \ll J$. Using the low-energy expansions of the spin operators in Eq. (71), we can express the low-energy Hamiltonian as $H = H_0 + H_1$, where H_0 is described by a sum over the free bosonic modes in Eq. (69) on each chain. Here, H_1 describes interchain interactions and is as follows:

$$\begin{aligned} H_1 = J'\sum_{y=1}^{3}\int_{x=0}^{L}dx\Bigg\{&2\tilde{M}^2 + 2\mathcal{S}^z_{y;0}\mathcal{S}^z_{y+1;0} \\ &+ \sum_{\sigma=\pm}(1 - e^{2i\sigma\tilde{\delta}})\mathcal{S}^z_{y;\pi+2\sigma\tilde{\delta}}\mathcal{S}^z_{y+1;\pi-2\sigma\tilde{\delta}} \\ &+ \frac{1}{2}[\mathcal{S}^+_{y;\pi}\partial_x\mathcal{S}^-_{y+1;\pi} + \text{H.c.}] \\ &+ \sum_{\sigma=\pm}\left[\left(\frac{1+e^{2i\sigma\tilde{\delta}}}{2}\right)\mathcal{S}^+_{y;2\sigma\tilde{\delta}}\mathcal{S}^-_{y+1;2\sigma\tilde{\delta}} + \text{H.c.}\right]\Bigg\}, \end{aligned} \tag{75}$$

where again $\tilde{M} = ML/(L+1)$.

The first term $2\tilde{M}^2$ with scaling dimension 0 is the most relevant, but is trivially a constant. The second term is marginal with scaling dimension 2, and renormalizes the Luttinger parameters and the velocities of the bosonic fields ϕ, θ in Eq. (69). The third term is relevant at $\tilde{M} = 0$ with scaling dimension 1, and becomes marginal as magnetization increases, approaching a scaling dimension 2 as $\tilde{M} \to M_{\rm sat}$. This term is responsible for the SDW phase that arises when

relevant. The fourth term, which involves a derivative, is marginal at $\tilde{M} = 0$ with scaling dimension 2 and becomes increasingly relevant with increasing magnetization, saturating to a scaling dimension of $\frac{3}{2}$ as $\tilde{M} \to M_{\rm sat}$. This is a "twist" term that favors the cone or XY phase that orders perpendicular to the magnetic field. The last term is always irrelevant, with scaling dimension $\geqslant 2$ and can be neglected in the analysis of this theory.

Apart from the trivial constant term, the SDW and the "twist" terms are the most relevant ones and have competing scaling dimensions as magnetization varies from 0 to saturation. With the exception of some subtleties that arise from the TST boundaries (we discuss this in later sections), standard scaling arguments can be made about these two operators. For small M, the SDW term dominates, and the system orders into a collinear SDW in which the ordering momentum $\pi - 2\tilde{\delta}$ scales linearly with magnetization. The twist interaction dominates over the SDW at a larger magnetization, and the system orders into a conelike state. Since there is no spontaneous breaking of continuous symmetry in one dimension, the SDW and cone order are not really ordered states, but are Luttlnger liquids with one gapless mode. This competition between cone and SDW phase was discussed for 2D triangular lattice in Ref. 11, where critical magnetization $M_{\rm crit}$ at which the quantum phase transition from the SDW to the cone phase takes place was evaluated. The TST has the same critical $M_{\rm crit} = 0.64 M_{\rm sat}$ as the 2D case, except that the cone state obtained in this quasi-1D regime is smoothly connected to the cone phase obtained in the high-field region in Sec. IV.

Equation (75) is not complete as it does not account for several less-obvious relevant terms which are allowed by the lattice symmetry of the problem. This will be considered in more detail later. Within the SDW phase, it is possible to lock the SDW momentum to a commensurate value by accounting for high-order umklapp processes. The first of these leads to a commensurate SDW, which is in fact identical to the $\frac{1}{3}$ plateau with the "up-up-down" structure. This is discussed extensively later in Sec. VI.

Other more relevant intrachain interaction terms may appear due to fluctuations that are not accounted for in the naive bosonization in Eq. (73). We will discuss these effects in Appendix C 2.

C. SDW

In the region of low to intermediate magnetization and small J', we can neglect all terms in H_1 except the marginal one and the SDW interaction. Using bosonization [Eq. (73)], the Hamiltonian can be rewritten as follows:

$$H_{\rm SDW} = \sum_{y=1}^{3} \int dx \frac{v}{2}[(\partial_x \phi_y)^2 + (\partial_x \theta_y)^2] + \frac{2J'}{\beta^2}\partial_x\phi_y \partial_x \phi_{y+1} + \gamma_{\rm SDW} \cos\left[\frac{2\pi}{\beta}(\phi_y - \phi_{y+1}) - \frac{\pi - 2\tilde{\delta}}{2}\right], \quad (76)$$

where the bare SDW coupling is given by $\gamma_{\rm SDW} = J' A_1^2 \sin(\tilde{\delta}) > 0$.

1. Scaling considerations

Renormalization group arguments give considerable insight into the physics of Eq. (76). All but the last term in $H_{\rm SDW}$ are scale invariant, and can be considered a fixed-point Hamiltonian. The remaining SDW term, proportional to $\gamma_{\rm SDW}$, is not, and renormalizes under the scale transformation $x \to bx$, according to the usual linearized relation

$$\gamma_{\rm SDW}(b) = b^{2-\Delta_{\rm SDW}} \gamma_{\rm SDW}, \quad (77)$$

where $b > 1$ is an arbitrary scale factor. As discussed in the previous section, $\Delta_{\rm SDW} < 2$, so that the SDW interact is *relevant*, and grows in strength under rescaling. Equation (77) is valid for small dimensionless $\gamma_{\rm SDW}(b)$, and therefore the weak-coupling regime is limited by the condition $\gamma_{\rm SDW}(b) < v$. This defines an "SDW correlation length" $\xi_{\rm SDW}$ such that $\gamma_{\rm SDW}(b) = v$:

$$\xi_{\rm SDW} \sim (v/\gamma_{\rm SDW})^{1/(2-\Delta_{\rm SDW})}. \quad (78)$$

In the weakly coupled chain regime, $\gamma_{\rm SDW}$ is small and so $\xi_{\rm SDW}$ is large. On scales large compared to this correlation length, we expect that the bosonic modes appearing inside the SDW term become "pinned" to values which minimize this interaction. This pinning corresponds to the creation of well-established SDW order.

Due to the divergence of $\xi_{\rm SDW}$, however, the establishment of SDW order can be prevented by finite-size effects, even for reasonably large systems accessible by DMRG. For a finite system of length L, we must compare the SDW correlation length to L, and it is expected that physical quantities will be functions of the dimensionless ratio $\Xi_{\rm SDW} \equiv \xi_{\rm SDW}/L$. For $\Xi_{\rm SDW} \ll 1$, SDW-like behavior is expected, but when $\Xi_{\rm SDW} \gtrsim 1$, there may be a nontrivial crossover. This occurs particularly in the case of the TST, for which an analysis, detailed below, shows that the crossover is *discontinuous*.

2. $L = \infty$

For an infinitely *long* system $\Xi = 0$, we can understand the nature of the SDW state by simply minimizing the $\gamma_{\rm SDW}$ term in Eq. (76). When the *width* is also infinite, i.e., in two dimensions, one can simultaneously minimize each cosine term (for each y) independently. This occurs by taking

$$\frac{2\pi}{\beta}\phi_y\Big|_{d=2} = \varphi + \frac{\pi - 2\tilde{\delta}}{2} y, \quad (79)$$

where φ is an arbitrary constant (x and y independent) phase. Allowing for small gradients of φ, which might be present due to fluctuations or perturbations and by substituting Eq. (79) into Eq. (73), we see that the spin operator can then be represented as

$$S_y^z(x)\big|_{d=2} \sim \tilde{M} + \frac{\partial_x \varphi}{2\pi} - A_2 \sin\left[\varphi(x) - \frac{\pi - 2\tilde{\delta}}{2}(2x - y)\right], \quad (80)$$

which indeed is the classic form for a spin density wave with wave vector $\frac{\pi - 2\tilde{\delta}}{2}(-2, 1)$. This corresponds to an ideal two-dimensional SDW state, and φ gives the "sliding" or "phason"[36] mode of the SDW. For generic irrational $\tilde{\delta}/\pi$, φ remains a gapless pseudo-Goldstone mode associated with translational symmetry breaking. In two dimensions, the

zero-point fluctuations of this mode do not, however, destroy long-range SDW order.

Now, consider the case of the TST ladder, where $y = 1,2,3$ and periodic boundary conditions are applied. In this case, it is generically impossible to simultaneously minimize each cosine term separately. Instead, the minimum occurs when

$$\frac{2\pi}{\beta}\phi_y\Big|_{L=\infty,\mathrm{TST}} = \varphi + \frac{2\pi}{3}y, \tag{81}$$

where again φ is an arbitrary constant, reflecting the invariance of Eq. (76) under uniform translations of all the ϕ_y. Again, one can express the spin operator here using this form

$$S^z_y(x)\big|_{L=\infty,\mathrm{TST}} \sim \tilde{M} + \frac{\partial_x\varphi}{2\pi} - A_2\sin\left[\varphi(x) - (\pi - 2\tilde{\delta})x + \frac{2\pi}{3}y\right]. \tag{82}$$

In contrast with Eq. (79), the minimum configuration in the TST, Eq. (81) is *independent* of $\tilde{\delta}$, manifesting in Eq. (82) as a difference dependence on y from Eq. (80). The difference is due to the frustration of the intrinsic 2D SDW order by periodic boundary conditions, which tend to lock the SDW order to a commensurate form in the y direction. Interestingly, the two results coincide when $\tilde{\delta} = \pi/6$, which corresponds to the case $M = M_{\mathrm{sat}}/3$. At this point, the periodicity of the TST and the SDW order are compatible.

As in the 2D case, at the level of Eq. (76) applied to the TST, the uniform translation mode φ remains gapless. Unlike the 2D case, however, in one dimension, the zero-point fluctuations of this mode are sufficient to disrupt long-range SDW order, which instead manifests as power-law correlations. Nevertheless, the short-distance physics is still that of an SDW, and moreover the 1D fluctuations are easily accounted for theoretically. This is accomplished simply by treating φ as a free massless boson, as we discuss below in Sec. V C3.

3. *Finite length $L < \infty$*

As we have discussed in Sec. V A, for a finite-length chain, we must impose the boundary conditions $\phi_y(x = 0) = \phi_y(x = L) = 0$. These conditions are *incompatible* with the values, in Eq. (81), which minimize the SDW term in the infinitely long case. This means that end effects strongly affect, and tend to suppress, SDW ordering. What do we expect? For short systems, where $\Xi \gg 1$, the end effects will dominate, and the effects of the SDW interaction become negligible. In other words, all components ϕ_y will be largely not affected by the SDW term, and the system should behave similarly to three decoupled chains of finite length. For long systems $\Xi \ll 1$, the SDW pinning should be effective far from the boundaries, and only the pseudo-Goldstone mode $\tilde{\Phi}_0$ will behave like a massless field (pinned at the boundaries).

Let us now address the crossover. It is convenient to first make a change of basis[34] from the ϕ_1,ϕ_2,ϕ_3 to new fields Φ_0,Φ_1,Φ_2:

$$\begin{pmatrix}\phi_1\\ \phi_2\\ \phi_3\end{pmatrix} = \begin{pmatrix}1/\sqrt{3} & 1/\sqrt{2} & 1/\sqrt{6}\\ 1/\sqrt{3} & 0 & -2/\sqrt{6}\\ 1/\sqrt{3} & -1/\sqrt{2} & 1/\sqrt{6}\end{pmatrix}\begin{pmatrix}\Phi_0\\ \Phi_1\\ \Phi_2\end{pmatrix}. \tag{83}$$

The dual fields θ_y transform similarly. Note that the center-of-mass field is just proportional to the SDW phase introduced earlier: $\Phi_0 = \frac{\sqrt{3}\beta}{(2\pi)}\varphi$. The boundary conditions $\phi_y = 0$ at the ends translate to $\Phi_i = 0$ at the ends. The SDW Hamiltonian now reads as $H_{\mathrm{SDW}} = H^{(0)}_{\mathrm{SDW}} + H^{(1)}_{\mathrm{SDW}}$, where the harmonic part

$$H^{(0)}_{\mathrm{SDW}} = \sum_{n=1}^{3}\int dx\left[\frac{\tilde{v}_n}{2\kappa_n}(\partial_x\Phi_n)^2 + \frac{\tilde{v}_n\kappa_n}{2}(\partial_x\Theta_n)^2\right] \tag{84}$$

is expressed in terms of renormalized stiffnesses $\kappa_0^{-2} = 1 + 4J'/(\beta^2 v)$ and $\kappa_{1,2}^{-2} = 1 - 2J'/(\beta^2 v)$ and velocities $\tilde{v}_n = v/\kappa_n$. Its interacting part [the analog of the second line in Eq. (76) written in the new basis] reads as

$$H^{(1)}_{\mathrm{SDW}} = \gamma_{\mathrm{SDW}}\int dx\, 2\cos\left[\frac{2\pi}{\sqrt{2}\beta}\Phi_1 - \frac{\pi - 2\tilde{\delta}}{2}\right] \times\cos\left[\frac{2\pi}{\beta}\sqrt{\frac{3}{2}}\Phi_2\right] + \cos\left[\frac{2\pi}{\beta}\sqrt{2}\Phi_1 + \frac{\pi - 2\tilde{\delta}}{2}\right]. \tag{85}$$

Note that the center-of-mass mode $\Phi_0 \propto \varphi$ does not enter in Eq. (85). Thus, it behaves as a free massless boson, independent of the strength of the SDW coupling. The distinction between δ and $\tilde{\delta}$ in the SDW Hamiltonian is not important when analyzing the crossover, and will be dropped in this section from now on.

To analyze the crossover, we first carry out the renormalization group procedure by integrating out fluctuations of the fields due to modes with wavelength less than the system size L. In doing so, we replace γ_{SDW} by its renormalized value at this scale,

$$\gamma_{\mathrm{SDW}} \to \gamma_{\mathrm{SDW}}(L) = L^{-\Delta_{\mathrm{SDW}}}\gamma_{\mathrm{SDW}}. \tag{86}$$

Note that we have done the coarse-graining step of the RG of integrating out modes, but we have not rescaled any fields or coordinates, so as to keep the original units unchanged for clarity. Under this coarse-graining transformation, the quadratic terms in the Hamiltonian remain unmodified.

In this renormalized Hamiltonian, it is appropriate to carry out a classical saddle-point approximation for Φ_1 and Φ_2, which are the fields pinned by the SDW coupling. The SDW potential in Eq. (85) is minimized by $\Phi_2 = 0$, which is compatible with the boundary condition, and so, we can impose this condition. Then, only Φ_1 enters the saddle-point condition in a nontrivial way. For simplicity, we specialize to the case $\delta = \pi/6$, or $M = M_{\mathrm{sat}}/3$. Then, we may define $\Psi = \frac{2\pi}{\sqrt{2}\beta}\Phi_1 + \frac{2\pi}{3}$, for which the saddle-point Hamiltonian, neglecting the decoupled Φ_0 term, becomes

$$H_{\mathrm{class}} = \int_0^L dx\,\{K(\partial_x\Psi)^2 - \gamma_{\mathrm{SDW}}(L)(\cos[2\Psi] + 2\cos[\Psi])\}, \tag{87}$$

with $K = \beta^2\tilde{v}_1/4\pi^2\kappa_1$.

The γ_{SDW} term is clearly minimized by $\Psi = 0$, while the open boundaries require $\Psi(0) = \Psi(L) = 2\pi/3$, causing the strong suppression of SDW order by the ends. There can be a nontrivial configuration $\Psi(x)$ which minimizes the functional

$H_{\rm class}$. To bring out the crossover physics, we transform to dimensionless coordinates, letting

$$x = \sqrt{K/\gamma_{\rm SDW}(L)}z, \tag{88}$$

which gives

$$H_{\rm class} = \epsilon_0 \int_0^{\tilde{L}} dz\,\{(\partial_z\Psi)^2 - (\cos[2\Psi] + 2\cos[\Psi])\}, \tag{89}$$

with

$$\epsilon_0 = \sqrt{K\gamma_{\rm SDW}(L)}, \tag{90}$$

$$\tilde{L} = (L/\xi)^{1-\Delta_{\rm SDW}/2} = \Xi_{\rm SDW}^{\Delta_{\rm SDW}/2-1}, \tag{91}$$

$$\xi_{\rm SDW} = (K/\gamma_{\rm SDW})^{1/(2-\Delta_{\rm SDW})}. \tag{92}$$

Note that Eq. (92) agrees, at the level of scaling, with Eq. (78) obtained earlier from general arguments. For the purpose of minimization, the overall prefactor ϵ_0 is irrelevant, so it is clear already from Eq. (89) that the properties are a function of the scaling variable $\Xi_{\rm SDW}$ only, as expected.

We are now prepared for the saddle-point approximation, which consists in minimizing Eq. (89). Starting from the Euler-Lagrange equation, which has the usual "energy" integral of motion, one obtains

$$\left(\frac{d\Psi}{dz}\right)^2 = C - (2\cos[\Psi] + \cos[2\Psi]), \tag{93}$$

where the integration constant ("energy") C is fixed by the condition $d\Psi(z=\tilde{L}/2)/dz = 0$ as $C = (2\cos[\Psi_{1/2}] + \cos[2\Psi_{1/2}])$, where we denote $\Psi_{1/2} \equiv \Psi(z=\tilde{L}/2)$. As a result, the mid-ladder value of Ψ is implicitly given by the following integral:

$$\int_{\Psi_{1/2}}^{2\pi/3} \frac{d\varphi}{\sqrt{2\cos[\Psi_{1/2}] + \cos[2\Psi_{1/2}] - 2\cos[\varphi] - \cos[2\varphi]}} = \frac{\tilde{L}}{2}. \tag{94}$$

The full crossover (in this saddle point-approximation) is obtained from Eq. (94). First, we observe that in the limit $\Psi_{1/2} \to 0$, the above integral diverges logarithmically, implying that, indeed, $\Psi(\tilde{L}/2) = 0$ in the infinite-size limit. The short system size limit is less obvious. For small $\tilde{L}$, we must choose $\Psi_{1/2}$ to minimize the integral. However, if we make the obvious choice to let $\Psi_{1/2} = 2\pi/3 - \epsilon$, with $\epsilon \to 0^+$, one finds that the integral in fact does not vanish, but approaches the *constant* value $\pi/\sqrt{6}$. In fact, the integral as a function of $\Psi_{1/2}$ has a nonmonotonic dependence, and the minimum value of the integral is $\approx 1.1436 < \pi/\sqrt{6} = 1.2826$, which is achieved for $\Psi_{1/2} \approx 1.3178 < 2\pi/3 = 2.0944$. Regardless, the lower bound on the integral implies that there is a minimum dimensionless length $\tilde{L}_{\rm min} \geqslant 2.28$, such that for $\tilde{L} < \tilde{L}_{\rm min}$, the minimum action solution is simply $\Psi_{1/2} = 2\pi/3$, i.e., $\Psi(z) = 1/2$ for *all* z. For such short systems, the boundary conditions *completely* disrupt the SDW order, and the system behaves as though it were just decoupled chains. The transition from $\tilde{L} < \tilde{L}_{\rm min}$ to $\tilde{L} > \tilde{L}_{\rm min}$ is evidently discontinuous since $\Psi_{1/2}$ must jump from a value $\Psi_{1/2} \leqslant 1.3178$ at $\tilde{L} = \tilde{L}_{\rm min} + \epsilon$ to $\Psi_{1/2} = 2\pi/3$ for shorter systems. To precisely determine the value of $\tilde{L}_{\rm min}$ requires a comparison of the action of the nontrivial and trivial solutions to see where they cross.

What are the consequences of this transition? In numerics, the transition can be probed by varying L *or* varying J'/J at fixed L. In either case, on crossing the transition, one expects a sharp change from SDW-like behavior for $\tilde{L} > \tilde{L}_{\rm min}$ to decoupled chainlike behavior for $\tilde{L} < \tilde{L}_{\rm min}$. In the SDW-like regime, the two modes Φ_1, Φ_2 may be considered to have developed a gap, and consequently, the entanglement entropy of a bipartite cut of the sample is reduced compared to the decoupled chainlike regime. Specifically, in the SDW-like regime, a logarithmic growth with L is expected and consistent with central charge $c = 1$, while in the decoupled chain regime, the behavior should be closer to $c = 3$. *At* the transition, a sharp *drop* with increasing L of the entanglement entropy is expected. More detailed predictions can be made for the spin density profile $\langle S_y^z(x)\rangle$. We make such a comparison in the following section.

D. DMRG results for SDW

A number of measurements in the DMRG give evidence of the SDW state. As discussed in the previous section, the SDW regime of long TSTs can be described by pinning the fields $\Phi_1 = \Phi_2 = 0$, and allowing for gapless fluctuations of the free massless boson field Φ_0. In the semiclassical approximation discussed in Sec. V C3, one can do somewhat better by using the Φ_0 fluctuations *and* replacing $\Phi_2 \to 0$ and $\Phi_1(x) \to \frac{\sqrt{2}\beta}{2\pi}[\Psi(x) - \frac{2\pi}{3}]$, with $\Psi(x)$ given by the solution of Eq. (93). In this way, one obtains from Eq. (73)

$$\langle S_y^z(x)\rangle = \tilde{M} + \frac{2-y}{2\pi}\partial_x\Psi(x) - \frac{A_1}{X^{\eta_{\rm SDW}}} \times \sin\left[(2-y)\left(\Psi(x) - \frac{2\pi}{3}\right) - (\pi - 2\tilde{\delta})x\right]. \tag{95}$$

Here, the quantity

$$X = \left[\frac{2(L+1)}{\pi}\sin\left(\frac{\pi|x|}{L+1}\right)\right] \tag{96}$$

arises from the quantum average over the free boson field Φ_0, which is evaluated along the lines of Ref. 18, with the result that the exponent

$$\eta_{\rm SDW} = \frac{\pi\kappa_0}{3\beta^2} = \frac{\kappa_0}{6}\frac{1}{2\pi\mathcal{R}^2}. \tag{97}$$

For $M = M_{\rm sat}/3$ and small J', we estimate $\kappa_0 \approx 1$ and $2\pi\mathcal{R}^2 \approx 1 - 1/\{2\ln[6\sqrt{8/(\pi e)}]\} = 0.72$ (see Appendix A of Ref. 11), which leads to $\eta_{\rm SDW} \approx 0.23$, so the spin density profile decays quite slowly with distance from the boundary in the SDW regime. Note that the $y = 2$ chain does not depend on Ψ, so one can directly compare the numerically obtained magnetization profile for the "nonfrustrated" chain with Eq. (95) (see Fig. 14).

One may wonder about the selection of the $y = 2$ chain. For the geometry of our simulations, the model has full translational symmetry $y \to y + 1$ in the y direction. This symmetry is broken by our *combined* choice of saddle point $\Psi = \Phi_0 = 0$ in the bulk *and* the boundary condition

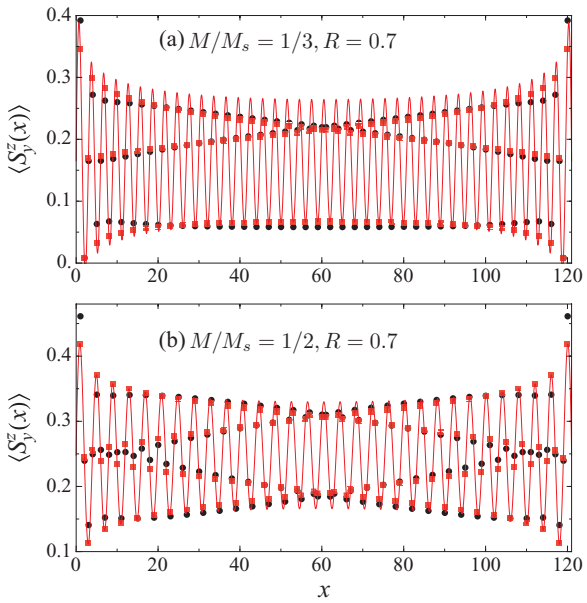

FIG. 14. (Color online) S_z profile for $R = 0.7$ at (a) $M/M_s = \frac{1}{3}$ plateau and (b) $M/M_s = \frac{1}{2}$ in the SDW state for the nonfrustrated chain (see text). We show the DMRG results by (black) circles and the theoretical prediction [Eq. (95)] by (red) solid line/square. The theoretical line captures all the DMRG data points, which appear to form three different curves. The (red) squares show the $S^z(x)$ values at discrete lattice site positions x, as obtained from Eq. (95).

$\Phi_0 = 0$ at the edges. Examination of the interaction term in Eq. (85) shows that there are apparently two other minimum solutions, $\Psi = \pi$ and $\Phi_2 = \pm\beta/\sqrt{6}$. In the infinite system, these are *equivalent* to the one we have chosen, insofar as they give identical results for all operators if we make a suitable translation of Φ_0. However, the choice of boundary condition for Φ_0 prevents this translation and results in a broken-symmetry state. By a different choice of the otherwise equivalent saddle points, we can obtain formulas analogous to Eq. (95) but with the $y = 1$ or 3 chains independent of Ψ. In principle, for a finite system, even the discrete translational symmetry should be unbroken, but the restoration of this symmetry is probably only at extremely low energies at which tunneling occurs between these minima, and indeed we find the symmetry to be spontaneously broken in our DMRG simulations.

In the decoupled regime $\tilde{L} < \tilde{L}_{\min}$, it is more appropriate to just calculate the spin expectation value using the free theory [Eq. (84)] for all three fields Φ_0, Φ_1, Φ_2. Then, we obtain, instead of Eq. (95), the result that

$$\langle S_y^z(x)\rangle = \tilde{M} + \frac{A_1}{X^{\eta_{\rm dc}}} \sin[(\pi - 2\tilde{\delta})x], \tag{98}$$

where the "decoupled chains" exponent is

$$\eta_{\rm dc} = \frac{\pi(\kappa_0 + \kappa_1 + \kappa_2)}{3\beta^2}. \tag{99}$$

In the same small-J' approximation, this gives $\eta_{\rm dc} \approx 3\eta_{\rm SDW}$, so that $\eta_{\rm dc} \approx 0.610$. Note that there is a much more rapid decay of the spin density profile from the boundary in this regime.

We compare the spin density profile in Eq. (95) with our DMRG data and find reasonable agreement. Figure 14 shows a comparison of numerical data with magnetization profile of the nonfrustrated chain, i.e., the $y = 2$ result of Eq. (95), while Fig. 15 shows that of frustrated chains $y = 1,3$.

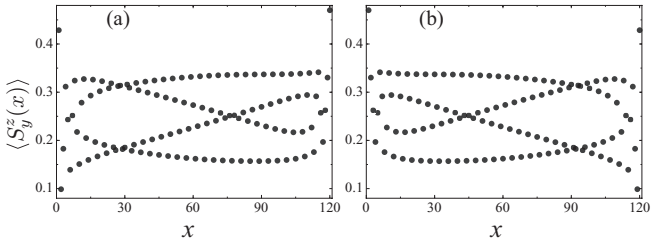

FIG. 15. S^z profile of DMRG result for SDW state at $M/M_s = \frac{1}{2}$, $R = 0.7$ for frustrated chains, (a) $y = 1$ and (b) $y = 3$. We can see from these plots that the translational symmetry is spontaneously broken, and that the SDW is strongly affected by boundaries. The DMRG data are seen to obey the symmetry $\langle S_1^z(x)\rangle = \langle S_3^z(L + 1 - x)\rangle$, which follows from Eq. (95).

We can also measure in DMRG the central charge via entanglement entropy, which yields $c = 1$ for the SDW phase as opposed to $c = 3$ for decoupled chains. This is shown in Fig. 16, where the plots show that at magnetizations $M/M_s = \frac{1}{6}, \frac{1}{2}$ for $R = 0.5$, the central charges obtained from numerics are $c = 0.9, 0.95$, respectively. These values are very close to the predicted $c = 1$, which gives evidence for the SDW.

Another measurement we can perform is the transverse spin-spin correlation function, which should decay exponentially to support the SDW state. We observe exactly this behavior from our simulations, as shown in Fig. 17. Finally, power-law behavior is expected for the "octupolar" correlation function[7]

$$\left\langle \left[\Pi_{y=1}^3 S_y^+(x)\right]\left[\Pi_{y=1}^3 S_y^-(x')\right]\right\rangle \sim C_{\eta_3}(x,x'). \tag{100}$$

The operator $\Pi_{y=1}^3 S_y^+(x)$ may be thought of as inserting a soliton, an extra period, into the SDW. This correlation

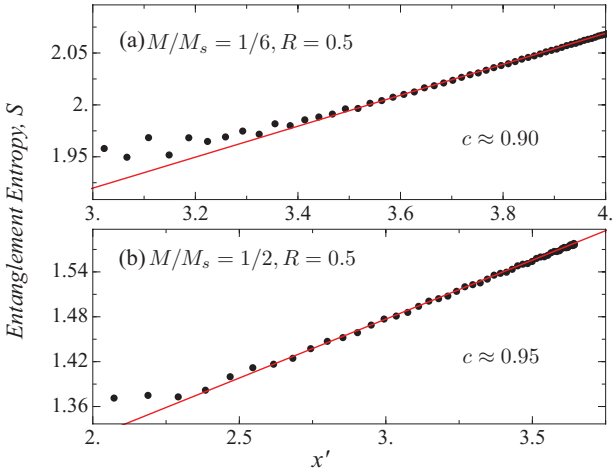

FIG. 16. (Color online) Entanglement entropy for SDW phase for $R = 0.5$ at (a) $M/M_s = \frac{1}{6}$ below the $\frac{1}{3}$ plateau and (b) $M/M_s = \frac{1}{2}$ above the $\frac{1}{3}$ plateau. Due to large finite-size effects of this measurement, we chose to run our simulations on a larger system size $N_x = 180$ in (a), to compare to a smaller size $N_x = 120$ in (b).

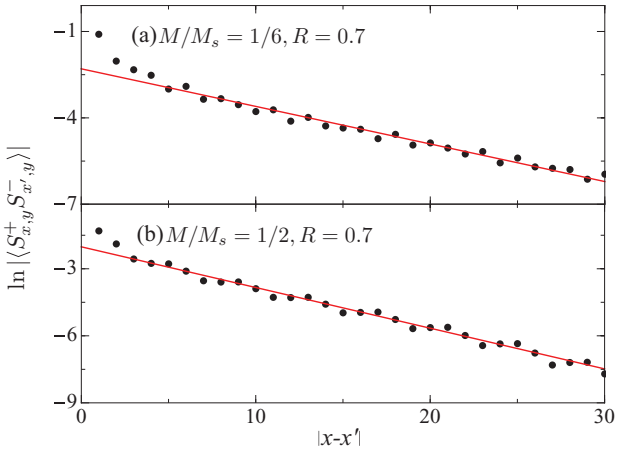

FIG. 17. (Color online) The transverse spin-spin correlation function on a log-linear scale for $R = 0.7$ and at magnetizations (a) $M/M_s = \frac{1}{6}$ and (b) $M/M_s = \frac{1}{2}$, both in the SDW state for system size $N_x = 120$ and $x' = N_x/2$. Data points are shown as (black) circles, while the (red) line is a fit to a pure exponential function.

function decays in the thermodynamic limit with the power-law exponent

$$\eta_3 = \frac{3\beta^2}{2\pi\kappa_0} = \frac{1}{2\eta_{\mathrm{SDW}}}. \tag{101}$$

We indeed observe such power-law behavior in the DMRG, as shown in Fig. 18. Fitting these data (for $M/M_s = \frac{1}{2}$, $R = 0.7$) gives $\eta_3 = 3.1 \pm 0.2$, while the S^z profile in Fig. 14 for the same parameters is fit to $\eta_{\mathrm{SDW}} = 0.2 \pm 0.1$, yielding the product $\eta_3\eta_{\mathrm{SDW}} = 0.62 \pm 0.31$. The uncertainties for each exponent are crudely estimated by tracing out the boundary values when the fitting starts to mismatch the DMRG result. The slow decay of the S^z profile and strong boundary effects as seen in Fig. 14 induce significant uncertainties in the estimate

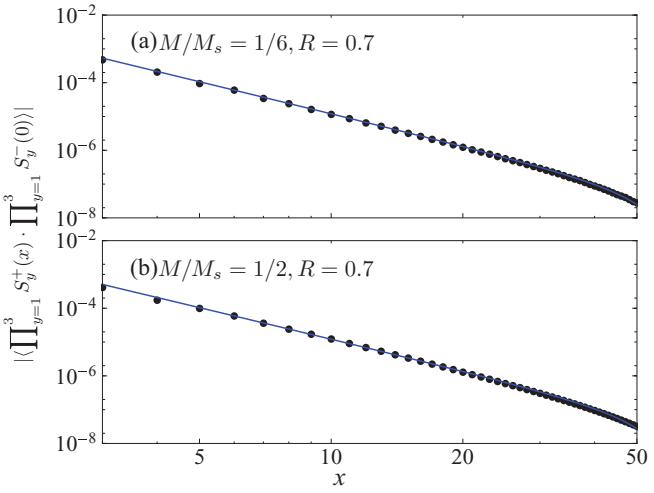

FIG. 18. (Color online) The "octupolar" correlation function $\langle[\Pi_{y=1}^3 S_y^+(x)][\Pi_{y=1}^3 S_y^-(x')]\rangle$ with $x' = N_x/2$, shown on a log-log scale. We show for $R = 0.7$ at magnetizations (a) $M/M_s = \frac{1}{6}$ and (b) $M/M_s = \frac{1}{2}$ in the SDW state. Our DMRG data points are plotted in (black) circles, while the theoretical fit to Eq. (100) is shown as (blue) line.

for η_{SDW}, so we consider the degree of agreement to the expected value $\eta_3\eta_{\mathrm{SDW}} = \frac{1}{2}$ satisfactory.

VI. $M = M_{\mathrm{sat}}/3$ PLATEAU

Magnetization plateaux are observed frequently in models of frustrated magnetism and in a number of experiments on such materials. Theoretically, we define a magnetization plateau as a ground state of a spin system in a magnetic field h, such that for a range of fields $h_1 < h < h_2$, the magnetization (along the field) $M(h) = M_{\mathrm{p}}$ is constant. This implies that the magnetization is a good quantum number, and, since by assumption the only term in the Hamiltonian coupling to the applied field is hM, that the ground-state wave function itself is independent of the field in this range. Moreover, since the magnetization M is just the total spin S^z_{tot} along the field direction, the symmetry under rotations generated by S^z_{tot} is unbroken. Thus, there can be no spin expectation values normal to the field. Furthermore, no other nearby states must cross the ground state (in energy) in this field range since it remains the ground state, and thus, since states with different magnetization must have energy depending linearly on the field, there must be a *spin gap* to excitations which carry nonzero spin S^z relative to the plateau state.

There are restrictions on such gapped states, following from the Lieb-Schultz-Mattis theorem and related arguments.[37] One way to understand them is to map the spins to hard-core bosons, where the boson number $n_i = S^z_i + \frac{1}{2}$. A gapped, insulating ground state of bosons in one dimension must have an *integer* number of bosons *per unit cell*. This implies that the total spin $\sum_{i\in\mathrm{u.c.}}\langle S^z_i\rangle$ per unit cell must be an *integer* if the unit cell contains an even number of sites, and must instead be a *half integer* if the unit cell contains an odd number of sites. Often, such gapped plateau states may be considered as ordered states with spins arranged in some pattern parallel and antiparallel to the field within a unit cell.

A prominent feature in the phase diagram we obtain is a magnetization plateau at one third of the saturation magnetization $M = M_{\mathrm{sat}}/3$. This has been extensively studied in the literature for the isotropic model[9,10] $R = 0$, where it is usually regarded as a result of quantum "order by disorder." The structure of the plateau state in that case is indeed in agreement with a semiclassical approach[3] and has a unit cell consisting of two up and one down spin, forming a three-sublattice enlargement of the primitive triangular lattice unit cell. Based on a combination of our DMRG studies and an analytic analysis of the quasi-1D limit $J'/J \ll 1$ (below), we show that, in the 2D system, the plateau state persists in the full range of anisotropies $0 < R \leqslant 1$ and forms a single phase throughout. For the one-dimensional TST, however, we find that the plateau, while present in the isotropic regime, *terminates* before reaching the decoupled chains limit. Both these results can be understood from the relation between the plateau state and the SDW phase, as will be explained in the next section.

A. Plateau states from SDW

The collinear SDW state shares many of the expected elements of the plateau phase. It has an unbroken U(1)

symmetry, even in the 2D limit, and exponentially decaying transverse correlations in the TST. It has rather long-range oscillating correlations of the component of the spin parallel to the field, and consequently a markedly modulated $\langle S^z_y(x)\rangle$ profile in finite systems. The distinction between the SDW and the plateau phase is that the former is generically incommensurate and gapless.

Both these differences may be removed due to further interactions neglected up to now, which *pin* the gapless phason mode φ at specific discrete values. This has been discussed at length already in Ref. 11 for the two-dimensional case. There, it was argued that an infinite sequence of plateaux occur at $T = 0$ within the SDW phase, the strongest of these being the $\frac{1}{3}$ plateau, and that all these plateaux exist at arbitrarily small J'/J. In the two-dimensional system, the plateau width (in a magnetic field) can be estimated to scale as $J(J'/J)^{9/2}$ (see Ref. 11). Here, we will restrict the discussion to the TST, and find that one-dimensional fluctuations suppress most of these plateaux, including the $\frac{1}{3}$ plateau for sufficiently small J'/J.

The plateau formation is due to additional interactions neglected in the sine-Gordon Hamiltonian presented so far in Eqs. (84) and (85), which involve *higher harmonics* of the phason mode φ. The allowed terms are obtained directly from a symmetry analysis. The action of the symmetries of the problem on φ may be understood directly from the expression for the spin operator in the SDW phase of the TST in Eq. (82). Under each symmetry, which is a lattice space-group operation, φ must be chosen to transform appropriately *so that* $S^z_y(x)$ *is a scalar*. This dictates the following transformation rules:

(1) translation along x, $x \to x+1$: $\varphi \to \varphi + \pi - 2\delta$;
(2) translation along y, $y \to y+1$: $\varphi \to \varphi - 2\pi/3$;
(3) 2D inversion, $x \to -x$, $y \to 2-y$: $\varphi \to -\pi/3 - \varphi$.

In addition, there is a "gauge invariance" arising because of the ambiguity of φ due its definition as a phase variable, which forces the invariance of the Hamiltonian under *local* shifts of φ by 2π. Note that in this section, we always consider the infinite-L limit, and neglect the difference between $\tilde{\delta}$ and δ.

Using the local gauge invariance, we seek terms of the form

$$H_{\text{pin}} = \sum_n \int dx t_n \sin(n\varphi + \alpha_n), \tag{102}$$

where t_n and α_n are arbitrary parameters. (In general, we can also allow α_n to be a slowly varying linear function of x, which is important for a full analysis of commensurate to incommensurate transitions, but we do not require this here for the more limited purpose of just identifying the relevant plateau states.) Using the translational symmetry along y, we immediately obtain the constraint that $t_n = 0$ unless n is a multiple of 3, and so we set $n = 3k$. The inversion symmetry then forces $\alpha_n = 0 \pmod{2\pi}$, so finally, we find

$$H_{\text{pin}} = \sum_{k\in\mathbb{Z}} \int dx t_k \sin 3k\varphi, \tag{103}$$

where we have redefined the t_k appropriately. Now, it remains to apply translation symmetry along x. This simply gives the condition that $3k(\pi - 2\delta)$ is an integer multiple of 2π. Writing $\delta = \pi M = (\pi/2)M/M_{\text{sat}}$, we have

$$\frac{M}{M_{\text{sat}}} = \frac{3k-2p}{3k}, \tag{104}$$

with k, p integers. This gives a rational family of potential magnetization plateaux, the strength of which decreases with increasing k.

An actual plateau occurs for a given value of magnetization characterized by integers k, p only if the associated term t_k is *relevant,*[7] when considered as a perturbation to the low-energy Hamiltonian of the SDW state, which is just the free massless field theory for φ. The scaling dimension of the operator in Eq. (103) is easily obtained as $\Delta_{3k} = 9k^2\eta_{\text{SDW}} = 3\pi k^2\kappa_0/\beta^2$ [cf. Eq. (97)] and, therefore, under RG, we find

$$t_k(b) = t_k b^{2-\Delta_{3k}} = t_k b^{2-9k^2\eta_{\text{SDW}}}. \tag{105}$$

Here, t_k is relevant, and a magnetization plateau appears when $\Delta_{3k} < 2$. Consider the case $k = 1$, which corresponds to the case $M = M_{\text{sat}}/3$ and small J'/J. There (recall Sec. V D), $\eta_{\text{SDW}} \approx 0.23$ so $\Delta_3 \approx 2.07 > 2$, and thus t_1 is *irrelevant*. Because Δ_{3k} increases quadratically with k, clearly all other potential plateaux with larger k are absent in the quasi-1D limit. Thus, we expect that for $J'/J \ll 1$, the SDW state remains stable, and there are no magnetization plateaux.

With increasing J', however, η_{SDW} decreases, owing to its dependence on κ_0 in Eq. (97). Including this dependence, and using the quasi-1D formula for κ_0 [in the text following Eq. (84)], we obtain the condition that t_1 becomes relevant, i.e., $\Delta_3 < 2$, when $J'/J > 0.17$. We believe that this is still in the domain where the quasi-1D approach is valid. The result predicts that the $\frac{1}{3}$ plateau appears only for $R < 0.83$ in the TST. At fixed $M = M_{\text{sat}}/3$, the transition from the gapless SDW to gapped plateau state at this value of R or J'/J is in the Kosterlitz-Thouless universality class, as is well known for the quantum sine-Gordon model. Consequently, the gap vanishes exponentially on approaching the transition from the more isotropic side, and the ground-state energy itself shows only an unobservably weak essential singularity at the transition. We note that other potential plateaux with $n = 3k \geqslant 6$ are so strongly suppressed by fluctuations that we do not expect any to occur, at least in the quasi-1D regime.

It is interesting to consider the spin structure on the plateau. This depends on the sign of $t \equiv t_1$. For $t > 0$, the $\sin 3\varphi$ pinning term in Eq. (103) is minimized by three values with equal energy, $\varphi = -\pi/6 + 2\pi n/3$, with $n = 0,1,2$. For these values, using Eq. (82), the spin density profile takes the form

$$\left\langle S^z_y(x)\right\rangle_{t>0} = \tilde{M} + A_1 \sin\left[\frac{\pi}{6} + \frac{2\pi}{3}(x-y-n)\right]. \tag{106}$$

This equation describes a three-sublattice structure with two spins "up," i.e., with $\langle S^z_y(x)\rangle > \tilde{M}$, when $x - y - n = 0,1 \pmod 3$ and one spin "down," when $x - y - n = 2 \pmod 3$. This is the semiclassical up-up-down state, and has precisely the same qualitative structure as predicted semiclassically in the isotropic limit $J' = J$.

For the other case $t < 0$, the minima occur for $\varphi = +\pi/6 + 2\pi n/3$, and the spin density profile becomes

$$\left\langle S^z_y(x)\right\rangle_{t<0} = \tilde{M} - A_1 \sin\left[\frac{\pi}{6} - \frac{2\pi}{3}(x-y-n)\right]. \tag{107}$$

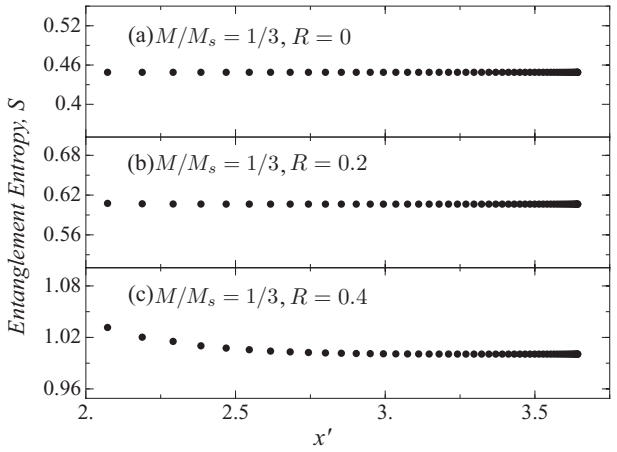

FIG. 19. Entanglement entropy at (a) $R = 0$, (b) $R = 0.2$, and (c) $R = 0.4$ in the $\frac{1}{3}$ plateau state. We see that the entanglement entropy approaches a constant for large x', which corresponds to a central charge of $c = 0$ in the ordered state.

This describes instead a three-sublattice structure with two spins nominally "down," with $x - y - n = 0,2 \,(\text{mod } 3)$, and the remaining one up. This state does not have a natural semiclassical picture, and instead corresponds to the "quantum" version of the plateau, discussed for the two-dimensional lattice in Ref. 11. A caricature of this state is a three-site unit cell with two sites forming a spin-singlet entangled pair, and the third (the "up" site) polarized along the field. Our DMRG results are consistent with the up-up-down configuration [Eq. (106)], suggesting that $t > 0$ case is realized.

We should stress that, apart from the quantitative estimate of κ_0, nothing in this section depends upon the quasi-1D approach. The conditions for the existence and stability of the plateaux arising out of the SDW state are otherwise completely general results based only on symmetries of the TST and general arguments.

B. DMRG results for plateau

In this section, we discuss how we use DMRG to probe into the $\frac{1}{3}$ plateau. The first observation of its existence is the constant entanglement entropy for the ranges of R on the $\frac{1}{3}$ plateau, as shown in Fig. 19. This shows an ordered state which corresponds to central charge $c = 0$, in Eq. (12). Furthermore, we can measure the transverse spin-spin correlations, which should decay exponentially in the $\frac{1}{3}$ plateau. We show this measurement in Fig. 20, for $R = 0.2$ as well as the isotropic case $R = 0$.

In Figs. 21(a) and 21(b), we plot the S^z profile of the spins forming the three sublattices on the $\frac{1}{3}$ plateau. Near $x = L/2$, we see a perfect up-up-down structure, with some boundary effects on the edges of the chain. This gives definitive evidence of the robustness of the $\frac{1}{3}$ plateau in these ranges of anisotropies. Moreover, in Fig. 21(c), we see that the plateau persists up until $R \approx 0.8$, at which point, the system undergoes a Kosterlitz-Thouless transition that destroys the $\frac{1}{3}$ plateau. As described in the previous sections, this is a signature of the 1D TST only: in 2D, the plateau is even more robust, extending down to $R = 1$. This is further discussed in Sec. VIII A.

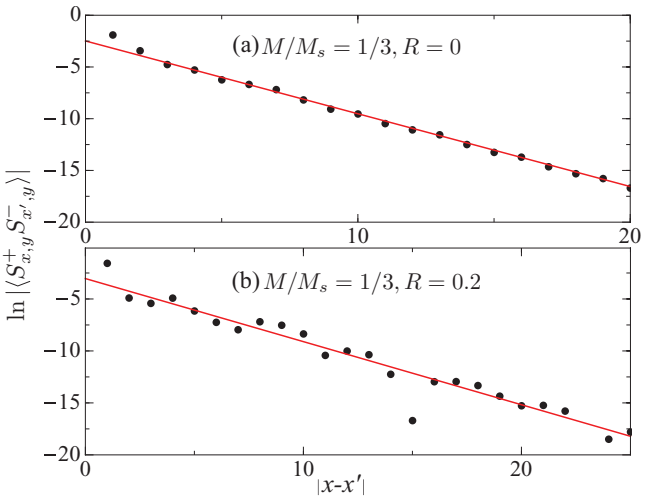

FIG. 20. (Color online) Log plot for transverse spin-spin correlation function at (a) $R = 0$ and (b) $R = 0.2$ in the $\frac{1}{3}$ plateau state for system size $N_x = 120$ and $x' = N_x/2$. Data points are shown as (black) circles, while the (red) line is a fit to the exponential function.

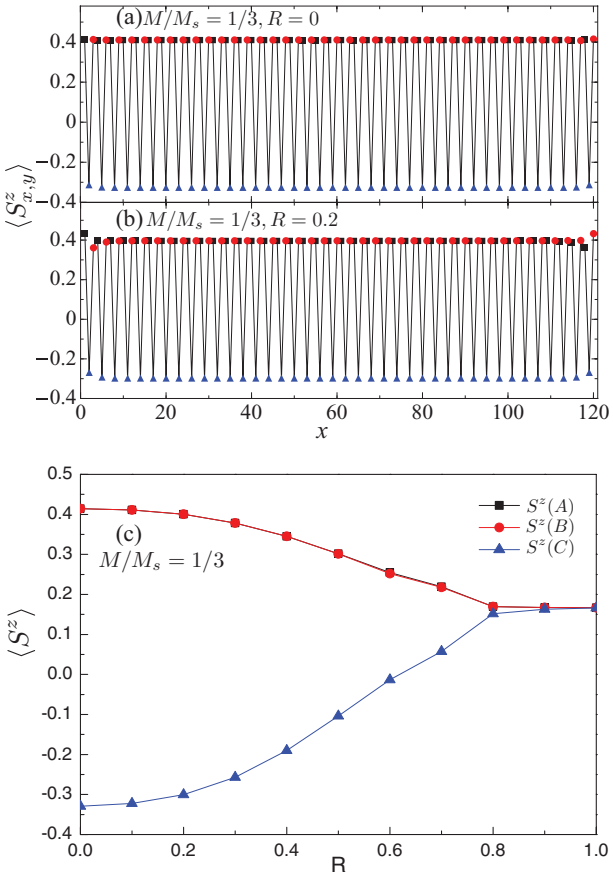

FIG. 21. (Color online) S^z profile for the $\frac{1}{3}$ plateau state at (a) $R = 0.0$ and (b) $R = 0.2$. We show data for the three sublattices, showing the up-up-down structure, as square (black), circle (red), and triangles (blue). There are slight boundary effects near the end of the chains, near $x = 0, 120$; however, the chains are well ordered toward the center. (c) Shows the S^z profile at $M/M_s = \frac{1}{3}$ as a function of R. We observe that the width of the plateau decreases and eventually vanishes near $R \approx 0.8$.

To characterize the properties of the plateau as well as its width, we will adopt the following method, which takes advantage of the total spin conservation due to the presence of the U(1) symmetry with a magnetic field along the z axis. In this case, we can work in a given total spin sector $S^z = \sum_i S_i^z$, and get the corresponding ground-state energy $E(S^z)$:

$$E(S^z,h) = E(S^z) - h \cdot S^z. \tag{108}$$

Then, the energy difference between two adjacent spin S^z sectors is given by

$$\delta E(S^z,h) = E(S^z+1,h) - E(S^z,h). \tag{109}$$

Generally, at small magnetic field h, $E(S^z+1,h) > E(S^z,h)$, so $\delta E(S^z,h) > 0$. However, $E(S^z+1,h) \leqslant E(S^z,h)$ when h is large enough, so $\delta E(S^z,h) \leqslant 0$. Therefore, the boundaries of the plateau can be determined when $E(S^z+1,h) = E(S^z,h)$, with the upper boundary $h_c^2(S^z)$ and lower boundary $h_c^1(S^z)$ of the plateau given by

$$\begin{aligned} h_c^2(S^z) &= E(S^z+1) - E(S^z), \\ h_c^1(S^z) &= E(S^z) - E(S^z-1). \end{aligned} \tag{110}$$

Finally, the corresponding width of the plateau can also be obtained as

$$W(S^z) = h_c^2(S^z) - h_c^1(S^z). \tag{111}$$

In DMRG, the boundaries of the $\frac{1}{3}$ plateau can be computed using Eq. (110) by fixing the total spin to $S^z = \frac{NM_s}{3}$. Here, $M_s = \frac{1}{2}$ is the saturation magnetization, and N is the total number of sites. As shown in Figs. 22(a) and 22(b), both the upper and lower boundaries of the $\frac{1}{3}$ plateau are determined using different system sizes and anisotropies. The corresponding width of the plateau is also given in Fig. 22(c) using Eq. (111). From this, we can see that the plateau is very robust and remains finite when the anisotropy R is small, and decreases with increasing R. Interestingly, the plateau still remains finite even R is very large, i.e., $R = 0.7$, although the width W is very small. In the region $0.7 < R \leqslant 1$, finite-size scaling of the data shows that the width of the plateau is zero within the numerical error, for example, at the decoupled chain limit $R = 1$.

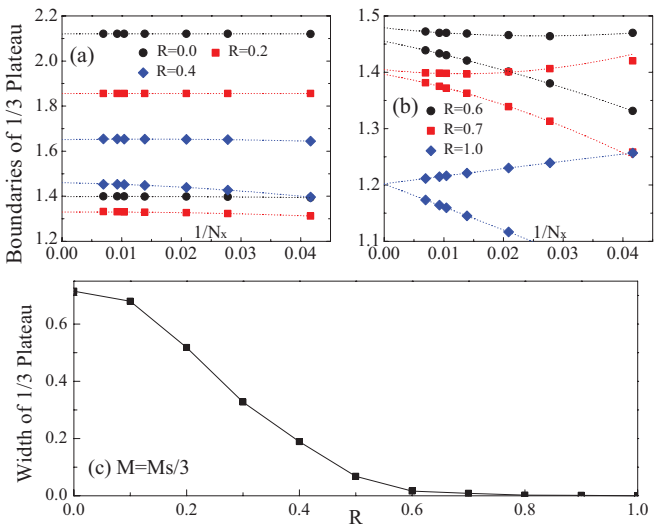

FIG. 22. (Color online) Finite-size scaling of the boundaries of the $\frac{1}{3}$ plateau for $L_y = 3$ TST for different anisotropies (a) $R = 0.0,0.2,0.4$ and (b) $R = 0.6,0.7,1.0$. (c) Width of the $\frac{1}{3}$ plateau as a function of R.

VII. LOW-FIELD REGIME

At zero field, there is already considerable work on the spatially anisotropic Heisenberg model in two dimensions.[10,38–43] Away from the quasi-1D region, i.e., for $0 < R \lesssim 0.8$, the ground state of the 2D model is unambiguously magnetically ordered, in a coplanar spiral with an incommensurate wave vector that varies continuously with R. With increasing anisotropy, the ground state is less clear, and is quite difficult to resolve numerically, owing to the fact that correlations between chains set in only at extremely long length scales for small J'/J. A controlled renormalization group approach predicts, however, that in the limit $0 < J'/J \ll 1$, the system develops a *collinear* magnetic state instead of the spiral one.[12] Such a collinear state is qualitatively distinguished from the spiral one by its pattern of symmetry breaking, which leaves a residual U(1) spin rotation symmetry about the ordering axis, in contrast to the spiral state which fully breaks SU(2) symmetry with no residual continuous invariance remaining.

Here, we turn to the situation in the one-dimensional TST. We argue that in this case the spiral order is converted by 1D quantum fluctuations into a fully gapped state with spontaneous *staggered dimerization*. The argument is quite general and is expected to hold for any 1D system with local noncollinear order and a half-integer spin per unit cell. Furthermore, specifically for the TST, we show that the tendency to short-range spiral order is *more* robust than in 2D, and unlike in 2D, it prevails over collinear order even in the limit of arbitrarily small J'/J. Thus, staggered dimerization is predicted at zero field for all $0 \leqslant R < 1$ for the TST. See Appendix C 1 for an alternative calculation that leads to the same conclusion as the one presented below.

Given the presence of dimerization in zero field, we can discuss the behavior in low fields, or more properly for small magnetization, in terms of the elementary excitations of the symmetry-broken dimerized state, which are domain-wall solitons. We obtain in this way different gapless phases at low field, including the SDW state discussed previously from the quasi-1D point of view.

A. Zero-field dimerization from spiral order

In the following, we assume that on short space and time scales, the spins establish a similar spiral order to that of the 2D system. This notion can be made more systematic by considering spin tubes made by wrapping the triangular lattice into cylinders with larger circumference. Once the circumference is large enough compared to the correlation length of the spiral order, the latter should become well established. It seems reasonable to regard this as being the case already for the circumference-three TST studied here. This is corroborated also by the close correspondence of the phase diagram in the weakly anisotropic limit $R \ll 1$ and the expected semiclassical one, as discussed already in Sec. III.

With this assumption, the description of the TST should be that of a nonlinear σ model (NLσM) for the spiral order, confined to the finite-width cylinder. This starting point is similar to the one of Haldane[44] applied to unfrustrated spin chains of spin S, which locally establish collinear Néel order. From this formulation, Haldane established the existence of a featureless gapped state for integer S, while it is known that chains with half-integral S harbor a gapless Bethe chainlike phase instead. The case of the TST is distinct from Haldane's analysis, however, owing to the different symmetry of the order. While the collinear Néel case is described by a vector O(3) NLσM, the spiral case is instead described by a NLσM with a *matrix* SO(3) order parameter.[45] Here, the matrix may be constructed from the local spin order

$$\mathbf{S}_i \sim m(\hat{\mathbf{n}}_1 \cos \mathbf{q}\cdot\mathbf{r}_i + \hat{\mathbf{n}}_2 \sin \mathbf{q}\cdot\mathbf{r}_i), \tag{112}$$

where $\hat{\mathbf{n}}_1$ and $\hat{\mathbf{n}}_2$ specify the plane of the spiral, with $\hat{\mathbf{n}}_1 \cdot \hat{\mathbf{n}}_2 = 0$, $\mathbf{q}$ the spiral wave vector, and m the amplitude of the quasistatic moment. One can construct from this the SO(3) matrix

$$\mathcal{O} = (\hat{\mathbf{n}}_1|\hat{\mathbf{n}}_2|\hat{\mathbf{n}}_3)\,, \tag{113}$$

with $\hat{\mathbf{n}}_3 = \hat{\mathbf{n}}_1 \times \hat{\mathbf{n}}_2$.

If on short space and time scales, spiral order is present, we expect that an appropriate effective NLσM action is given by

$$S_{\mathrm{NL}\sigma\mathrm{M}} = \frac{1}{2g}\int dx\, d\tau \left\{ \frac{1}{v}\mathrm{Tr}[\partial_\tau \mathcal{O}^T \partial_\tau \mathcal{O}] + v\,\mathrm{Tr}[\partial_x \mathcal{O}^T \partial_x \mathcal{O}] \right\}. \tag{114}$$

Note that, for a quasi-1D system with circumference L_y, the effective coupling constant $g \sim c/L_y \ll 1$ for large L_y, with some constant two-dimensional coupling constant c.

Famously, in Haldane's analysis of spin chains with a vector O(3) order parameter, the naive NLσM action must be supplemented by a topological term.[44] Topology of the order parameter is also important here, but its nature is rather distinct from Haldane's case. For clarity, we compare and contrast the two situations here. The vector O(3) order parameter comprises a manifold isomorphic to the sphere S^2. Its topology is summarized by the homotopy groups $\Pi_1(S^2) = 0$ and $\Pi_2(S^2) = \mathbb{Z}$. The former implies that there are no nontrivial loops on the sphere and, correspondingly, no *singular* point defects in two dimensions. The latter, second homotopy group implies that there are classes of nontrivial *smooth* configurations of the order parameter in two dimensions, parametrized by an integer. These configurations are skyrmions, lacking any singularity. Because of the lack of any singularity, the skyrmions appear in a continuum limit of the O(3) vector NLσM, and modify the physics of the NLσM through a topological θ term, which gives a phase factor to configurations with nonzero skyrmion number. Based on this NLσM with θ term, Haldane postulated distinctly different behavior for integer and half-integer spin chains.

In the matrix SO(3) case, the order-parameter manifold is $S^3/\mathbb{Z}_2$, and the corresponding homotopy groups are $\Pi_1(S^3/\mathbb{Z}_2) = \mathbb{Z}_2$ and $\Pi_2(S^3/\mathbb{Z}_2) = 0$. The trivial second fundamental group means that *nonsingular* configurations of the order parameter have no topological distinctions. This implies that a continuum limit exists in which there are no topological defects and there is no topological term. Instead, the nonvanishing first homotopy group implies that there are *singular* point defects in two dimensions, with an Ising character. Note that in our theory, these are point defects in space-time, or *instantons*. Such defects are well known in classical two-dimensional noncollinear magnets, and are known as $\mathbb{Z}_2$ vortices.[46] They do not appear in the continuum NLσM, but are allowed in a lattice theory. Instead, the proper way to treat them is to *embed* the continuum theory in a larger one in which the defects appear as *operator insertions*, with some fugacity and selection rules. This situation is familiar from the Kosterlitz-Thouless analysis of the classical XY model, in which the naive continuum theory is just the Gaussian spin-wave line, and the defects are point vortices which are treated as a kind of Coulomb gas.[36] It occurs also in the quantum analysis of $(2+1)$-dimensional collinear antiferromagnets, where the singular defects are hedgehogs or monopoles. The separation of these defects and the continuum theory is the basis of the theory of deconfined quantum criticality.[47]

With this understanding, we may first consider the SO(3) matrix NLσM *without* any $\mathbb{Z}_2$ vortices, which is simply described by Eq. (112). There is no topological term. This SO(3) NLσM is, like all NLσM's in two dimensions for non-Abelian groups, asymptotically free. Lacking any quantum phase factors, we expect simply that it develops a gap at a length scale $\xi \sim e^{g_0/g} \sim e^{\frac{g_0}{c}L_y}$, and that order-parameter (hence spin) correlations decay exponentially beyond this scale. The gap itself behaves as $\Delta \sim v/\xi$. Note the difference from Haldane's case, where the θ term, which is nontrivial for half-integer spin, fundamentally alters the behavior of the continuum NLσM, leading to gapless behavior in the half-integer spin case. Here, there is no topological term, and the system is always gapped with exponential spin correlations.

Now, we can consider the role of the $\mathbb{Z}_2$ vortex instantons. Such a vortex is described in the field theory by an operator ψ, which inserts the vortex at a particular space-time point. It is crucial to consider the quantum numbers of a $\mathbb{Z}_2$ vortex, i.e., how the operator ψ transforms under physical symmetries. The relevant operations are time reversal, translation, and inversion. It can be argued (we discuss this in Appendix D) that the vortex operator is invariant under time reversal and translations along y, and transforms under the other two operations, translation along x, T_x and inversion P according to

$$T_x : x \to x+1,\ \psi \to (-1)^{L_y}\psi, \tag{115}$$

$$P : x \to -x, y \to -y,\ \psi \to (-1)^{L_y}\psi. \tag{116}$$

From the above properties, we see that *for odd L_y, ψ has the transformation properties of a staggered dimerization operator*. In general, two operators with the same symmetry are expected to have nonzero overlap in the operator sense, and their correlations will be proportional. Thus, for odd L_y, the $\mathbb{Z}_2$ vortex operator ψ can be viewed as a staggered dimerization order parameter.

Let us consider the correlations of ψ. Its two-point correlation function is obtained by inserting two $\mathbb{Z}_2$ vortices in the system at separated space-time points. When they are widely separated, the result should be just the product of

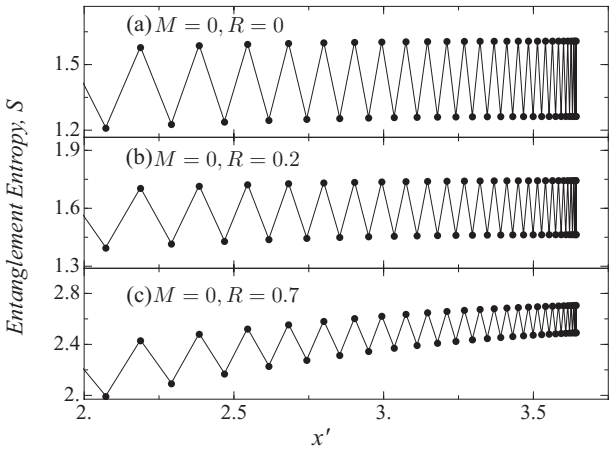

FIG. 23. Entanglement entropy at (a) $R = 0$, (b) $R = 0.2$, and (c) $R = 0.7$ at zero field. The oscillatory behavior with periodicity 2 shows the dimerized ground state.

two independent $\mathbb{Z}_2$ vortices. Naively, using Eq. (112), such a vortex has an action which diverges logarithmically with the system size. However, its *effective* action is expected to be finite, due to the vanishing order and stiffness beyond the scale ξ. Roughly, the effective action for a single vortex is thus obtained by replacing the system size by ξ, so $S_v \sim \frac{1}{g} \ln \xi \sim g_0/g^2$. Then, we expect that

$$\lim_{x\to\infty} \langle \psi(x)\psi(0)\rangle \sim e^{-2S_v} \sim e^{-g_0/g^2} \sim e^{-cL_y^2}, \qquad (117)$$

with some constant c. The saturation to a finite value as $x \to \infty$ implies $\langle\psi\rangle \neq 0$, and hence, for odd L_y, the existence of staggered dimer order. For even L_y, there is no connection of $\mathbb{Z}_2$ vortices to dimerization, so although the former are present, the system forms simply a featureless gapped state.

We can probe into this state by measuring the entanglement entropy in DMRG for a range of anisotropies at zero field. We show this in Fig. 23, where an oscillatory behavior of period 2 gives clear evidence of the dimerized phase described above.

B. Gapless states in low but nonzero field

As argued in the previous section, the ground state in zero field is a nonmagnetic dimerized state with a gap to all excitations. As a consequence of the gap, the ground state is unchanged by application of a sufficiently small field. The ground state changes when the field is large enough that a state with nonzero spin crosses the energy of the spin-zero ground state. Generally, if the transition to a state of nonzero magnetization occurs continuously, we can think that the state with nonzero magnetization consists of a dilute set of elementary excitations above the zero-field ground state.

We must consider therefore the elementary excitations of the dimerized state, and in particular those which carry nonzero spin (as these couple to the field). The most important such excitations are the topological *soliton* excitations which are characteristic of the broken Ising symmetry of the dimerized state. Such solitons are domain walls, connecting the two distinct dimerized ground states. As is well known from the study of the Majumdar-Gosh chain,[48] solitons of this type carry spin, and in particular for the TST, one can readily argue

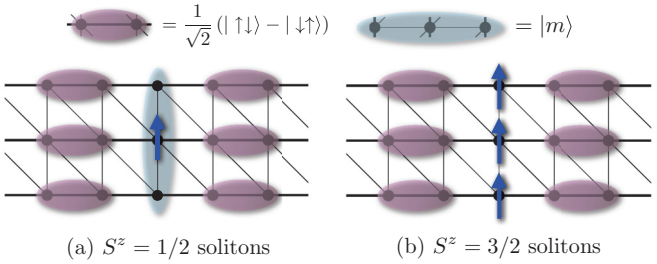

FIG. 24. (Color online) Toy picture of solitons. The blue shade, covering three sites, in (a) corresponds to the $S_z = \frac{1}{2}$ soliton in Eq. (118), while the three blue arrows in (b) correspond to a single $S_z = \frac{3}{2}$ soliton.

that the solitons carry half-integer spin, namely, $S^z = \frac{1}{2}, \frac{3}{2}$, as shown in Fig. 24. Both values of the spin are possible, and generally differ in energy. The solitons are topological excitations insofar as they are nonlocal: they can not be created by the action of any local operator on a dimerized ground state. In addition to the topological soliton excitations, nontopological excitations carrying spin $S^z = 1$ also exist. They can be visualized either by replacing a singlet dimer by a triplet of aligned spins, or as a bound pair of $S^z = \frac{1}{2}$ solitons.

Generally, if the magnetized state is realized as a dilute system of *non*topological $S^z = 1$ triplons, then the dimerization is not disrupted and must persist for $M > 0$. Numerically, however, the dimerization appears to be disrupted at all nonzero M. We will assume henceforth that the magnetized state (at small $M > 0$) should be regarded as a collection of topological soliton excitations, and neglect the $S^z = 1$ triplons.

In general, the excitations can be characterized by spatial quantum numbers in addition to spin. For an excitation localized in x in the TST, we may consider the transformations under translations along y, T_y, and under inversion P. From Fig. 24, it is clear that the $S^z = \frac{3}{2}$ soliton is invariant under both. However, this is not the case for the $S^z = \frac{1}{2}$ soliton, which has additional structure. In general, out of the three nondimerized spins in the "core" of the domain wall, we can form three linearly independent states with $S^z = \frac{1}{2}$:

$$|m\rangle = \frac{1}{\sqrt{3}}\left[\zeta^m \begin{pmatrix}\downarrow\\ \uparrow\\ \uparrow\end{pmatrix} + \begin{pmatrix}\uparrow\\ \downarrow\\ \uparrow\end{pmatrix} + \frac{1}{\zeta^m}\begin{pmatrix}\uparrow\\ \uparrow\\ \downarrow\end{pmatrix}\right], \qquad (118)$$

where $\zeta = e^{2\pi/3}$ and $m = 0, \pm 1$. These are simply momentum eigenstates along the three-site chain. The state $|0\rangle$ is invariant under the T_y and P operations, while the *chirality* eigenstates $|\pm\rangle$ form a two-dimensional irreducible representation. In general, the chirality states would differ in energy from the scalar one. If we crudely model the soliton core as a three-site antiferromagnetic Heisenberg chain, then we see that the chirality states have lower energy, so we expect that the elementary solitons take this form. Consequently, there are two chirality "flavors" to the $S^z = \frac{1}{2}$ solitons.

To understand the impact of the solitons, we will need the relation between the microscopic lattice operators and those which describe the solitons. The simplest to consider is the dimerization operator, or the bond kinetic energy $B_{x,y} = \vec{S}_{x,y} \cdot$

$\vec{S}_{x+1,y}$. This is negative on singlet bonds and has zero average on bonds with uncorrelated spins. In a ground state, it oscillates with period 2 in the x direction. However, the singlets are shifted over by one sublattice on crossing a soliton, so

$$B_{x,y} \sim \overline{B} + (-1)^{x+N(x)}\epsilon_0, \tag{119}$$

where $\overline{B}$ is the nonzero average, and ϵ_0 is the amplitude of the bond modulation. We have defined $N(x) = \sum_{x'<x} a^\dagger_{+,x'}a_{+,x'} + a^\dagger_{-,x'}a_{-,x'} + a^\dagger_{3,x'}a_{3,x'}$, which is the number of solitons to the left of the position x. The $N(x)$ factor accounts for the shift in the singlet position on crossing each domain wall.

Next, we turn to the spin density operator $S^z_{x,y}$. We are interested in its action on states which consist of a low density of solitons. It is helpful to consider a caricature of these states in which solitons are described by a wave function which is a product of columns of singlets, spaced by occasional nonsinglet columns with either the chiral $S^z = \frac{1}{2}$ form, or fully aligned $S^z = \frac{3}{2}$ spins, as shown in Fig. 24. If the operator $S^z_{x,y}$ acts on a column x which is part of a singlet, it converts that singlet to an $S^z = 0$ triplet state. This triplet costs a nonzero energy equal to the zero-field spin gap, and having $S^z = 0$ gains no energy back from the magnetic field. Thus, if we restrict our description to a low-energy one, below the zero-field spin gap, we can simply take $S^z_{x,y}$ to annihilate the state in this case. If, however, x is located at the position of a soliton, then $S^z_{x,y}$ gives back a low-energy state, which consists either of the original soliton or one with reversed chirality. Notably, in moving down the 1D system, solitons alternate between odd and even columns of the lattice. Thus, a nonzero spin is only measured when $S^z_{x,y}$ acts on an even or odd site, if the number of solitons to the left of the position x is fixed. This lets us write the following expression for the spin operator:

$$\begin{aligned} S^z_{x,y} \sim{}& [1 + (-1)^{x+N(x)}][a^\dagger_{+,x}a_{+,x} + a^\dagger_{-,x}a_{-,x} \\ &+ \zeta^y a^\dagger_{+,x}a_{-,x} + \zeta^{-y}a^\dagger_{-,x}a_{+,x} + a^\dagger_{3,x}a_{3,x}], \end{aligned} \tag{120}$$

where $a_{+,x}$,$a_{-,x}$ are annihilation operators for chiral $S^z = \frac{1}{2}$ solitons, and $a_{3,x}$ is an annihilation operator for an $S^z = \frac{3}{2}$ soliton.

Finally, we consider the spin-raising operator $S^+_{x,y}$, containing the XY components of the spin. Acting on a site which is part of a singlet bond, the raising operator converts the singlet to an $S^z = 1$ triplet, with amplitude $\mp 1/\sqrt{2}$ depending upon whether the site is the left or right member of that singlet. The triplet with $S^z = 1$ has overlap with the state of two adjacent $S^z = \frac{1}{2}$ solitons (as well as other states not in the low-energy sector). Simple algebra shows that, for instance,

$$\begin{pmatrix} |s\rangle \\ |\uparrow\uparrow\rangle \\ |s\rangle \end{pmatrix} = \tfrac{1}{3}\big[|+\rangle|+\rangle + |-\rangle|-\rangle - \tfrac{1}{2}(|+\rangle|-\rangle + |-\rangle|+\rangle)\big] + \cdots, \tag{121}$$

where on the left-hand side, $|s\rangle$ represents the singlet state, and the columns represent the three columns in the TST. On the right-hand side, the state has been decomposed into soliton states, and the ellipsis represents higher-energy states. Here, we took the triplet to reside in the middle row. The other triplets can be obtained by translation, as the chirality states are translational eigenstates. From this construction, we obtain the analogous relation to Eq. (120),

$$\begin{aligned} S^+_{x,y} \sim{}& (-1)^{x+N(x)} \sum_{m=\pm} [\zeta^{my} a^\dagger_{m,x} a^\dagger_{m,x+(-1)^{x+N(x)}} \\ &+ a^\dagger_{m,x} a^\dagger_{-m,x+(-1)^{x+N(x)}}]. \end{aligned} \tag{122}$$

The low-energy excited eigenstates will not consist of localized quasiparticles but delocalized ones, as solitons may hop between columns of the same sublattice, i.e., even or odd x. As a consequence, the states are eigenstates of the x momentum k_x, which is defined *modulo* π rather than the usual 2π, due to the doubled background unit cell of the dimerization. In the dilute limit, we should consider only the states near the minimum energy of the corresponding energy bands. For the $S^z = \frac{3}{2}$ solitons, which are inversion symmetric, if this minimum is nondegenerate, it must occur at $k_x = 0$ or $k_x = \pi/2$. We expect it to occur at the latter $k_x = \pi/2$ value, owing to the dominant antiferromagnetic spin correlations. For the $S^z = \frac{1}{2}$ solitons, inversion symmetry implies instead that if the positive chirality ($q = +1$) soliton has minimum energy at $k_x = q_0$, then the negative chirality soliton has its minimum energy at $k_x = -q_0$. We are not aware of a general argument to fix the momentum q_0, however, and expect it is generically nonzero. We have checked this by a crude and uncontrolled variational calculation of the soliton dispersion, which indeed gives minimum energy states with opposite nonzero momenta for opposite chirality (this calculation gives $q_0 = \pi/6$, but we do not expect this to be accurate).

With this in mind, we focus only on the minimum energy states and take a continuum limit, writing

$$a_{\pm,x} \sim \psi_\pm(x) e^{\pm i q_0 x}, \tag{123}$$

$$a_{3,x} \sim \Psi(x) e^{i\frac{\pi}{2}x}, \tag{124}$$

where $\psi_m(x)$ and $\Psi(x)$ are taken as slowly varying continuum boson fields. Then, Eqs. (120) and (122) become

$$\begin{aligned} S^z_{x,y} \sim{}& [1 + (-1)^{x+N(x)}] \Bigg[\sum_{m=\pm} \psi^\dagger_m \psi_m \\ &+ \sum_m e^{im(2q_0 x + \frac{2\pi}{3}y)} \psi^\dagger_m \psi_{-m} + \Psi^\dagger \Psi \Bigg], \end{aligned} \tag{125}$$

$$\begin{aligned} S^+_{x,y} \sim{}& 2i \sin q_0 \sum_m e^{im(2q_0 x + \frac{4\pi}{3}y)} m (\psi^\dagger_m)^2 \\ &+ 2\cos q_0 (-1)^{x+N(x)} \sum_m e^{im(2q_0 x + \frac{4\pi}{3}y)} (\psi^\dagger_m)^2 \\ &+ 2\cos q_0 (-1)^{x+N(x)} \psi^\dagger_+ \psi^\dagger_-. \end{aligned} \tag{126}$$

We are now in a position to write an effective continuum theory to describe the low magnetization state in terms of bosonic field operators ψ_m for $S^z = \frac{1}{2}$ solitons with chirality m and Ψ_m for the $S^z = \frac{3}{2}$ solitons, all taken near their band

minima. By symmetry, it takes the form

$$H_{\rm low} = \int dx \left\{ \sum_{m=\pm} \psi_m^\dagger \left(-\frac{1}{2m_1}\partial_x^2 + \epsilon_{1/2} - h/2 \right) \psi_m + \Psi^\dagger \left(-\frac{1}{2m_2}\partial_x^2 + \epsilon_{3/2} - 3h/2 \right) \Psi + V[\psi_+^\dagger\psi_+, \psi_-^\dagger\psi_-, \Psi^\dagger\Psi] \right\}. \quad (127)$$

Here, V is a general potential of quartic order and higher in the fields, representing interactions of the solitons. We have dropped terms above which mix the different soliton species, e.g., ones which might annihilate one $S^z = \frac{3}{2}$ soliton while creating three $S^z = \frac{1}{2}$ solitons. Most such terms, at least at low order, are prohibited by various symmetries, such as translation and inversion symmetry, at least for a generic incommensurate wave vector q_0 for the $S^z = \frac{1}{2}$ solitons.

Consider increasing the magnetic field h from zero. The ground state remains the soliton vacuum, i.e., the dimerized state, until the energy of a state with nonzero solitons crosses the energy of the vacuum. Assuming repulsive interactions between solitons, this occurs when the energy of a single soliton vanishes, and this type of soliton will enter the system. We must compare the energies $\epsilon_{1/2} - h/2$ and $\epsilon_{3/2} - 3h/2$, and see which vanishes first on increasing h. If the $S^z = \frac{3}{2}$ soliton energy is large, $\epsilon_{3/2} > 3\epsilon_{1/2}$, then the $S^z = \frac{1}{2}$ solitons will appear, at $h = 2\epsilon_{1/2}$. Conversely, if $\epsilon_{3/2} < 3\epsilon_{1/2}$, then the $S^z = \frac{3}{2}$ solitons will appear at $h = 2\epsilon_{3/2}/3$. The critical ratio $\epsilon_{3/2}/\epsilon_{1/2} = 3$ is valid at infinitesimal soliton density, i.e., $M \to 0^+$. At larger magnetization, interactions amongst solitons may become important, and will probably tend to disfavor the $S^z = \frac{1}{2}$ solitons further, since these must occur at a higher density and hence interact more strongly. Since in any case we do not know the energies $\epsilon_{3/2}, \epsilon_{1/2}$, we can not actually use this criteria quantitatively. Instead, we simply consider both types of soliton liquids as possibilities, and determine their properties at a phenomenological level.

Let us consider first the $S^z = \frac{1}{2}$ case. Then, we can neglect the Ψ particle, which has an energy gap even when the ψ_q solitons enter the system. The structure of the solitonic state is determined to a degree by the potential V in Eq. (127). By symmetry, it has the form

$$V[n_+, n_-, 0] = \frac{a}{2}(n_+^2 + n_-^2) + b n_+ n_-. \quad (128)$$

With $a > 0$ for stability, the state depends upon the coefficient b. If we assume $b < a$, then it is favorable for both solitons to enter the system in equal amounts, and the system forms a one-dimensional Bose liquid of particles with two flavors. Owing to the strong quantum fluctuations in one dimension, this is a Luttinger liquid phase with two independent massless bosonic modes, associated to the two conserved densities. In the CFT terminology, this is a state with central charge $c = 2$. If instead $b > a$, it is preferable for the system to choose one state of soliton only. In this case, there is a spontaneously broken discrete symmetry (inversion P), and only a single massless bosonic mode, or $c = 1$. We focus on the former case $b < a$, which we argue *describes the same phase* as the semiclassical incommensurate planar state.

To see this, we show that the spin correlations in the two-flavor $S^z = \frac{1}{2}$ soliton liquid have the same form as those in the 1D incommensurate planar phase, described in Sec. III E. In the soliton liquid, we can use the usual bosonization of bosons for each of the two species $\psi_m \sim \sqrt{\bar{n}_s/2} e^{-i\theta_m}$, $\psi_m^\dagger \psi_m \sim \bar{n}_s/2 + \partial_x \phi_m/\pi$ (and $\Psi^\dagger\Psi = 0$), where ϕ_m is the dual field to the boson phase θ_m. With this, we may conveniently represent the nonlocal operator $N(x) = \bar{n}_s x + \sum_m \phi_m/\pi$, where $\bar{n}_s$ is the mean soliton density. Note since each soliton carries $S^z = \frac{1}{2}$ spread over the TST of width 3, the average magnetization *per site* is $M = \frac{1}{3}\bar{n}_s/2 = \bar{n}_s/6$. Then,

$$B_{x,y} \sim \overline{B} + \epsilon_0 \cos[(\pi + 2\delta)x + \varphi], \quad (129)$$

$$S^z_{x,y} \sim \{1 + \cos[(\pi + 2\delta)x + \varphi]\} \times \left(M + \frac{\partial_x \varphi}{6\pi} + n_s \cos\left[\theta_+ - \theta_- + 2q_0 x + \frac{2\pi}{3} y \right] \right), \quad (130)$$

$$S^+_{x,y} \sim 2i \sin q_0 \sum_m e^{im(2q_0 x + \frac{2\pi}{3} y)} m e^{2i\theta_m} + 2\cos q_0 \cos[(\pi + 2\delta)x + \varphi] \times \left(e^{i(\theta_+ + \theta_-)} + \sum_m e^{im(2q_0 x + \frac{2\pi}{3} y)} e^{2i\theta_m} \right). \quad (131)$$

Here, $2\delta = \pi\bar{n}_s = 2\pi M/3$ and $\varphi = \phi_+ + \phi_-$. We can compare the above to the semiclassical result. In the semiclassical limit, the bosonic phases $\theta_\pm$ are weakly fluctuating, while $\phi_\pm$ and hence φ are strongly fluctuating. Then, the dominant terms in the spin operators, with smallest scaling dimension, are those which do not contain any of the strongly fluctuating phases,

$$S^z_{x,y} \sim M + n_s \cos\left[\tilde{\theta} + 2q_0 x + \frac{2\pi}{3} y \right], \quad (132)$$

$$S^+_{x,y} \sim -4 \sin q_0 \, e^{i\theta} \sin\left[\tilde{\theta} + 2q_0 x + \frac{2\pi}{3} y \right], \quad (133)$$

where we defined $\theta = \theta_+ + \theta_-$ and $\tilde{\theta} = \theta_+ - \theta_-$. This can be directly compared to Eqs. (20) of Sec. III E. We see that the *form* of the spin operators is identical to that in the incommensurate coplanar state. Thus, we can regard the $S^z = \frac{1}{2}$ chiral soliton liquid as another limit of the same phase.

Let us turn to the case of the $S^z = \frac{3}{2}$ soliton liquid. As there is no chirality quantum number in this case, the state can be simply viewed as a Luttinger liquid without spin, and is expected to be described by a $c = 1$ theory of a single massless boson. We argue that this $S^z = \frac{3}{2}$ soliton liquid is in fact another SDW phase very similar to the one obtained by the quasi-one-dimensional approach of Sec. V C. While one might have expected to find the *identical* SDW phase in this way, we instead find that the $S^z = \frac{3}{2}$ soliton liquid is a SDW state with a different SDW wave vector, in particular with $Q_y = 0$, contrasting with the value $Q_y = 2\pi/3$ obtain from the quasi-1D approach. If the $S^z = \frac{3}{2}$ liquid indeed occurs, therefore, we presumably require a phase transition to the other SDW state upon increasing magnetization.

To observe the SDW structure of the $S^z = \frac{3}{2}$ soliton liquid, we again consider the spin correlations. Now we have no chiral solitons, $\psi_m^\dagger \psi_m = 0$. This immediately implies that *there are no low-energy excitations with spin* $S^z = 1$ *and hence no low-energy content to the* $S^\pm$ *operators*. Thus, XY correlations decay exponentially in this phase, exactly as in the the SDW phase. To examine the S^z correlations, we can bosonize the nonchiral bosons. This gives $\Psi \sim \sqrt{\overline{n}_s} e^{i\vartheta}$, $\Psi^\dagger \Psi \sim \overline{n}_s + \partial_x \varphi/\pi$, with dual phases φ, ϑ. Now, $N(x) = \overline{n}_s x + \varphi/\pi$, and we note the relation between the magnetization and soliton density is changed to $M = \overline{n}_s/2$ since the solitons have spin $S^z = \frac{3}{2}$. We see then that

$$S^z_{x,y} \sim \{1 + \cos[(\pi + 2\delta)x + \varphi]\} \left(M + \frac{\partial_x \varphi}{2\pi} \right). \qquad (134)$$

Higher harmonics of the above cosine also appear in a more careful treatment. Note that the incommensurability is different in this case: $2\delta = \pi \overline{n}_s = 2\pi M$. Equation (134) can be compared to the corresponding formula (82) for the quasi-1D SDW state in the TST. We see that it is identical, save for the presence of a factor $2\pi y/3$ inside the cosine in the quasi-1D case. This shows that the two states have the same structure, save for a difference in the SDW wave vector, as mentioned above.

VIII. DISCUSSION

In this paper, we have presented a comprehensive analysis of the field-anisotropy phase diagram of the three-leg spin-$\frac{1}{2}$ triangular spin tube, of interest primarily as an approximation to the corresponding two-dimensional Heisenberg model on the anisotropic triangular lattice. Pronounced quantum effects, strongly deviating from the expectations based on classical analysis, occur throughout the phase diagram. In this section, we will discuss the implications of our results for two dimensions, and how robust these quantum effects are to other modifications to the model.

A. Implications for two dimensions

Throughout the paper, we have commented on how results obtained in the one-dimensional TST geometry apply to the two-dimensional spin-$\frac{1}{2}$ system. Here, we summarize these connections, with particular attention to the phase diagram in 2D. With a few exceptions, the phases we obtained for the TST have straightforward analogs in 2D and consequently we expect the 2D diagram to be only slightly modified.

For example, on the isotropic line $R = 0$, away from very small field, all the phases we found are precisely those expected from the semiclassical analysis of Refs. 3 and 4. We expect the semiclassical analysis to only work better in 2D, so the same coplanar and plateau states, and their incommensurate analogs for small anisotropy $0 < R \ll 1$ should occur there as well. We note that all coplanar states are intrinsically stabilized by quantum effects.

Perhaps the most striking feature amongst these states is the $\frac{1}{3}$ magnetization plateau, which extends well beyond the semiclassical regime in our phase diagram for the TST (Fig. 22). In addition to the TST, we have also studied the $\frac{1}{3}$ magnetization plateau for $L_y = 6$ cylinders (see Fig. 25).

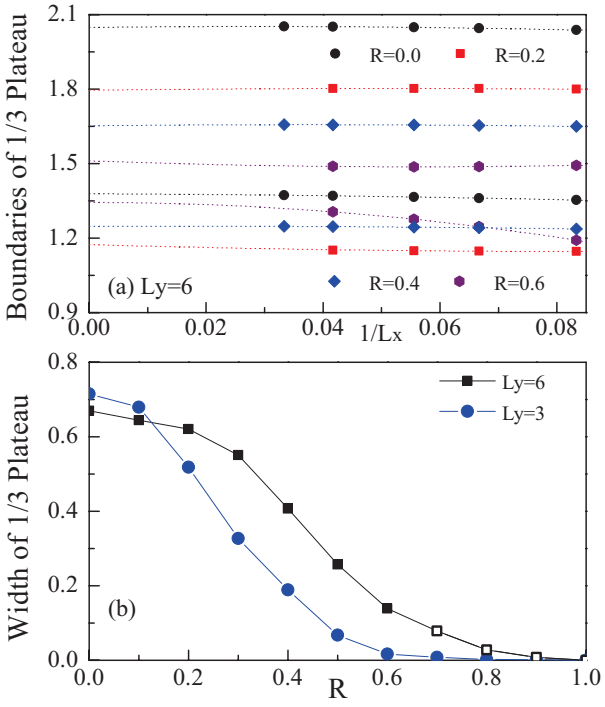

FIG. 25. (Color online) Finite-size scaling of the boundaries of the $\frac{1}{3}$ plateau for cylinders of width $L_y = 6$, and different anistropies: (a) $R = 0.0, 0.2, 0.4, 0.6$. (b) Width of the $\frac{1}{3}$ plateau as a function of R for cylinder of width $L_y = 6$, shown as (black) squares. The data points at $R > 0.6$ (hollow square) are based on a preliminary finite-size scaling for quasi-2D system with $L_x \sim L_y$. The plateau width for $L_y = 3$ (blue circles), from Fig. 22, is shown for comparison.

Close to the isotropic limit $R \ll 1$, the plateau width is only slightly changed by the increase in width from $L_y = 3$ to 6, and its value $\Delta h \approx 0.7J$ agrees well with previous numerical studies.[9,10,49,50] This trend in width is consistent with our picture that for small R, the phases proximate to the plateau are commensurate planar *ordered* ones in the 2D limit. The broken U(1) symmetry of these phases makes them sensitive to infrared quantum fluctuations in the 1D geometry since of course continuous symmetries are unbroken in 1D. Hence, in the thinner cylinders, the commensurate plateau state competes slightly more effectively against the planar phases than in two dimensions, leading to a wider plateau for smaller circumference.

In the intermediate region $0.2 \lesssim R \lesssim 0.7$, the trend is much more striking and *opposite* to that for small R: the plateau width is seen to increase significantly compared with that for $L_y = 3$. The same is true in the larger anisotropy limit $0.7 \lesssim R < 1$, for which our preliminary results, based on the finite-size scaling for quasi-2D systems with $L_x \approx L_y$ (for such highly anisotropic systems, we were unable to converge the $L_x \to \infty$ limit), still suggests a finite $\frac{1}{3}$ plateau, consistent with analytical arguments put forward in Ref. 11 and in Sec. VI. The increase of the plateau width is understood as being due to a greater stability of crystal phases in two dimensions. Our DMRG results strongly support existence of the 2D magnetization plateau state for *all* values of spatial anisotropy $0 < R < 1$.

Several experimental spin-$\frac{1}{2}$ materials with the triangular lattice structure have indeed been observed to support a $\frac{1}{3}$ magnetization plateau, including the well-documented material Cs_2CuBr_4 (Refs. 51 and 52) as well as $Ba_3CoSb_2O_9$, studied more recently.[53] A notable exception is Cs_2CuCl_4, which is isostructural to Cs_2CuBr_4, but does *not* exhibit a magnetization plateau.[54] In our opinion, as explained in detail in Ref. 11, the plateau is destabilized in this case by three-dimensional coupling, which is stronger (relative to the appropriate J) in the Cs-based magnet in comparison with the Br-based one,[55] with perhaps strong Dzyaloshinskii-Moriya (DM) interactions in Cs_2CuCl_4 playing an additional role.[56]

The SDW phase dominates a large fraction of the phase diagram for the TST. This is an entirely quantum phase (since it requires modulation of the *length* of the static moments), which in 2D exhibits incommensurate collinear long-range order along the field direction. Being of quantum origin, one may wonder whether the SDW persists into 2D. Based on renormalization group arguments, discussed extensively in Ref. 11, we know that the SDW indeed must exist in the quasi-1D regime $J' \ll J$, when interchain correlations are relatively weak. We expect that the region occupied by the SDW may be somewhat curtailed in 2D relative to that in the TST, but that it still is quite large. This is based on intuition and numerical evidence that interchain correlations remain suppressed for relatively large J' due to frustration.

Experimental verification of this magnetic state is clearly called for. In this regard, we would like to point out a recent series of experiments on quasi-1D spin-$\frac{1}{2}$ material $LiCuVO_4$. While much of the interest in this material stems from the high-field nematic phase predicted[57] and observed[58] to occur near the saturation field, several experimental studies[59–62] have found strong evidence in favor of an incommensurate longitudinal SDW phase in the intermediate range of magnetic fields. To understand this finding better, it is important to realize that the interchain exchange in this material is of zigzag (triangular) type albeit of predominantly ferromagnetic sign.[63] The considerations of Sec. V make it clear that the SDW phase is not sensitive to the sign of interchain J' and should appear in the model with ferromagnetic J' as well (see for example Ref. 64 for explicit calculations). We thus would like to posit that a recent neutron scattering study,[65] which observed longitudinal spin fluctuations but no transverse ones, is very much consistent with SDW phase scenario. Like the spin nematic phase, which is expected to occur at much higher magnetic fields, the SDW phase does not support low-energy transverse spin excitations. It would also be interesting to seek evidence of a SDW state in Cs_2CuBr_4.

The above aspects of the TST and 2D phase diagrams are qualitatively similar. Qualitative differences are expected at low and high fields. At zero field, the TST exhibits a dimerized phase, which we attribute (Sec. VII) to quantum fluctuation effects specific to one dimension. In 2D, most of the zero-field line should exhibit incommensurate spiral order, with a small region of collinear antiferromagnet at small J'/J, as argued in Ref. 12. At high field, near saturation, where the TST shows both coplanar and cone phases, we saw in Sec. IV D2 that in 2D only the coplanar state occurs. This is a rather surprising result since the coplanar state might be considered more quantum than the cone. This observation poses a tricky problem of

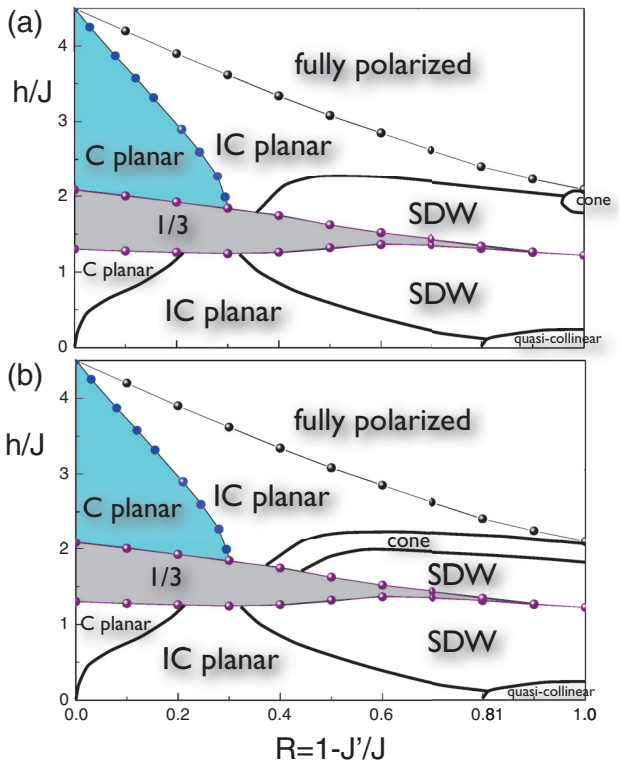

FIG. 26. (Color online) Schematic phase diagrams for the two-dimensional $S = \frac{1}{2}$ system. The shaded regions and boundaries containing full circles are based on preliminary DMRG results for circumference $L_y = 6,9$ systems in addition to the TST with $L_y = 3$. Other boundaries are drawn by hand using the considerations described in the text. Two possible schematics are drawn, differing in the extent of the cone phase. In (a), it is limited to the quasi-1D regime, while in (b), it extends to enclose the SDW state. The latter possibility is more classical. Intermediate or more complex cases are also possible. See text for further explanations.

connecting the limit of field approaching saturation at fixed small J', where the coplanar state is expected, to the limit of vanishing J' at fixed field slightly below saturation, where we instead expect a cone state. In 2D, therefore, a phase boundary must emanate from the saturation point at $J' = 0$, and we do not presently understand where this boundary extends to.

Putting together all these considerations, we can construct schematic phase diagrams for two dimensions. The two simplest possibilities we could construct are shown in Fig. 26. The quasi-1D analysis, which was carried out directly in 2D in Ref. 11, demands the cone, SDW, and plateau phases at nonzero field and small J'/J. It also requires a collinear antiferromagnetic state at zero field and small J'/J. This collinear state is expected to be rapidly destroyed in favor of the SDW as the field is imposed. It is likely to become canted as it does so, but in the absence of a detailed description of this narrow region descending from the collinear antiferromagnet at zero field, we label it "quasicollinear" in the figures. Near the isotropic line, the semiclassical description requires commensurate (C) planar and incommensurate (IC) planar states, as well as the $\frac{1}{3}$ plateau. Finally, near saturation, the dilute spin-flip approach becomes exact, and the solution of the BS equation required the IC planar phase. The shaded

phases and the boundaries containing circles are taken from preliminary DMRG results for more two-dimensional systems with $L_y = 6,9$ lattice spacings around the circumference. The remaining phase boundaries are drawn arbitrarily to connect the known regions demanded by the above reasoning in the simplest possible manner consistent with scaling. The principal uncertainty in the diagrams is the extent of the cone phase. We expect it to occupy a relatively small portion of the phase space, despite the fact that it is the classical ground state everywhere below saturation except on the $R = 0$ line! In the first schematic, Fig. 26(a), the cone state occupies the minimum possible area, while a more semiclassical situation might be as shown in Fig. 26(b).

1. Comparison to other work

It is interesting to compare our results to those of Tay and Motrunich,[10] which is the only other comprehensive study of the full anisotropy-field phase diagram of which we are aware. We caution that a strict comparison is not possible because both their and our predictions for 2D are somewhat schematic, being based on conjectural extrapolation of results for the 1D TST (us) and finite clusters (them). Nevertheless, one notices immediately similarities between their schematic 2D phase diagram, Fig. 10 of their paper, and our Fig. 3. First, the region near the isotropic line is in both cases quite close to semiclassical predictions. Small differences appear at low fields, where indeed quantum effects of the finite systems studied in both works are probably maximal. Second, near the saturation field, they also find a wide range of incommensurate planar phase (called incommensurate V in their study). Our analytical BS analysis indicates that this phase in fact extends over the full range of anisotropy, a fact which was not resolved in their diagram. Third, both studies indicate the robustness of the $\frac{1}{3}$ plateau. As already mentioned above, our results for the width of the plateau $\Delta h \approx 0.8J$ at the isotropic point $R = 0$ agree well with those of Refs. 9 and 10. The more recent exact diagonalization study[49] predicts smaller width, about $0.5J$, but this is based on extrapolating Δh from small-size clusters. For $R > 0$, Ref. 10 is the only one we can compare with, and qualitative agreement is quite good. Our DMRG work completes the phase diagram, demonstrating the $\frac{1}{3}$ plateau existence for all $J' > 0$.

The major distinction between the two works is in our finding of the SDW state in a wide field anisotropy range, where Tay and Motrunich postulate separate spin liquid, spiral (corresponding to our cone state), and quasi-1D regimes. In our work, renormalization group arguments rather clearly establish the SDW phase in the small J'/J regime in 2D, which is the quasi-1D region of Tay and Motrunich. We think it likely that even in 2D, the SDW phase extends to $R \approx 0.5$.

B. Suppressing the quantum effects

As remarked above, we predict two types of quantum states, coplanar phases and collinear SDWs, in the 2D $S = \frac{1}{2}$ model. While remarkably robust in this case, these quantum phases can be suppressed by other changes to the model: larger spins $S > \frac{1}{2}$, three-dimensional coupling, and Dzyaloshinskii-Moriya (DM) interactions.

1. Higher spin

We first consider $S > \frac{1}{2}$, and find that the quantum phases are strongly suppressed. We begin with the vicinity of the saturation field. In Sec. IV D2, we showed that for $S = \frac{1}{2}$ the system forms a coplanar state in this limit for all $0 < J'/J \leqslant 1$. This is surprising since except for the isotropic case, the coplanar phase is not a classical ground state. Using the calculations sketched below, we find that with increasing S, the classical results are recovered, with the coplanar phase restricted to increasingly narrow region near the isotropic limit, where it occurs due to classical degeneracy.

To do so, we use the representation below,[22] which is more convenient than the Holstein-Primakoff one:

$$S^{\dagger}_{\mathrm{r}} = \sqrt{2S}[1 + (K_s - 1)b^{\dagger}_{\mathrm{r}}b_{\mathrm{r}}]b_{\mathrm{r}}, \quad S^{z}_{\mathrm{r}} = S - b^{\dagger}_{\mathrm{r}}b_{\mathrm{r}}, \quad (135)$$

where $K_s = \sqrt{1 - 1/(2S)}$. This expression reproduces the matrix elements of spin-raising and -lowering operators between states with different magnetization *exactly* within the two-magnon (two-spin-flip) subspace. The advantage of this form is that it requires no $1/S$ expansion. Note that for $S = \frac{1}{2}$, Eq. (135) reduces to Eq. (26), thanks to the hard-core condition $(b_{\mathrm{r}})^2 = 0$, while for large $S \gg 1$, we recover Holstein-Primakov asymptote $K_s \sim -1/(4S)$. Note that for $S \geqslant 1$, the hard-core constraint is not required and as a result the U term is absent from the two-magnon Hamiltonian.[25] The Hamiltonian within the two-magnon subspace retains the form in Eq. (28), but now the interaction term is a bit more complicated:

$$\begin{aligned} V(\mathsf{k},\mathsf{k}',\mathsf{q}) &= \frac{1}{2}(J(\mathsf{q}) + J(\mathsf{k}+\mathsf{q}-\mathsf{k}')) - SK_s(J(\mathsf{k}+\mathsf{q}) \\ &\quad + J(\mathsf{k}'-\mathsf{q}) + J(\mathsf{k}) + J(\mathsf{k}')), \\ J(\mathsf{k}) &= 2J\cos[\mathsf{k}_x] + 4J'\cos\left[\frac{\mathsf{k}_x}{2}\right]\cos\left[\frac{\sqrt{3}\mathsf{k}_y}{2}\right]. \end{aligned} \quad (136)$$

Numerical solution of the BS equation (44) for the two-dimensional triangular lattice, which proceeds along the same lines as in Sec. IV D, finds that for higher spins $S \geqslant 1$, near the saturation field the coplanar phase near the isotropic limit is limited to a region $J' > J'_{\mathrm{cr}} > 0$, with a cone phase obtaining instead for $J' < J'_{\mathrm{cr}}$. The critical value monotonically increases with S, taking the values $J'_{\mathrm{cr}}/J \approx 0.1, 0.5, 0.61$ for $S = 1$, $\frac{3}{2}$, and 2, respectively. These findings show that the absence of the cone state for $S = \frac{1}{2}$ found here is a very unusual feature of the most quantum case. Larger, more classical spins do recover the classically expected state, although still in a limited range of J'/J.

We next turn to the SDW phase. Since this state is rooted in the one-dimensional limit, we consider just the limit of weakly coupled chains for $S > \frac{1}{2}$ and in particular $S = 1$. We find that the SDW is completely absent in this case.

To see this, we consider a magnetic field above the lower critical field h_{Δ} needed to overcome the nonzero Haldane gap ($\Delta_{s=1} \approx 0.41J$ for $J' \ll J$). This turns the gapped [and, essentially, decoupled (see Refs. 40, and 66)] spin-1 chains into critical Luttinger liquids.[27,67,68] It turns out that these critical chains are characterized by a Luttinger parameter $K = 1/(4\pi\mathcal{R}^2) \geqslant 1$ for all values of the magnetic field above

the gap closing h_Δ.[67,68] This immediately implies that the scaling dimension of the longitudinal spin density operator $\mathcal{S}^z_{\pi-2\delta}(x)$ in Eq. (72) is $K > 1$ as well, which makes interchain SDW coupling in Eq. (76) (which has twice this scaling dimension) strictly irrelevant. As a consequence, the SDW phase does not occur in the quasi-1D limit. Since this was its most stable regime in the $S = \frac{1}{2}$ case, it may well be that the SDW phase is totally absent for $S = 1$! It would be interesting to check this in future simulations.

What replaces the SDW? The large value of K implies an increased tendency to spin ordering transverse to the field direction, and indeed the twist term [fourth term in Eq. (75)] is instead always relevant, leading to stabilization of the cone state. This result is supported by analytical[27] and numerical[69] studies of the spin-1 zigzag ladder. For example, Ref. 69 finds a finite vector chirality (that is, a cone state) for all values of the magnetization in the case of $J_1 - J_2$ spin-1 chain, along the $J_1 = J_2$ line.

Note that above we found that the cone state was also stabilized for small J'/J in the vicinity of saturation. It is likely then that the cone phase evolves smoothly between the 1D limit $J'/J = 0^+$ and the approach to saturation at finite J'/J. Moreover, the presence of the cone state at small J' implies the absence of any magnetization plateau in that regime. The predictions appear quite similar to those of the semiclassical analysis of Ref. 4, which suggests that the full phase diagram for $S = 1$ might be well described semiclassically. It is clear that in particular the $\frac{1}{3}$ plateau must terminate at some finite (and perhaps not particularly small) value of the J'/J ratio in this case.

2. Three-dimensional coupling

Another experimentally relevant modification of the spin-$\frac{1}{2}$ Hamiltonian is three-dimensional coupling. We consider the simplest case of unfrustrated antiferromagnetic interplane exchange interaction J'' between identical triangular layers. Provided the three-dimensional coupling is unfrustrated, we expect that the particular form is not too important. Such an interaction is expected to make the spin system more classical and thus to promote the classical cone state over the coplanar one.

Considering again the regime near saturation, one may readily solve the BS equation, appropriately modified to the three-dimensional situation. We indeed find that high-field coplanar configuration changes to the cone one for sufficiently large J''/J ratio. When the triangular lattice is isotropic, $J' = J$, this occurs for $(J''/J)_{\rm cr} \approx 0.2$, in agreement with the calculation in Ref. 23. Not unexpectedly, the critical J'' becomes smaller for weaker inter-chain exchange J'. For example, for $J'/J = 0.75$, as perhaps appropriate for Cs_2CuBr_4, we find $(J''/J)_{\rm cr} \approx 0.15$, while for $J'/J = 0.34$ (the Cs_2CuCl_4 case), $(J''/J)_{\rm cr} \approx 0.034$. One-dimensional scaling arguments, described in Appendix B 3, suggest that $(J''/J)_{\rm cr} \sim (J'/J)^2$ when $J'/J \ll 1$, in agreement with the numerical values listed above.

In the 1D limit $J'/J \ll 1$, introduction of unfrustrated $J''/J \ll 1$ disfavors SDW order in favor of a cone phase. This is discussed in detail in Sec. V of Ref. 11. Thus, three-dimensional coupling, if unfrustrated, tends to remove all quantum features of the phase diagram.

3. Dzyaloshinskii-Moriya interactions

A variety of DM interactions can be present in anistotropic triangular lattice systems, depending upon the crystal symmetry and microscopic details. This can lead to diverse effects which are difficult to discuss without being more specific. For the materials Cs_2CuCl_4 and Cs_2CuBr_4, the symmetry-allowed DM interactions were obtained and discussed in detail in Ref. 11. Here, we describe only the effects of the dominant DM term in those materials, which can be written as

$$H_{\rm DM} = \sum_{x,y} \mathbf{D} \cdot \mathbf{S}_{x,y} \times (\mathbf{S}_{x-1,y+1} - \mathbf{S}_{x,y+1}) \qquad (137)$$

in the notation of this paper, with the DM vector $\mathbf{D} = D\hat{\mathbf{a}}$ oriented along the crystallographic a axis, normal to the triangular planes.

Although small, a nonzero D has significant effects in both zero field and when a magnetic field is applied normal to the triangular plane, i.e., parallel to the DM vector. In these situations, unlike the J' interchain coupling, it is not frustrated either by the dominant chain interactions J or by the applied magnetic field. It tends to favor the cone state (or a spiral in zero field), and can obliterate the more quantum coplanar and SDW phases completely if sufficiently strong in this field orientation. Indeed, with this field orientation, an arbitrarily weak DM coupling inevitably forces the state in immediate proximity to the saturated state to be a cone phase, for all values of J'/J. This occurs because the DM coupling splits the degeneracy of the two minimum energy spin wave modes, already at the single spin wave level, making a two-component condensate impossible when the spin-flip magnons are sufficiently dilute.

We note, however, that when the magnetic field is applied normal to the a axis, i.e., in the triangular plane, it itself frustrates the DM interaction. In this situation, the DM interaction is largely ineffective and has only minimal perturbative effects on the spin correlations. These field orientations are therefore optimal for observing quantum effects.

C. Experimental implications and future directions

Our study indicates that a number of "quantum" ordered states may be found in $S = \frac{1}{2}$ anisotropic triangular lattice systems. These states are not so exotic as quantum spin liquids, and are well characterized by their symmetries and associated order parameters. They are instead quantum in the weaker sense that they can not be obtained in the classical limit. Most notably, we obtained a SDW state whose order involves (quasi)periodic modulation of the *length* of the spin expectation value, along the field direction. We suggest this state occupies a wide swath of the field-anisotropy phase diagram, provided perturbations to our model are not too strong.

The particular material Cs_2CuBr_4 appears a good candidate for the observation of the SDW state since three-dimensional coupling is known to be relatively weak there, and experiments have already identified the $\frac{1}{3}$ magnetization plateau. Direct observation of the SDW would consist of observing the incommensurate ordering wave vector evolving monotonically with field, for fields above and below the plateau, and correlating this wave vector with the average magnetization. We expect it to approximately follow the 1D relation $q = \pi(1 - M/M_s)$,

away from the plateau. Given its 1D origin, one might well also expect that the inelastic spectra retain 1D features, such as spinon continua, in the SDW state and even in the plateau state above the gap. Of course, at low energy, in the vicinity of the SDW wave vector, we expect the collective phason mode to dominate. There must therefore be significant rearrangement of the spectra on passing from low to high energy. A more detailed understanding of the spectral evolution with energy, field, and anisotropy may make an interesting subject for future study.

In Cs_2CuBr_4, many additional features suggestive of phase transitions were identified above the $\frac{1}{3}$ plateau in the magnetization process with an in-plane field.[52] Our study indicates that few such transitions should be expected in the pure J-J' model. Likely, additional DM interactions [beyond the one given in Eq. (137)] and perhaps further neighbor couplings are at play. Study of their effects is a possible avenue for more research.

More generally, the richness and surprisingly quantum nature of field-anisotropy phase diagram of the relatively weakly frustrated triangular lattice suggests that the behavior on more frustrated lattices such as the kagome and pyrochlore may be even more interesting. The methods used here should be helpful in attacking these problems.

ACKNOWLEDGMENTS

We would like to thank A. Chubukov, R. Coldea, A. Kolezhuk, M. Mourigal, F. Mila, M. Takigawa, and M. Zhitomirsky for discussions and communications. We acknowledge support from the Center for Scientific Computing at the CNSI and MRL: an NSF MRSEC (DMR-1121053) and NSF CNS-0960316. This research was supported in part by the National Science Foundation under Grants No. NSF DMR-1206809 (L.B., R.C., and H.J.), No. NSF PHY11-25915 (H.C.J.), and No. NSF DMR-1206774 (O.A.S.).

APPENDIX A: SINE-GORDON MODEL AND COMMENSURATE-INCOMMENSURATE TRANSITIONS

In this Appendix, we summarize the commensurate-incommensurate transition (CIT) within the sine-Gordon model, which appears in multiple places throughout the paper. We consider the sine-Gordon action in $d+1$ dimensions, with the form

$$\mathcal{S}_{\rm sg} = \int d^d\mathbf{x}\, d\tau \left\{ \frac{\kappa}{2}(\partial_\tau \vartheta)^2 + \sum_\mu \frac{\rho_\mu}{2}(\partial_\mu \vartheta)^2 - \lambda \cos\left[n(\vartheta - qx)\right] \right\}, \tag{A1}$$

where ϑ is the sine-Gordon field. We can write an alternative expression in terms of the shifted field $\hat{\vartheta} = \vartheta - qx$ so that

$$\mathcal{S}_{\rm sg} = \int d^d\mathbf{x}\, d\tau \left\{ \frac{\kappa}{2}(\partial_\tau \hat{\vartheta})^2 + \sum_\mu \frac{\rho_\mu}{2}(\partial_\mu \hat{\vartheta})^2 + \delta\partial_x\hat{\vartheta} - \lambda\cos[n\hat{\vartheta}] \right\}, \tag{A2}$$

with $\delta = \rho_x q$. In general, large δ prefers an incommensurate state, where the field $\hat{\vartheta}$ is nonuniform and unpinned, while for small δ, a commensurate phase occurs, where $\hat{\vartheta}$ is pinned to a fixed value by the cosine term. The detailed nature of the sine-Gordon model depends upon dimensionality, so we treat the $d = 1$ and $d \geqslant 2$ cases separately.

1. $d \geqslant 2$: Mean-field transition

For $d \geqslant 2$, the fluctuations of the phase field $\hat{\vartheta}$ are small even in the absence of the sine-Gordon term, i.e., for $\lambda = 0$. This can be seen from the fact that, already at the Gaussian level, the free boson propagator is nondivergent at small momentum for $d \geqslant 2$. This implies that the fluctuations of ϑ are bounded, and one can therefore treat the entire problem by a saddle-point approximation. Moreover, one can show that fluctuation effects are negligible in the (quantum) CIT for $d \geqslant 2$. More formally, $D = d + 1 = 2 + 1$ is the upper critical dimension for the CIT.

Therefore, in this case we may proceed by simply minimizing the action in Eq. (A2). The minimum action configuration is independent of the $d-1$ coordinates normal to x and τ. This gives

$$\mathcal{S}_{\rm sg} = L_\perp^{d-1}\beta E_{\rm 1D}, \tag{A3}$$

where $L_\perp$ is the system width in the directions normal to x, and β is the length of the imaginary-time integration. The one-dimensional energy is then

$$E_{\rm 1D} = \int dx \left\{ \frac{\rho}{2}(\partial_x\hat{\vartheta})^2 + \delta\partial_x\hat{\vartheta} - \lambda\cos(n\hat{\vartheta}) \right\}, \tag{A4}$$

where $\rho = \rho_x$. Notice that δ only appears as a boundary term, which means that the energy depends on δ only through the winding number $N = (\hat{\vartheta}(x = L) - \hat{\vartheta}(x = 0))\frac{n}{2\pi}$. Consider the case $N = 0$. Then, the solution is uniform, i.e., $\hat{\vartheta} = 2\pi k/n$, with $k = 0,1,2,\ldots$. With $N = 1$, one obtains a well-known soliton solution of the sine-Gordon model,[36] which reads as

$$\hat{\vartheta}(x) = \frac{4}{n}\arctan\left\{ e^{\pm n\sqrt{\frac{\lambda}{\rho}}(x - x_0)} \right\}, \tag{A5}$$

where x_0 is the location of the center of the soliton. Note that the soliton has a width $w \sim \sqrt{\rho/\lambda}$ and energy $E \sim \sqrt{\rho\lambda}$. This gives a critical value

$$\delta_c = 4\sqrt{\rho\lambda}/\pi, \tag{A6}$$

such that, for $\delta < \delta_c$, domain-wall solitons cost positive energy and so, are unfavorable, resulting in a commensurate wave vector. For $\delta > \delta_c$, it is favorable for solitons to be present, and the minimum energy configuration will be an array of solitons which characterize an incommensurate phase.

Equation (A6) defines the *location* of the CIT phase boundary. We may also discuss its critical properties. On the commensurate side, no solitons are present, which implies the winding number $N = 0$ precisely, and the ground-state energy and field configuration are independent of δ. Thus, there is no visible critical behavior in the ground state (hence in equal-time correlations) in the commensurate phase. On the incommensurate side, however, the minimum energy configuration of $\hat{\varphi}(x)$ depends upon δ. It can be considered as

an array of solitons, whose main characteristic is the spacing ℓ between solitons. This spacing is determined by the balance of the negative energy to introduce a soliton (which favors many solitons with a short spacing) and the repulsive energy of interaction between solitons (which favors large spacing). The repulsive interaction is exponentially small in the separation ℓ in units of the width w. Hence, the energy of the array is

$$E_{1D} = E_{1D}^{C} - (\delta - \delta_c)\frac{2\pi L}{n\ell} + c\sqrt{\rho\lambda}\frac{L}{\ell}e^{-\ell/w}, \quad \text{(A7)}$$

where c is an unimportant constant, and L/ℓ is the total number of solitons. Minimizing this over ℓ, one finds the critical behavior, to leading logarithmic accuracy,

$$\ell \sim w \ln\left[\frac{\delta_c}{\delta - \delta_c}\right] \quad \text{(A8)}$$

for $0 < \delta - \delta_c \ll \delta_c$. The presence of the soliton array implies that the average gradient of the phase $\hat{\vartheta}$ is nonzero, which defines the *incommensurability* wave vector $\overline{q}$:

$$\overline{q} = \overline{\partial_x \hat{\vartheta}} = \frac{2\pi}{n\ell} \sim \frac{1}{w|\ln[\delta - \delta_c|/\delta_c]|}\Theta(\delta - \delta_c). \quad \text{(A9)}$$

The incommensurability $\overline{q}$ in the incommensurate phase gives the shift of the ordering wave vector from its commensurate value. Other critical properties at the CIT in $d \geqslant 2$ are readily obtained from the results above. For example, the ground-state energy density is simply the saddle-point value of E_{1D}, which scales as

$$\frac{E}{L} \sim -\frac{\delta - \delta_c}{|\ln(\delta - \delta_c)|}\Theta(\delta - \delta_c). \quad \text{(A10)}$$

2. $d = 1$: Quantum fluctuations

In the case $d = 1$, fluctuations of the phase field can not be neglected. This can be anticipated from the Gaussian level result that, in the absence of a sine-Gordon term, the free boson Green's function is logarithmically divergent at small momentum, signaling large fluctuations of ϑ. Hence, we must deal directly with the $(1 + 1)$-dimensional action

$$\mathcal{S}_{sg} = \int dx d\tau \left\{ \frac{\kappa}{2}(\partial_\tau \hat{\vartheta})^2 + \frac{\rho}{2}(\partial_x \hat{\vartheta})^2 + \delta\partial_x\hat{\vartheta} - \lambda\cos n\hat{\vartheta} \right\}. \quad \text{(A11)}$$

Once again, δ is the coefficient of a pure boundary term, which simply counts the number of solitons in the system. A finite density of solitons will be generated, provided the energy of a soliton for $\delta = 0$ is compensated by this boundary energy, which equals $2\pi\delta/n$. Thus, we need the energy of a soliton at $\delta = 0$, i.e., in the pure quantum sine-Gordon model.

We estimate this as follows. The scaling dimension of the cosine term Δ_n is easily calculated, and is equal to

$$\Delta_n = \frac{n^2}{4\pi\sqrt{\kappa\rho}}. \quad \text{(A12)}$$

The cosine is relevant when $\Delta_n < 2$, and irrelevant if $\Delta_n > 2$. When it is irrelevant, there is no pinning of the phase field at low energies. A state of this type is known as a "floating phase," and because of the lack of pinning, the state becomes immediately incommensurate for any nonzero δ, i.e., $\delta_c = 0$, and there is no CIT.

When the cosine is relevant, then when $\delta = 0$, the phase is pinned at low energies, and the energy of a soliton is nonzero. We need to estimate this energy to locate the value δ_c which defines the CIT. We do this by renormalization group (RG) arguments. Renormalizing out to a length ξ, the cosine is reduced by fluctuations by an amount proportional to $\xi^{-\Delta_n}$, so $\lambda_{\text{eff}} \sim \lambda\xi^{-\Delta_n}$. For a possible soliton of width ξ, the energy cost is of order

$$\epsilon_s \sim \frac{\rho}{\xi}\left(\frac{2\pi}{n}\right)^2 - \lambda_{\text{eff}}\xi. \quad \text{(A13)}$$

The actual soliton size is determined by optimizing this over ξ, which gives

$$\xi \sim \left(\frac{\rho}{\lambda n^2}\right)^{\frac{1}{2-\Delta_n}}, \quad \text{(A14)}$$

and thus an energy cost for the soliton of order

$$\epsilon_s \sim \lambda^{\frac{1}{2-\Delta_n}}\left(\frac{\rho}{n^2}\right)^{\frac{1-\Delta_n}{2-\Delta_n}}. \quad \text{(A15)}$$

This energy should equal the energy gain $2\pi\delta_c/n$ from the boundary term at the CIT, which gives

$$\delta_c \sim \sqrt{\lambda\rho}\left(\frac{\lambda}{\rho}\right)^{\frac{\Delta_n}{4-2\Delta_n}}. \quad \text{(A16)}$$

Note that this approaches the mean-field result of the previous section when $\Delta_n \to 0$, and becomes very suppressed when $\Delta_n \to 2^-$ (since we must assume $\lambda < \rho$ for consistency of the treatment).

We now turn to the critical behavior, which in $1 + 1$ dimensions is a storied problem in critical phenomena. It is sometimes referred to as a Pokrovsky-Talapov transition, due to the solution by those authors.[70] We recapitulate the essence of the argument. As in the mean-field case, for $\delta < \delta_c$, there are no solitons in the system, and the ground-state energy is independent of δ, i.e., there is no sign of criticality in any static quantity. However, the excitation gap for creating a soliton vanishes linearly with $\delta_c - \delta$. For $0 < \delta - \delta_c \ll \delta_c$, we expect a low density of solitons to be present in the system, again determined by the balance of the (negative) single-soliton energy and the repulsive soliton-soliton interactions.

We must, however, in this case treat the problem quantum mechanically. In particular, we must consider the effects of interactions properly in the low-density limit. In this limit, the kinetic energy and momentum of individual solitons is vanishingly small, and well-known results for low-energy scattering apply. In particular, for short-range repulsively interacting particles in one dimension, the probability of transmission *vanishes* in the low-energy limit. Thus, effectively, regardless of the microscopic strength of the interaction or of its short-distance structure, the solitons behave at low densities as though they were *hard-core* particles, which can not pass one another. To model this behavior, we can treat the solitons as *fermions*. Interactions at longer distances beyond the local hard core are weak and unimportant, so the fermions are effectively *free*.

The free fermion problem is trivially soluble, so we can easily obtain the critical behavior. When $\delta > \delta_c$, we simply fill the negative-energy fermion states to form a Fermi sea. The sine-Gordon model has Lorentz invariance, so the dispersion of the solitons must be relativistic, hence the energy for a single soliton is

$$E_{\rm sol} = \sqrt{\epsilon_s^2 + v^2 k^2} - \frac{2\pi}{n}\delta, \tag{A17}$$

where the velocity $v = \sqrt{\rho/\kappa}$, and $\epsilon_s = 2\pi\delta_c/n$. The Fermi momentum k_F is determined by the condition $E_{\rm sol} = 0$. It will be small near the CIT, so we may expand the relativistic dispersion into its nonrelativistic limit

$$E_{\rm sol}(k_F) = -\frac{2\pi}{n}(\delta - \delta_c) + \frac{k_F^2}{2m} = 0, \tag{A18}$$

with $m = \epsilon_s/v^2$. This determines the Fermi momentum

$$k_F = \left[\frac{4\pi m}{n}(\delta - \delta_c)\right]^{1/2} \sim \sqrt{\delta - \delta_c}. \tag{A19}$$

The density of solitons is just k_F/π, as usual for spinless fermions, so the incommensurability is thus

$$\overline{q} = \frac{2\pi}{n}\frac{k_F}{\pi} = \frac{2k_F}{n} \sim \sqrt{\delta - \delta_c}. \tag{A20}$$

The square-root behavior is quite distinct from the logarithmic one in $d \geqslant 2$. We may also easily obtain the behavior of the ground-state energy density, as the total energy of the Fermi sea,

$$\frac{E}{L} = \int_{-k_F}^{k_F} \frac{dk}{2\pi}\left[\frac{k^2}{2m} - \frac{2\pi}{n}(\delta - \delta_c)\right] \sim -(\delta - \delta_c)^{3/2}\Theta(\delta - \delta_c). \tag{A21}$$

Many more results, e.g., for correlations in the incommensurate phase, can be readily obtained from the free fermion formulation, but we leave this to the reader to discover for themselves in the literature.

APPENDIX B: DETAILED CALCULATIONS OF BS

In this Appendix, we present our solutions to the Bethe-Salpeter (BS) equation in Eq. (44). This equation applies only near saturation field, where the system can be modeled as dilute (hard-core) bosons. We substitute our ansatz, Eq. (46), into the BS equation. With the constraint equation (45), which enforces $s = \frac{1}{2}$, we obtain a set of linear equations for the constants A_i, which can be written in a matrix form as

$$\begin{pmatrix} \tau_{11} & \tau_{12} & \tau_{13} & \tau_{14} & \tau_{15} & \tau_{16} & \tau_{17} \\ 2J\tau_{21} & 2J\tau_{22}+1 & 2J\tau_{23} & 2J\tau_{24} & 2J\tau_{25} & 2J\tau_{26} & 2J\tau_{27} \\ 2J\tau_{31} & 2J\tau_{32} & 2J\tau_{33}+1 & 2J\tau_{34} & 2J\tau_{35} & 2J\tau_{36} & 2J\tau_{37} \\ 2J'\tau_{41} & 2J'\tau_{42} & 2J'\tau_{43} & 2J'\tau_{44}+1 & 2J'\tau_{45} & 2J'\tau_{46} & 2J'\tau_{47} \\ 2J'\tau_{51} & 2J'\tau_{52} & 2J'\tau_{53} & 2J'\tau_{54} & 2J'\tau_{55}+1 & 2J'\tau_{56} & 2J'\tau_{57} \\ 2J'\tau_{61} & 2J'\tau_{62} & 2J'\tau_{63} & 2J'\tau_{64} & 2J'\tau_{65} & 2J'\tau_{66}+1 & 2J'\tau_{67} \\ 2J'\tau_{71} & 2J'\tau_{72} & 2J'\tau_{73} & 2J'\tau_{74} & 2J'\tau_{75} & 2J'\tau_{76} & 2J'\tau_{77}+1 \end{pmatrix} \begin{pmatrix} A_0 \\ A_1 \\ A_2 \\ A_3 \\ A_4 \\ A_5 \\ A_6 \end{pmatrix} = \begin{pmatrix} 1 \\ 2J \\ 0 \\ 2J' \\ 0 \\ 2J' \\ 0 \end{pmatrix}, \tag{B1}$$

where we have defined

$$\tau_{lm}(k,k';\Omega) \equiv \int_q \frac{\mathbf{T}_l(q)\mathbf{T}_m(q)}{\epsilon(k+q)+\epsilon(k'-q)+\Omega}, \tag{B2}$$

$$\mathbf{T}(q) = [1, \cos q_x, \sin q_x, \cos q_y, \sin q_y, \cos(q_x - q_y), \sin(q_x - q_y)], \tag{B3}$$

and $\Omega \propto |h - h_{\rm sat}|$. Although the $\tau'_{lm}s$ are integrals over simple trigonometric functions and other known quantities, e.g., the dispersion, these integrals are divergent in both one and two dimensions and must be treated with care. It is possible, however, to analyze them asymptotically. Once these integrals are evaluated, we can solve for the constants A_i to obtain $\Gamma(q)$ from our ansatz (46). In the next two sections, we take the reader through our asymptotic analysis.

1. Asymptotic behavior of τ_{lm} for the 2D case

In this section, we calculate the τ_{lm}'s for the 2D case. As aforementioned, we are interested in performing asymptotic analysis in the limit $\Omega \to 0$, as the full integrals are too complicated to evaluate fully. We can partition the integrals into the the first two subleading terms $B_{lm}\ln(\Omega) + C_{lm}$, where the constants B,C are independent of Ω. We can consider two cases: one with the same incoming momenta, i.e., the cone phase with $\Gamma_1 = \Gamma(\mathbf{Q},\mathbf{Q},0) = \Gamma(-\mathbf{Q},-\mathbf{Q},0)$, and the other with different incoming momenta, i.e., the coplanar phase with $\Gamma_2 = \Gamma(\mathbf{Q},-\mathbf{Q},0) + \Gamma(\mathbf{Q},-\mathbf{Q},-2\mathbf{Q})$. Here, the wave vector $\mathbf{Q}$ minimizes the dispersion relation in Eq. (29), which can now be substituted into Eq. (B2). After some algebraic simplifications, we obtain

$$\tau_{lm} = \frac{1}{4\pi^2}\int_0^{2\pi} dq_x \int_0^{2\pi} dq_y \frac{\mathbf{T}_l(p)\mathbf{T}_m(p)}{a + b\cos q_y}. \tag{B4}$$

The exact forms of a,b will depend on whether the incoming momenta are the same or different. In this Appendix, we will only present our results for $l = m = 1$, in which case, we can integrate analytically over q_y in Eq. (B4), and obtain the following:

$$\tau_{11} = \int_0^{2\pi} dq_x \frac{1}{\sqrt{a^2 - b^2}}. \tag{B5}$$

To proceed further, we need to specify the exact form of a and b.

(1) *Same incoming momenta*: For the same incoming momenta, a,b take on the form

$$a = \Omega + J[2 + j^2 - (2 - j^2)\cos q_x],$$
$$b = J[-2j^2 \cos(q_x/2)], \tag{B6}$$

where we define $j \equiv J'/J$. The integrand diverges near $q_x = 0$ like $1/q_x$ in the limit $\Omega \to 0$, and thus, the integral is logarithmically divergent. After some analysis, the integral takes on the form

$$\tau_{11} \sim -\frac{1}{2\pi j\sqrt{4 - j^2}} \ln(\Omega) + \frac{\ln[2j(4 - j^2)]}{\pi j\sqrt{4 - j^2}}. \tag{B7}$$

(2) *Different incoming momenta*: For this case, a,b are as follows:

$$a = \Omega + J[2 + j^2 + (-2 + j^2)\cos(q_x) + j\sqrt{4 - j^2}\sin(q_x)]$$
$$b = -2Jj[j\cos(q_x/2) + \sqrt{4 - j^2}\sin(q_x/2)]. \tag{B8}$$

The integrand now has two divergent points at $q_x = 0$ and $q_x = -2\arccos(1 - j^2/2)$. Therefore, in comparison with the previous case, the logarithmic term doubles, and the integral takes on the form

$$\tau_{11} \sim -\frac{1}{\pi j\sqrt{4 - j^2}} \ln(\Omega) + \frac{2\ln[j(4 - j^2)]}{\pi j\sqrt{4 - j^2}}. \tag{B9}$$

2. τ_{lm} for the TST case

In computing the τ_{lm}'s for the TST, we turn the two-dimensional integral in the previous section into a single integral over q_x and a sum over q_y. As one can imagine, the asymptotic behaviors differ in the TST from the 2D in that, in the limit $\Omega \to 0$, the integrals diverge as $1/\sqrt{\Omega}$. Therefore, the two subleading terms of the integrals are $B_{lm}/\sqrt{\Omega} + C_{lm}$, where again B,C are independent of Ω. We present our results for $l = m = 1$ for the two cases of the same and differing incoming momenta.

(1) For the *same incoming momenta*, we obtain the following expression:

$$\tau_{11} = \frac{1}{6\sqrt[4]{j^2 - j + 1}\sqrt{\Omega}} + \frac{4}{3\sqrt{9j^2 + 24\sqrt{(j-1)j+1}\,j - 24j + \frac{36(j-1)}{(j-1)j+1} + 36}} + O(\sqrt{\Omega}), \tag{B10}$$

where again $j \equiv J'/J$.

(2) We now compute τ_{11} for the case of *differing incoming momenta*, in which case the integral evaluates to

$$\tau_{11} = \frac{1}{3\sqrt[4]{(j-1)j+1}\sqrt{\Omega}} + \frac{1}{3\sqrt{3}\sqrt{j(3j + 4\sqrt{(j-1)j+1} - 4)}} + O(\sqrt{\Omega}). \tag{B11}$$

3. Weakly coupled chains limit

In this section, we analytically check the results of Sec. IV D 2 in the limit of weakly coupled chains $J' \ll J$. Recall that the calculation was done for a full two-dimensional lattice. Hereafter, we will use Cartesian coordinates (x,y) for convenience. In this limit, we can express the spin-flip operator as a continuous function of x, which is along the chain direction, while keeping the chain index $\mathsf{y} \in \mathcal{Z}$ discrete. Then, from Eq. (71), we write this operator as $\Psi_{\mathsf{y}}(\mathsf{x}) \sim S^+_{\mathsf{y},\pi}(\mathsf{x})$, where its low-energy theory is described by the following action:

$$\mathcal{S}_{1D} = \sum_{\mathsf{y}} \int d\mathsf{x}\, d\tau \Big\{ \Psi^\dagger_{\mathsf{y}} \left(\partial_\tau - \frac{1}{2m}\partial^2_{\mathsf{x}} - \mu \right) \Psi_{\mathsf{y}} - t(\Psi^\dagger_{\mathsf{y}} i\partial_{\mathsf{x}} \Psi_{\mathsf{y}+1} + \text{H.c.}) + u\Psi^\dagger_{\mathsf{y}}\Psi^\dagger_{\mathsf{y}}\Psi_{\mathsf{y}}\Psi_{\mathsf{y}} + v\Psi^\dagger_{\mathsf{y}}\Psi^\dagger_{\mathsf{y}+1}\Psi_{\mathsf{y}+1}\Psi_{\mathsf{y}} \Big\}. \tag{B12}$$

The spin-flip (magnon) mass $m = 1/J$ follows from the quadratic dispersion of the magnon mode near momentum π in a fully polarized chain. Additional interaction terms describe the hard-core constraint (u term) as well as the transverse ($t = J'_{xy}/2$) and longitudinal ($v = 2J'_z$) parts of the interchain exchange interaction J'. Note that the t term contains a spatial derivative with respect to x, which reflects the frustration of the interchain exchange by the triangular geometry. In addition, this term contains a factor of i from the staggered factor $(-1)^x = e^{i\pi x}$ in Eq. (71), and from the fact that x takes half-integer values on odd chains [see Eq. (2), Fig. 1(a), and Appendix D6 of Ref. 11].

We can analyze each term of Eq. (B12) through simple dimensional analysis, which will deem all these terms to be relevant under RG. Denoting the spatial scale along x as L, we can conclude that $\tau \sim L^2$, Ψ_{y} scale as $1/\sqrt{L}$, while the three interaction terms t, u, and v scale as L. Hence, these are *relevant* interactions and must be included in our analysis of the low-energy theory.

We can Fourier transform Eq. (B12) and write the Hamiltonian that corresponds to this action

$$H_{1D} = \sum_{\mathsf{k}} \Psi^\dagger_{\mathsf{k}} \left(\frac{\mathsf{k}_x^2}{2m} + 2t\mathsf{k}_x \cos[\mathsf{k}_y] - \mu \right) \Psi_{\mathsf{k}} + \frac{1}{2N} \sum_{\mathsf{k},\mathsf{k}',\mathsf{q}} V(\mathsf{k},\mathsf{k}',\mathsf{q}) \Psi^\dagger_{\mathsf{k}+\mathsf{q}} \Psi^\dagger_{\mathsf{k}'-\mathsf{q}} \Psi_{\mathsf{k}'} \Psi_{\mathsf{k}}. \tag{B13}$$

Here, $V(\mathsf{k},\mathsf{k}',\mathsf{q}) = V(\mathsf{q}) = 2u + 2v\cos[\mathsf{q}_y]$. Note that while the range of k_x is not restricted, $-\infty < k_x < \infty$, that of k_y is limited by the lattice $-\pi \leqslant \mathsf{k}_y \leqslant \pi$. This single-particle dispersion contains two degenerate moment at $\mathsf{Q}_1 = (-2tm, 0)$ and $\mathsf{Q}_2 = (2tm, \pi)$.

The single-particle dispersion has two degenerate minima, at $\mathsf{Q}_1 = (-2tm, 0)$ and $\mathsf{Q}_2 = (2tm, \pi)$. We can now compute the renormalized couplings Γ_1, Γ_2 in a similar manner as the previous sections. However, we alter our ansatz of the BS equation (44) to take the form $\Gamma(\mathsf{q}) = A_0 + A_1\cos[\mathsf{q}_y]$ because the odd contribution $\propto \sin[\mathsf{q}_y]$ vanishes under the integral as the denominator in Eq. (44) is even for all combinations of incoming and transferred momenta.

Computing Γ_1,Γ_2 requires one to solve two linear equations for A_0,A_1, which involve 2D integrals over functions with denominators such as $[\mathsf{k}_x^2/m + 16mt^2\sin^2[\mathsf{k}_y/2] + \Omega]$ (for Γ_1) and $[(\mathsf{k}_x - 4mt\sin^2[\mathsf{k}_y/2])/m + 4mt^2\sin^2[\mathsf{k}_y] + \Omega]$ (for Γ_2). We first evaluate these integrals analytically by separating out the leading terms in $\ln[\Omega/(mt^2)]$, then taking the limit $u \to \infty$ to, again, enforce the $s = \frac{1}{2}$ constraint. The expressions are as follows:

$$\frac{\Gamma_1}{8\pi t} = \frac{1+\frac{4}{3}\gamma}{\left(1+\frac{4}{3}\gamma\right)\ln\Upsilon + 4\ln 2 + 4\gamma\left(\frac{4}{3}\ln 2 - 1\right)}, \tag{B14}$$

$$\frac{\Gamma_2}{8\pi t} = \frac{1}{\ln\Upsilon + 2\ln 2}, \tag{B15}$$

where $\gamma = v/(\pi t)$ and $\Upsilon = 16mt^2/\Omega$. Given these forms, we can conclude that $\Gamma_1 > \Gamma_2$ for $\gamma \geqslant \gamma_c = 3\ln 2/(6 - 4\ln 2) \approx 0.644$. Since we are considering the isotropic Heisenberg model, where $\gamma = 4/\pi > \gamma_c$, we observe that the coplanar fan state prevails over the cone state in the $J' \ll J$ limit, in agreement with the full lattice approach in Eq. (48), once the parameters m,t,v are expressed in terms of exchange integrals.

With this approach, we can also estimate the width of the planar fan state near saturation field through simple dimensional analysis of Eq. (B12). Since the chemical potential $\mu = h_{\rm sat} - h$ scales as L^2 and the t interaction scales as L, the phase boundary between the planar and the lower-field phases must scale as $\Delta h \sim (J')^2/J$. This boundary separates the planar fan phase from the cone phase, a region in which a standard bosonization description of Sec. V becomes appropriate. Details of this analysis are presented in Appendix C 2.

Similar reasoning allows one to estimate the stability of the planar fan state with respect to interlayer coupling J'', which is always present in real materials. It is clear that (nonfrustrated) interlayer coupling corresponds to adding a simple single-particle hopping term between layers with a different z-coordinated $\int d\tau d\mathsf{x}\sum_{\mathsf{z}} J''(\Psi^\dagger_{\mathsf{y},\mathsf{z}}\Psi_{\mathsf{y},\mathsf{z}+1} + \text{H.c.})$ term to the action in Eq. (B12). Such a term also scales as L^2, which implies that the phase boundary between the planar and the cone phases in the J'-J'' plane takes on a quadratic shape, $J'' \sim (J')^2/J$.

APPENDIX C: ADDITIONAL ONE-DIMENSIONAL ANALYSIS

The purpose of this Appendix is to show that the TST geometry with three legs is unique in that the renormalized couplings generated through RG produce significantly different physics for $N = 3$ compared to that of $N > 3$, in the limit $J' \ll J$. Moreover, we show that the arguments given below further support our claims in Sec. VII for the existence of a dimerized state near low field. Finally, we conclude this Appendix with a more thorough analysis of the cone state near high fields.

1. Zero-field analysis by quasi-1D methods

We start with the zero-field case of Eq. (1) in the limit of decoupled chains $J' \ll J$, where each Heisenberg chain can be bosonized using the Wess-Zumino-Witten $\mathrm{SU}(2)_1$ theory, with central charge $c = 1$. In this theory, the spin operator can be decomposed into its uniform $\mathbf{M}_y(x) = \mathbf{J}_{R,y}(x) + \mathbf{J}_{L,y}(x)$ and staggered $\mathbf{N}_y(x)$ magnetizations

$$\mathbf{S}_{x,y} \to a_0[\mathbf{M}_y(x) + (-1)^x\mathbf{N}_y(x)], \tag{C1}$$

and its scalar product can be written in the continuum limit

$$\mathbf{S}_{x,y}\cdot\mathbf{S}_{x+1,y} \to (-1)^x\epsilon_y(x), \tag{C2}$$

where $\epsilon_y(x)$ is the staggered dimerization. With $J' = 0$, this theory describes the Luttinger liquid fixed point of the decoupled chains. The scaling dimensions of these continuum operators $\mathbf{M}$, $\mathbf{N}$, and ϵ determine the relevance of each operator as it perturbs this fixed point. The uniform magnetization has scaling dimension 1, whereas both the staggered spin magnetization and the staggered dimerization have scaling dimension $\frac{1}{2}$. These three continuum operators form a closed operator algebra with well-defined operator product expansions (OPEs) used widely in literature.[11–13,71–74] For instance, the product of $\mathbf{J}_R$ and $\mathbf{N}$ can be expanded as

$$J^a(x,\tau)N^b(x',\tau') = \frac{i\epsilon^{abc}N^c(x,\tau) - i\delta^{ab}\epsilon(x,\tau)}{4\pi\left[v(\tau-\tau') - i(x-x') + a_0\sigma_\tau\right]}, \tag{C3}$$

where τ is the imaginary time, $v = \pi J a_0/2$ is the spin velocity, and a_0 is the short-distance cutoff.

Let us now consider interchain Hamiltonian perturbing the decoupled Heisenberg chains

$$V = J'\sum_{y=1}^{3}\sum_x \mathbf{S}_y(x)[(\mathbf{S}_{y+1}(x) + \mathbf{S}_{y+1}(x-1)]. \tag{C4}$$

Perturbation theory is formulated by expanding the partition function $Z = \int e^{-S_0 - \int d\tau V}$ up to quadratic order, i.e.,

$$Z \simeq \int e^{-S_0}\left[1 - \int_\tau V + \frac{1}{2}\mathrm{T}\int_{\tau_1}\int_{\tau_2} V(\tau_1)V(\tau_2)\right], \tag{C5}$$

with an implied short-time cutoff $\alpha = a_0/v$. Here, T is the time-ordering operator. To utilize this perturbation theory and the OPEs, we express Eq. (C4) in terms of continuum operators [Eqs. (C1) and (C2)]:

$$V_1 = 2a_0^2J'\sum_{y=1}^{3}\sum_x \mathbf{M}_y(x)\cdot\mathbf{M}_{y+1}(x), \tag{C6}$$

$$V_2 = -a_0^2J'\sum_{y=1}^{3}\sum_x \mathbf{M}_y(x)\cdot\partial_x\mathbf{M}_{y+1}(x), \tag{C7}$$

$$V_3 = a_0^2J'\sum_{y=1}^{3}\sum_x \mathbf{N}_y(x)\cdot\partial_x\mathbf{N}_{y+1}(x), \tag{C8}$$

$$V_4 = -a_0^2J'\sum_{y=1}^{3}\sum_x \mathbf{N}_y(x)\cdot\frac{1}{2}\partial_x^2\mathbf{N}_{y+1}(x), \tag{C9}$$

where $V = V_1 + V_2 + V_3 + V_4$. It is *crucial* to realize that the periodic boundary conditions enforced in the y direction by the TST system (cf. Fig. 2) allows us to rewrite any operator $\mathcal{O}$ as

$$\sum_{y=1}^{3}\sum_x \mathcal{O}_y\mathcal{O}_{y+1} = \sum_{y=1}^{3}\sum_x \mathcal{O}_y\mathcal{O}_{y+2}. \tag{C10}$$

Using OPEs, one can show that the nearest-neighbor chain couplings of the staggered magnetization and dimerization enter in the third power of J':

$$V = J_3 \sum_{y=1}^{3} \sum_{x} \left(\mathbf{N}_y(x) \cdot \mathbf{N}_{y+1}(x) - \frac{3}{2} \epsilon_y(x) \epsilon_{y+1}(x) \right), \quad \text{(C11)}$$

where $J_3 > 0$ and $J_3 \propto (J')^3$. This is done by first generating $\partial_x \mathbf{N}_{y-1} \partial_x \mathbf{N}_{y+1}$ by quadratic in $V_3 + V_4$ terms. Next, this term is fused with V_1 to generate the $J_3 \propto (J')^3$ interaction. The calculations are similar to those described in Refs. 11–13 and 73 and 74, and refer the reader to these papers for more details.

In a 2D system,[11,12] however, we find that the generated term is instead quartic in J', with interaction constant $J_4 \sim (J')^4/J^3$ and is of the opposite (negative) sign $J_4 < 0$ in comparison with J_3 above. It turns out that $J_3 \sim (J')^3 > 0$ is a feature of the $N = 3$ TST model *only*: wider tubes with $N > 3$ are analogous to the 2D case, where the renormalized couplings $\sim (J')^4/J^3 < 0$. Note that this difference is important as it implies that spin tubes with $N > 3$ are not frustrated by the periodic BC along the y direction.

Going back to the $N = 3$ TST, both of the generated interactions in Eq. (C11) are strongly relevant (scaling dimension 1) and scale to strong coupling under RG transformations. It would appear that because of the greater numerical coefficient of $\epsilon_y \epsilon_{y+1}$ in Eq. (C11), it is the dimerized ground state that emerges from the competition in the strong coupling. However, this argument is not complete as it neglects the crucially important effect of marginally irrelevant in-chain backscattering term $\propto \mathbf{J}_R \cdot \mathbf{J}_L$, which in fact breaks the symmetry between the $\mathbf{N}_y \cdot \mathbf{N}_{y+1}$ and $\epsilon_y \epsilon_{y+1}$ interactions in favor of the first one.[12] This outcome is not unexpected as it is well known that in-chain marginal current-current interaction spoils the extended $SU(2)_R \times SU(2)_L$ symmetry of the Heisenberg chain by subleading logarithmic corrections which modify chain spin correlations as follows:[75,76]

$$\begin{aligned} \langle \mathbf{N}_y(x) \mathbf{N}_y(0) \rangle &= (\ln[x])^{1/2} x^{-1}, \\ \langle \epsilon_y(x) \epsilon_y(0) \rangle &= (\ln[x])^{-3/2} x^{-1}. \end{aligned} \quad \text{(C12)}$$

Essentially, the same mechanism promotes interchain $\mathbf{N}_y \cdot \mathbf{N}_{y+1}$ interaction over that of staggered dimerizations. In the infinite 2D lattice, this leads to the stabilization of the collinear antiferromagnetic phase,[12] which, however, is not possible in the TST geometry.

It is important to realize at this point that the relevant $J_3 \sum_y \mathbf{N}_y \cdot \mathbf{N}_{y+1}$ interaction, which describes nonfrustrated coupling of staggered magnetizations on neighboring chains, changes the geometry of the system into that of a *rectangular* spin tube. The renormalized, relevant coupling J_3 becomes comparable to the intrachain exchange J under RG and forces Néel vectors $\mathbf{N}_{1,2,3}$ to order into the familiar 120° pattern on every rung. Our 1D reasoning stops at this scale, but further progress can be made by assuming that the spin tube with $J_3 \sim J$ can be accessed from the opposite limit of the strong rung exchange $J_\perp \gg J$.[77] In this limit, the spins on each rung form three-spin triangles that interact via $J_\perp = J_3$, and are coupled to neighboring triangles by a weak exchange J. The ground state of each triangle is fourfold degenerate and is characterized by *two* quantum numbers, total spin $s_{\text{rung}} = \frac{1}{2}$ and chirality τ, which is itself another pseudo-spin-$\frac{1}{2}$ object. The physical meaning of τ is just a sense of either a clockwise or a counterclockwise rotation of the "unpaired" spin-$\frac{1}{2}$ in the ground state of the individual triangle. In other words, in addition to spin $\frac{1}{2}$, the ground state now carries finite momentum $\pm 2\pi/3$ due to chirality. Focusing on this low-energy subset of triangle's states, one can derive spin-orbital Hamiltonian[78]

$$\begin{aligned} H_{\text{so}} = \frac{J_\perp}{N} \sum_x \mathbf{s}_{\text{rung}}(x) \cdot \mathbf{s}_{\text{rung}}(x+1) \\ \times [1 + \alpha_N (\tau_x^+ \tau_{x+1}^- + \tau_x^- \tau_{x+1}^+)] \end{aligned} \quad \text{(C13)}$$

describing correlated dynamics of spins and chiralities. For the triangular ladder considered here, $N = 3$ and $\alpha_N = 4$. The presented arguments remain valid for any *odd* N, however. See Ref. 78 for $N = 5$ and Ref. 79 for $N > 5$. Analytical[77,80] and numerical[78,81,82] studies of the model (C13) find dimerized ground state, in agreement with our consideration in Sec. VII A. Figure 23, which shows oscillatory behavior of the entanglement entropy for different values of R, represents clear evidence of the dimerized ground state.

Finally, we conclude by discussing the way to generate an interaction of the uniform magnetizations from the next-neighboring chains. This is done by fusing V_1 in Eq. (C6) with itself, which yields, under Eq. (C5),

$$\begin{aligned} \delta H_{\text{MM}} = -\frac{(2J')^2}{2} \sum_y \int_x \int_{x'} \left\langle M_y^z(x,\tau) M_y^z(x',\tau') \right\rangle \\ \times M_{y-1}^z M_{y+1}^z. \end{aligned} \quad \text{(C14)}$$

Because the result is converging, the integral of the yth chain correlation function can be extended to the full $x - v\tau$ plane. This, using important short-distance cut-off $\sim a_0 \text{sign}(\tau)$ and $y = v\tau$ (see Ref. 74 for detailed discussion), leads to

$$\int_{-\infty}^{\infty} dx \int_{-\infty}^{\infty} dy \left(\frac{1}{[y + ix + a_0 \text{sign(y)}]^2} + \text{H.c.} \right) = 4\pi. \quad \text{(C15)}$$

As a result, we obtain for the amplitude of $\delta\gamma_{\text{MM}} = (J')^2/(\pi v)$, where v is magnetization-dependent spin velocity.

2. Cone state

Now, turn on the magnetic field. When a large enough magnetic field is applied to the TST, the "twist" order, the fourth term in Eq. (75), becomes more relevant than the SDW. This was discussed in previous papers for the two-chain ladder[27] as well as the 2D triangular lattice.[11,12] As both the SDW and the cone interaction amplitudes in Eq. (75) are of the order J', the relative importance of the two interactions can be estimated[12] from a comparison of their scaling dimensions $\Delta_{\text{saw}} = 1/(2\pi\mathcal{R}^2)$ and $\Delta_{\text{cone}} = 1 + 2\pi\mathcal{R}^2$. These two dimensions are equal when $2\pi\mathcal{R}^2 = (\sqrt{5} - 1)/2$, which takes place at sufficiently high magnetization $M \approx 0.6 M_{\text{sat}}$. Because of rather steep dependence $M(h)$ of the magnetization on the magnetic field near the saturation, this value of magnetization corresponds to $h \approx 0.9 h_{\text{sat}}$ (see Fig. 2 in Ref. 12). A similar conclusion is obtained by comparing mean-field transition temperatures of these two ordered states as functions of magnetization (see Ref. 11).

These arguments, however, are not complete because they do not take into account the fluctuation-generated interactions between spin densities on *next-nearest* chains. The most important of these in the presence of an external magnetic field is given by

$$V'_{\rm cone} = \delta\gamma_{\rm cone} \sum_y \int dx \mathcal{S}^+_{\pi,y} \mathcal{S}^-_{\pi,y+2} + \text{H.c.} \qquad \text{(C16)}$$

Even though the generated coupling constant is small $\delta\gamma_{\rm cone} \ll J'/J \ll 1$, this interaction does not involve spatial derivatives and has scaling dimension $2\pi\mathcal{R}^2$ which approaches $\frac{1}{2}$ as $h \to h_{\rm sat}$. Thus, this is a strongly relevant term.

In a 2D system,[11,12] $\delta\gamma_{\rm cone} \sim (J')^4/J^3 < 0$ as discussed in the previous section. [Note that Eq. (C16) is written in the "sheared" system of coordinates.] When translated into Cartesian coordinates, it implies antiferromagnetic (positive) exchange interactions between spins on next-nearest chains at the same position x along the chain.[12] Crucially, as emphasized in the previous section, the TST geometry allows for a stronger renormalized coupling, of the order of $\delta\gamma_{\rm cone} \equiv J_3 \sim (J')^3/J^2 > 0$.

The difference is due to slightly different routes to (C16) in 2D and $N = 3$ TST geometries. One can first show that, when you start from the original cone interaction

$$V_{\rm cone} = \gamma_{\rm cone} \sum_y \int dx \mathcal{S}^+_{\pi,y} \partial_x \mathcal{S}^-_{\pi,y+1} + \text{H.c.}, \qquad \text{(C17)}$$

one can couple the derivatives $\partial_x \mathcal{S}^\pm_\pi$ on the next-nearest chains y and $y+2$,

$$V''_{\rm cone} \sim \frac{\gamma^2_{\rm cone}}{v} \sum_y \int dx \partial_x \mathcal{S}^+_{\pi,y} \partial_x \mathcal{S}^-_{\pi,y+2} + \text{H.c.} \qquad \text{(C18)}$$

This step parallels calculations leading to Eq. (C11) with minor variation due to U(1) symmetry of the system in the presence of an external magnetic field. In this situation, the scaling dimension of the $\mathcal{S}_\pi$ field is smaller than $\frac{1}{2}$ which leads to a slightly different numerical prefactor in the renormalization. However, the functional dependence on J' remains the same. Second, for all $N > 3$ one also needs to generate

$$V'_{\rm MM} = -\delta\gamma_{\rm MM} \sum_y \int dx M^z_y M^z_{y+2}, \qquad \text{(C19)}$$

which was described in the end of the previous section (Appendix C 1). Here, $\delta\gamma_{\rm MM} \sim (J')^2/J$. Fusing next (C18) and (C19) together leads to the result (C16). In the $N = 3$ TST, however, the second step is not required due to Eq. (C10), and we end up with a larger coupling of the order $\delta\gamma_{\rm cone} \sim (J')^3/J^2 > 0$ in Eq. (C16).

To compare the original $V_{\rm cone}$ with the generated $V'_{\rm cone}$ quantitatively, we can estimate the RG scale ℓ at which the coupling constant of the interaction becomes of the order one (in units of spin velocity v). For Eq. (C17) this is, with logarithmic accuracy, $\ell_{\rm cone} \sim -\ln(J')/(2-\Delta_{\rm cone}) = -\ln(J')/(1-2\pi\mathcal{R}^2)$, while for Eq. (C16) it is $\ell_3 \sim -3\ln(J')/(2-2\pi\mathcal{R}^2)$. We immediately conclude that $\ell_3 < \ell_{\rm cone}$ for all values of $2\pi\mathcal{R}^2 \in (1, \frac{1}{2})$, i.e., that the generated cone interaction term Eq. (C16) is more relevant than the bare one for all values of magnetization in the case of $N = 3$ TST. Similar consideration allows us to analyze the competition between the generated cone $V'_{\rm cone}$ interaction and the SDW one, which is characterized by the RG scale $\ell_{\rm SDW} \sim -2\pi\mathcal{R}^2 \ln(J' \sin[\delta])/(4\pi\mathcal{R}^2 - 1)$. We find that $\ell_{\rm SDW} < \ell_3$ for $1 \geqslant 2\pi\mathcal{R}^2 \geqslant \sqrt{7} - 2 \approx 0.65$, which corresponds to low-to-intermediate range of magnetization $M \gtrsim 0.25$. At higher M, however, the modified cone interaction takes over the SDW one. (For the 2D case, the comparison is less conclusive as the result sensitively depends on numerical factors inside the argument of the logarithm.[11])

We now investigate the consequences of the strong $J_3 \equiv \delta\gamma_{\rm cone}$ interaction in Eq. (C16) for the TST problem. In the high-field region where SDW fluctuations are suppressed, the Hamiltonian of the system is given by the sum of H_0 in Eq. (69), the generated direct coupling $V'_{\rm cone}$ in Eq. (C16), and the original cone interaction $V_{\rm cone}$ in Eq. (C17), which now is a subleading one in comparison with (C16). With this, we perform Abelian bosonization form of the interaction potential and arrive at the following expression:

$$\begin{aligned} H^{\rm TST}_{\rm cone} = J_3 \int dx \{ &\cos[\beta(\theta_1 - \theta_2)] + \cos[\beta(\theta_2 - \theta_3)] \\ &+ \cos[\beta(\theta_3 - \theta_1)]\} + \frac{\beta J'}{2} \int dx \{\partial_x(\theta_1 + \theta_2) \\ &\times \sin[\beta(\theta_1 - \theta_2)] + \partial_x(\theta_2 + \theta_3) \sin[\beta(\theta_2 - \theta_3)] \\ &+ \partial_x(\theta_3 + \theta_1) \sin[\beta(\theta_3 - \theta_1)]\}. \end{aligned} \qquad \text{(C20)}$$

For $J_3 \gg J'$, which is the appropriate regime according to our RG arguments above, this potential is minimized by configurations with $\cos[\beta(\theta_y - \theta_{y+1})] = -1/2$ for all y. This allows for two different values of sine terms $\sin[\beta(\theta_y - \theta_{y+1})] = \pm\sqrt{3}/2$. In fact, different signs describe states with different vector chiralities defined as

$$\kappa^z_y = (\mathbf{S}_y \times \mathbf{S}_{y+1})_z \sim \sin[\beta(\theta_y - \theta_{y+1})]. \qquad \text{(C21)}$$

Thus, different signs of κ^z_y correspond to different senses of rotation (clockwise or counterclockwise) of $e^{i\beta\theta_y}$ as we go from one chain to the next. These chiralities also represent useful order parameter describing two degenerate cone states.[83]

To account for the subleading twist terms with spatial derivatives in Eq. (C20), we shift $\theta_y \to \theta_y + \upsilon x$, where υ is determined by the requirement that in the new ground state, the bosonic field θ is twistless, i.e., $\langle \partial_x \theta_y \rangle = 0$. Minimizing $H_0 + H^{\rm TST}_{\rm cone}$ over υ, we find

$$\upsilon = -\beta J' \langle \sin[\beta(\theta_y - \theta_{y+1})] \rangle \sim -J' \kappa^z_y. \qquad \text{(C22)}$$

This shows that the doubly degenerate cone state is characterized by incommensurate transverse spin correlations, by virtue of the relation $\mathcal{S}^+_y = (-1)^x e^{i\beta\theta_y} \to \exp[i(\pi + \upsilon)x + i\beta\theta_y]$. Depending on the spontaneously chosen vector chirality, Eq. (C21), transverse spin correlations are picked at either $Q_{1,x} = \pi + \upsilon$ (for $\kappa^z_y > 0$) or $Q_{2,x} = -\pi + \upsilon$ (for $\kappa^z_y < 0$) along the chain.

APPENDIX D: TRANSFORMATION PROPERTIES OF $\mathbb{Z}_2$ VORTICES

In this Appendix, we address the transformation properties of the $\mathbb{Z}_2$ vortex instanton operator ψ. We give several arguments. First, these properties have been implicitly obtained in the case of a three-leg spin tube, slightly different

from the one studied here, in Ref. 84. There, the authors explicitly evaluate the Berry phase contribution to the action for instantons on the lattice. Microscopically, the instantons are associated with columns of spatial *links* along the x direction of the cylinder (see below how this arises in another formulation). They showed that, due to the Berry phase, a single pair of instantons (an odd number of instantons can not occur) is accompanied by a weight

$$e^{iS_{\rm BP}} = e^{2\pi i S(x-x')}, \tag{D1}$$

where x and x' are the locations of the instantons. For half-integer spins, this gives an oscillating factor equal to $+1$ or -1 if the separation between instantons is even or odd, respectively. From this we can extract the transformation properties. If we translate *one* of the instantons, $x \to x+1$, we see that the weight in Eq. (D1) changes sign. This requires $\psi \to -\psi$, in agreement with Eq. (115). Under inversion P about a lattice site, the instantons, which live on the links, change from the even to odd sublattice of bonds and vice versa. Inverting a single instanton, therefore, changes the parity of x, and hence also the sign of the weight in Eq. (D1). Thus, again, ψ is odd under inversion, in agreement with Eq. (116). Since the instantons do not move under time reversal or translation along y, the invariance of ψ under these operations is obvious. Thus, for the case $L_y = 3$, for the model studied in Ref. 84, the symmetry of the instanton operator is determined as shown in the text.

We turn now to an alternative derivation of the transformation laws, which gives the general result, and clarifies its generality. Here, we follow the general strategy of Ref. 85, in which the $\mathbb{Z}_2$ vortices are explicitly separated from the smooth configurations of the SO(3) order parameter using a slave-particle construction. This is achieved by writing the unit vectors defining the SO(3) matrix in terms of a "slave spinon" z_α:

$$\hat{\mathbf{n}}_1 + i\hat{\mathbf{n}}_2 = \epsilon_{\alpha\beta} z_\beta \boldsymbol{\sigma}_{\alpha\gamma} z_\gamma, \tag{D2}$$

where the complex, two-component vector z_α is constrained to have unit norm $\sum_\alpha z_\alpha^* z_\alpha = 1$. This representation faithfully reproduces the orthonormality constraints on the $\hat{\mathbf{n}}_i$, but is two to one: the physical order parameter $\mathcal{O}$ is unchanged by the transformation $z_\alpha \to -z_\alpha$. This is actually a gauge invariance since the transformation is made locally. The $\mathbb{Z}_2$ vortex is a configuration in which, on encircling the center of the defect, z_α returns not to itself but to $-z_\alpha$.

As explained in Ref. 85, a low-energy effective theory, appropriate to describe the regime with a local spiral order, as well as a quantum disordered phase, is a $(2+1)$-dimensional $\mathbb{Z}_2$ gauge theory coupled to the spinon variables z_α. We refer the reader to Ref. 85 for details. The $\mathbb{Z}_2$ vortex in this theory appears as a configuration of a spinon field which has a discontinuity $z_\alpha \to -z_\alpha$ across a semi-infinite "cut" emanating from the vortex. This $\mathbb{Z}_2$ vortex is accompanied by an Ising vortex, the so-called vison, which is itself a defect with a nonzero Ising gauge field crossing the same semi-infinite cut. In this way, the topological defects of the spiral magnet become identified with the visons of the $\mathbb{Z}_2$ gauge theory.

The discussion in the previous paragraph applies to $\mathbb{Z}_2$ vortices in two-dimensional space, which are particles in the $(2+1)$-dimensional theory. We need to go from this to the description of instantons in the $(1+1)$-dimensional theory obtained by applying periodic boundary conditions in the y direction. A $(1+1)$-dimensional instanton can be viewed as an event in which a pair of $\mathbb{Z}_2$ vortices is nucleated: one of them winds around the cylinder and finally arrives back at the other $\mathbb{Z}_2$ vortex and annihilates it. We can, by the previous argument, consider the particles nucleated and annihilated to be visons in the gauge theory.

Such a process was considered in Ref. 86 (in the Supplemental Material), where it was shown that the operator representing this process in the Ising gauge theory has the transformation properties in Eqs. (115) and (116), i.e., this operator can be viewed as a staggered dimerization operator for odd L_y. There, a rectangular lattice gauge theory was studied, but the basic physics is quite general. Let us consider the translation. We ask about the amplitude to first wind one vison around the cylinder at position x, and then wind another at position $x+1$. The overall phase of the amplitude for both processes taken together gives the transformation property of the instanton operator under translation. The visons reside at the plaquette centers of the original lattice, and the winding trajectories form closed circles at fixed x, circumnavigating the cylinder. Together, these two events form two such circles that enclose one column of sites in the lattice. The fundamental property of a vison is that it has a mutual statistical interaction with "electric" gauge charges, with the wave function acquiring a phase of π whenever one encircles the other. For a $S = \frac{1}{2}$ system, a unit gauge charge is present at every lattice site: this represents the physical spin at each site. The net effect of the two events together is that one vison is wound around each site of the lattice between the two circles, leading to an overall amplitude of $(-1)^{L_y}$ for the two processes together. Here, L_y is the number of sites contained between the two circles. This gives the result in Eq. (115). Note that we may also roughly understand this phase factor by considering the smooth rotations of microscopic spins between the two contours, all of which rotate by 2π, and due to their $s = \frac{1}{2}$ spinor transformation properties, each acquires a minus sign. A similar argument shows that spatial inversion gives the same phase factor. Explicit calculations for these factors in the Ising gauge theory can be found in Ref. 86. Note that these arguments do not depend at all on the interactions in the model, just the presence of these symmetries and fundamental statistics of the particles.

[1] B. Bernu, C. Lhuillier, and L. Pierre, Phys. Rev. Lett. **69**, 2590 (1992).
[2] S. R. White, Phys. Rev. Lett. **69**, 2863 (1992).
[3] A. V. Chubukov and D. I. Golosov, J. Phys.: Condens. Matter **3**, 69 (1991).
[4] J. Alicea, A. V. Chubukov, and O. A. Starykh, Phys. Rev. Lett. **102**, 137201 (2009).
[5] K. Okunishi and T. Tonegawa, J. Phys. Soc. Jpn. **72**, 479 (2003).
[6] F. Heidrich-Meisner, I. A. Sergienko, A. E. Feiguin, and E. R. Dagotto, Phys. Rev. B **75**, 064413 (2007).

[7] T. Hikihara, T. Momoi, A. Furusaki, and H. Kawamura, Phys. Rev. B **81**, 224433 (2010).
[8] A. Honecker, J. Schulenburg, and J. Richter, J. Phys.: Condens. Matter **16**, S749 (2004).
[9] D. J. J. Farnell, R. Zinke, J. Schulenburg, and J. Richter, J. Phys.: Condens. Matter **21**, 406002 (2009).
[10] T. Tay and O. I. Motrunich, Phys. Rev. B **81**, 165116 (2010).
[11] O. A. Starykh, H. Katsura, and L. Balents, Phys. Rev. B **82**, 014421 (2010).
[12] O. A. Starykh and L. Balents, Phys. Rev. Lett. **98**, 077205 (2007).
[13] A. P. Schnyder, O. A. Starykh, and L. Balents, Phys. Rev. B **78**, 174420 (2008).
[14] H. Kawamura and S. Miyashita, J. Phys. Soc. Jpn. **54**, 4530 (1985).
[15] H. C. Jiang, M. Q. Weng, Z. Y. Weng, D. N. Sheng, and L. Balents, Phys. Rev. B**79**, 020409(R) (2009).
[16] C. Griset, S. Head, J. Alicea, and O. A. Starykh, Phys. Rev. B **84**, 245108 (2011).
[17] P. Calabrese and J. Cardy, J. Stat. Mech.: Theor. Exp. (2004) P06002.
[18] T. Hikihara and A. Furusaki, Phys. Rev. B **69**, 064427 (2004).
[19] M. E. Zhitomirsky, Phys. Rev. B **54**, 353 (1996).
[20] T. Matsubara and H. Matsuda, Prog. Theor. Phys. **16**, 569 (1956).
[21] E. Batyev and L. Braginskiı, ZhETF **87**, 1361 (1984) [Sov. Phys.–JETP **60**, 781 (1984)].
[22] E. G. Batyev, ZhETF **89**, 308 (1985) [Sov. Phys.–JETP **62**, 173 (1986)].
[23] T. Nikuni and H. Shiba, J. Phys. Soc. Jpn. **64**, 3471 (1995).
[24] H. T. Ueda and K. Totsuka, Phys. Rev. B **80**, 014417 (2009).
[25] A. K. Kolezhuk, F. Heidrich-Meisner, S. Greschner, and T. Vekua, Phys. Rev. B **85**, 064420 (2012).
[26] S. Sachdev, *Quantum Phase Transitions* (Cambridge University Press, Cambridge, 2001).
[27] A. Kolezhuk and T. Vekua, Phys. Rev. B **72**, 094424 (2005).
[28] A. Abrikosov, L. Gor'kov, and I. Dzyaloshinski, *Methods of Quantum Field Theory in Statistical Physics* (Dover, New York, 1975).
[29] S. T. Beliaev, ZhETF **34**, 417 (1958) [Sov. Phys.–JETP **7**, 289 (1958)].
[30] S. T. Beliaev, ZhETF **34**, 433 (1958) [Sov. Phys.–JETP **7**, 299 (1958)].
[31] I. Affleck and M. Oshikawa, Phys. Rev. B **60**, 1038 (1999).
[32] N. M. Bogoliubov, A. G. Izergin, and V. E. Korepin, Nucl. Phys. B **275**, 687 (1986).
[33] S. Qin, M. Fabrizio, L. Yu, M. Oshikawa, and I. Affleck, Phys. Rev. B **56**, 9766 (1997).
[34] D. C. Cabra, A. Honecker, and P. Pujol, Phys. Rev. B **58**, 6241 (1998).
[35] S. Eggert and I. Affleck, Phys. Rev. B **46**, 10866 (1992).
[36] P. Chaikin and T. Lubensky, *Principles of Condensed Matter Physics* (Cambridge University Press, Cambridge, UK, 2000).
[37] M. Oshikawa, M. Yamanaka, and I. Affleck, Phys. Rev. Lett. **78**, 1984 (1997).
[38] M. Q. Weng, D. N. Sheng, Z. Y. Weng, and R. J. Bursill, Phys. Rev. B **74**, 012407 (2006).
[39] S. Yunoki and S. Sorella, Phys. Rev. B **74**, 014408 (2006).
[40] T. Pardini and R. R. P. Singh, Phys. Rev. B **77**, 214433 (2008).
[41] R. F. Bishop, P. H. Y. Li, D. J. J. Farnell, and C. E. Campbell, Phys. Rev. B **79**, 174405 (2009).
[42] D. Heidarian, S. Sorella, and F. Becca, Phys. Rev. B **80**, 012404 (2009).
[43] A. Weichselbaum and S. R. White, Phys. Rev. B **84**, 245130 (2011).
[44] F. D. M. Haldane, Phys. Rev. Lett. **61**, 1029 (1988).
[45] T. Dombre and N. Read, Phys. Rev. B **39**, 6797 (1989).
[46] H. Kawamura and S. Miyashita, J. Phys. Soc. Jpn. **53**, 4138 (1984).
[47] T. Senthil, L. Balents, S. Sachdev, A. Vishwanath, and M. P. A. Fisher, Phys. Rev. B **70**, 144407 (2004).
[48] B. S. Shastry and B. Sutherland, Phys. Rev. Lett. **47**, 964 (1981).
[49] T. Sakai and H. Nakano, Phys. Rev. B **83**, 100405 (2011).
[50] S. Yoshikawa, K. Okunishi, M. Senda, and S. Miyashita, J. Phys. Soc. Jpn. **73**, 1798 (2004).
[51] T. Ono, H. Tanaka, H. Aruga Katori, F. Ishikawa, H. Mitamura, and T. Goto, Phys. Rev. B **67**, 104431 (2003).
[52] N. A. Fortune, S. T. Hannahs, Y. Yoshida, T. E. Sherline, T. Ono, H. Tanaka, and Y. Takano, Phys. Rev. Lett. **102**, 257201 (2009).
[53] Y. Shirata, H. Tanaka, A. Matsuo, and K. Kindo, Phys. Rev. Lett. **108**, 057205 (2012).
[54] Y. Tokiwa, T. Radu, R. Coldea, H. Wilhelm, Z. Tylczynski, and F. Steglich, Phys. Rev. B **73**, 134414 (2006).
[55] T. Ono, H. Tanaka, O. Kolomiyets, H. Mitamura, F. Ishikawa, T. Goto, K. Nakajima, A. Oosawa, Y. Koike, K. Kakurai *et al.*, Prog. Theor. Phys. Suppl. **159**, 217 (2005).
[56] K. Y. Povarov, A. I. Smirnov, O. A. Starykh, S. V. Petrov, and A. Y. Shapiro, Phys. Rev. Lett. **107**, 037204 (2011).
[57] M. E. Zhitomirsky and H. Tsunetsugu, Europhys. Lett. **92**, 37001 (2010).
[58] L. Svistov, T. Fujita, H. Yamaguchi, S. Kimura, K. Omura, A. Prokofiev, A. Smirnov, Z. Honda, and M. Hagiwara, Pis'ma v ZhETF **93**, 24 (2011) [JETP Lett. **93**, 21 (2011)].
[59] N. Büttgen, H.-A. Krug von Nidda, L. E. Svistov, L. A. Prozorova, A. Prokofiev, and W. Aßmus, Phys. Rev. B **76**, 014440 (2007).
[60] T. Masuda, M. Hagihala, Y. Kondoh, K. Kaneko, and N. Metoki, J. Phys. Soc. Jpn. **80**, 113705 (2011).
[61] N. Büttgen, P. Kuhns, A. Prokofiev, A. P. Reyes, and L. E. Svistov, Phys. Rev. B **85**, 214421 (2012).
[62] M. Takigawa (private communication).
[63] M. Enderle, C. Mukherjee, B. Fk, R. K. Kremer, J.-M. Broto, H. Rosner, S.-L. Drechsler, J. Richter, J. Malek, A. Prokofiev *et al.*, Europhys. Lett. **70**, 237 (2005).
[64] M. Sato, T. Hikihara, and T. Momoi, Phys. Rev. Lett. **110**, 077206 (2013).
[65] M. Mourigal, M. Enderle, B. Fåk, R. K. Kremer, J. M. Law, A. Schneidewind, A. Hiess, and A. Prokofiev, Phys. Rev. Lett. **109**, 027203 (2012).
[66] M. Sato and M. Oshikawa, Phys. Rev. B **75**, 014404 (2007).
[67] R. M. Konik and P. Fendley, Phys. Rev. B **66**, 144416 (2002).
[68] G. Fáth, Phys. Rev. B **68**, 134445 (2003).
[69] I. P. McCulloch, R. Kube, M. Kurz, A. Kleine, U. Schollwöck, and A. K. Kolezhuk, Phys. Rev. B **77**, 094404 (2008).
[70] V. L. Pokrovsky and A. L. Talapov, Phys. Rev. Lett. **42**, 65 (1979).
[71] A. O. Gogolin, A. A. Nersesyan, and A. M. Tsvelik, *Bosonization and Strongly Correlated Systems* (Cambridge University Press, Cambridge, UK, 2004).
[72] *Theoretical Methods for Strongly Correlated Electrons*, edited by D. Sénéchal, A. M. Tremblay, and C. Bourbonnais (Springer, New York, 2004), pp. 139–186.
[73] O. A. Starykh and L. Balents, Phys. Rev. Lett. **93**, 127202 (2004).
[74] O. A. Starykh, A. Furusaki, and L. Balents, Phys. Rev. B **72**, 094416 (2005).
[75] J. Voit, J. Phys. C: Solid State Phys. **21**, L1141 (1988).

[76]I. Affleck, D. Gepner, H. J. Schulz, and T. Ziman, J. Phys. A: Math. Gen. **22**, 511 (1989).
[77]H. Schulz, in *Strongly Correlated Magnetic and Superconducting Systems*, Vol. 478 of Lecture Notes in Physics, edited by G. Sierra and M. Martin-Delgado (Springer, Berlin, 1997), p. 136.
[78]K. Kawano and M. Takahashi, J. Phys. Soc. Jpn. **66**, 4001 (1997).
[79]V. Subrahmanyam, Phys. Rev. B **50**, 16109 (1994).
[80]E. Orignac, R. Citro, and N. Andrei, Phys. Rev. B **61**, 11533 (2000).
[81]S. K. Pati and R. R. P. Singh, Phys. Rev. B **61**, 5868 (2000).
[82]J.-B. Fouet, A. Läuchli, S. Pilgram, R. M. Noack, and F. Mila, Phys. Rev. B **73**, 014409 (2006).
[83]M. Sato, Phys. Rev. B **75**, 174407 (2007).
[84]D. Charrier, S. Capponi, M. Oshikawa, and P. Pujol, Phys. Rev. B **82**, 075108 (2010).
[85]S. Bhattacharjee, Phys. Rev. B **84**, 104430 (2011).
[86]H.-C. Jiang, H. Yao, and L. Balents, Phys. Rev. B **86**, 024424 (2012).